



University of  
Massachusetts  
Amherst

## **WILDFIRES IN THE NORTHEASTERN UNITED STATES: EVALUATING FIRE OCCURRENCE AND RISK IN THE PAST, PRESENT, AND FUTURE**

Item Type	Dissertation (Open Access)
Authors	Miller, Daniel R
DOI	<a href="https://doi.org/10.7275/13428743">10.7275/13428743</a>
Download date	2026-06-08 09:00:42
Link to Item	<a href="https://hdl.handle.net/20.500.14394/17738">https://hdl.handle.net/20.500.14394/17738</a>

**WILDFIRES IN THE NORTHEASTERN UNITED STATES: EVALUATING  
FIRE OCCURRENCE AND RISK IN THE PAST, PRESENT, AND FUTURE**

A Dissertation Presented

by

DANIEL R. MILLER

Submitted to the Graduate School of the  
University of Massachusetts Amherst in partial fulfillment  
of the requirements for the degree of

DOCTOR OF PHILOSOPHY

February 2019

Department of Geosciences

© Copyright by Daniel R. Miller 2019

All Rights Reserved

**WILDFIRES IN THE NORTHEASTERN UNITED STATES: EVALUATING  
FIRE OCCURRENCE AND RISK IN THE PAST, PRESENT, AND FUTURE**

A Dissertation Presented

by

DANIEL R. MILLER

Approved as to style and content by:

---

Raymond S. Bradley, Chair

---

Isla S. Castañeda, Member

---

Keith Nislow, Member

---

Julie Brigham-Grette, Department Head  
Department of Geosciences

## **DEDICATION**

For Jaime. Your light will keep shining bright through everyone you touched and loved.

## ACKNOWLEDGMENTS

This dissertation is the culmination of three years of hard but worthwhile and exciting work. While only one name may be on this thesis, this project could not have been done without the help of a multitude of people both at the University of Massachusetts – Amherst and scattered across the globe. I would like to thank my co-advisors, Dr. Raymond Bradley and Dr. Isla Castañeda, for their guidance and support. Despite being a world-renowned climate scientist and seemingly being in a different country every month, somehow Ray found time to answer all my questions, concerns, and thoughts. Isla is a remarkable scientist with an unparalleled work ethic who introduced me to the world of biogeochemistry and made me a better writer and scientist. Thank you for your enthusiasm and energy, and for shaping me into the scientist I am today.

I would also like to thank other people who were critical to the success of this dissertation. To Keith Nislow, thank you for agreeing to be on my dissertation committee and for providing me valuable help throughout the entirety of this project. To Julie Brigham-Grette and Mike Rawlins, thank you for being on my examination committee at the beginnings of my PhD. Many thanks to Jeff Salacup and the rest of the biogeochemistry lab group for your support and guidance over the years in the lab, and to the rest of the biogeochemistry lab group for their support and enthusiasm. To Dana MacDonald and Bill Patterson, thanks for your guidance and knowledge on charcoal records and analysis throughout my Basin Pond study.

I'd like to thank the Department of Geosciences at UMass for giving me the opportunity to pursue my graduate degrees here with world-renowned scientists and

researchers, and for providing me with summer funding through the Joseph Hartshorn Memorial Fund. I'd also like to thank the Department of Interior's Northeast Climate Adaptation Science Center and the United States Geological Survey (USGS) for providing funding for this research project. Special thanks to Debra Willard, coordinator of the Climate and Land Use Change Research and Development Program at the USGS, for providing funding for radiocarbon analysis on the Basin Pond sedimentary record. Thank you to the NECASC staff, fellows and the people that make everything operate smoothly on a daily basis. Special thanks to Toni Lyn Morelli, Addie Rose Holland, and Jeanne Brown for making the experience of being a fellow so enjoyable and worthwhile. The professional development I gained from being a fellow with the NECASC is one of the most valuable and memorable portions of my graduate work that I will take away into my future careers, and I am truly grateful for your support, mentoring, and friendship over the past several years.

Finally, none of this would have been possible without the support of my family and friends. Thank you, Mom, Dad, Carl, and the rest of my family for everything you have done for me and for making the move to Massachusetts smooth and welcoming. Thank you to all my friends who have helped make Massachusetts my home. In particular, thanks to Ari and Matt for your support and unending belief in me and my abilities – your friendship has helped me more than you know. Finally, a monumental thanks to Alyssa, for your love, patience, and support. You mean the world to me, and your kindness and empathy in the face of the unknown is always inspirational.

Here's to the future!

## ABSTRACT

### **WILDFIRES IN THE NORTHEASTERN UNITED STATES: EVALUATING FIRE OCCURRENCE AND RISK IN THE PAST, PRESENT, AND FUTURE**

FEBRUARY 2019

DANIEL R. MILLER, B.S., THE OHIO STATE UNIVERSITY

M.S., UNIVERSITY OF MASSACHUSETTS AMHERST

Ph.D., UNIVERSITY OF MASSACHUSETTS AMHERST

Directed by: Professor Raymond S. Bradley

Climate change is one of the most complex and challenging issues facing the world today. A changing climate will affect humankind in many ways and alter our physical environment, presenting ethical challenges in how we respond. The impact of climate change will likely be exacerbated in heavily populated regions of the planet, such as the Northeastern United States (NEUS). The NEUS is comprised of complex, sprawling urban centers and rural regions, both of which are vital to the economic and cultural character of the region. Furthermore, both urban and rural areas in the NEUS contain communities that have been historically susceptible to climate change (Horton et al. 2014). Over the past 120 years, average temperatures have increased by 2°F, precipitation has increased by 10%, and sea levels have also risen (Kunkel 2013).

One poorly understood consequence of climate change is its effects on extreme events such as wildfires. Robust associations between wildfire frequency and climatic variability have been shown to exist (Scholze et al. 2006; Westerling et al. 2006), indicating that future climate change may continue to have a significant effect on wildfire activity. The NEUS has been home to some of the most infamous and largest historic “megafires” in North America, such as the Miramichi Fire of 1825 and the fires of 1947

(Irland 2013). Although return intervals in most areas of the NEUS are high (hundreds of years), wildfires have played a critical role in ecosystem development and forest structure in the region (Carlson 2013). Therefore, predicting fire occurrence and vulnerability to large wildfires in the NEUS is economically and culturally relevant. However, predicting fire occurrence is not a simple task due to the nature of wildfire activity in the NEUS.

While in most regions of the world, natural factors such as lightning are the driving cause of wildfires, it has been estimated that the vast majority (>99%) of wildfires in the NEUS are caused by anthropogenic activity and not natural causes (Pyne 1982). Consequently, only studying data associated with fire occurrence (i.e. area burned, number of fires) is likely inadequate for the investigation the region's fire risk over time. Furthermore, little is known about how the direct (temperature & precipitation trends) and indirect (ecosystem-wide species distribution) effects of climate change will impact fire risk in the NEUS under future climate scenarios. Fully understanding the natural mechanisms that control fire risk and occurrence requires continuous records of past fires and climatic variability on centennial to millennial timescales. However, historical fire records in the NEUS are temporally limited, and do not provide an adequate analysis of the impacts of regional wildfire regimes, prior to human disturbance and anthropogenic climate change.

We find that regional climatic fire risk for the NEUS can be estimated most accurately using the Keetch Byram Drought Index (KBDI) from 20<sup>th</sup> century historical meteorological records from various stations located throughout the region. Regional fire risk is then estimated through 2100 AD, using the KBDI and dynamically downscaled regional climate models from CMIP5 climate models. Under RCP 8.5, average KBDI and max yearly KBDI is shown to increase by 300% and 500%, respectively, in an

exponential trend. Under RCP 4.5, KBDI is also expected to increase through 2100 AD to a lesser extent. Interestingly, these increases in regional fire risk are present regardless of increases in precipitation, indicating that future fire risk in the NEUS is driven largely by changes in temperature as opposed to precipitation.

In order to investigate long-term regional wildfire activity over the past millennium, we examine PAHs and macrocharcoal from a varved sedimentary record from Basin Pond, Fayette, Maine (USA). We find elevated concentrations of the PAH retene were found to be highly correlated with known large-scale regional wildfire events that occurred in 1761-1762, 1825, and 1947 (A.D.). To distinguish between biomass burning and anthropogenic combustion, we examined the ratio of the PAHs retene and chrysene. The new Basin Pond PAH records, along with a local signal of fire occurrence from charcoal analysis, offers the prospect of using this multi-proxy approach as a method for examining wildfire frequency at the local and regional scale in the NEUS.

Finally, we report seasonally resolved measurements of brGDGT production in the water column, in catchment soils, and in a sediment core from Basin Pond. We utilize these observations to help interpret a Basin Pond brGDGT-based temperature reconstruction spanning the past 900 years. This record exhibits similar trends to a pollen record from the same site and also to regional and global syntheses of terrestrial temperatures over the last millennium. However, the Basin Pond temperature record shows higher-frequency variability than has previously been captured by such an archive in the NEUS, potentially attributed to large scale atmospheric patterns. These new records of temperature variability and wildfire activity, when compared to regional hydroclimate records, shed insight into pre-historic wildfire risk in the NEUS.

# TABLE OF CONTENTS

	Page
DEDICATION .....	v
ACKNOWLEDGMENTS .....	vi
ABSTRACT .....	viii
LIST OF TABLES .....	xiv
LIST OF FIGURES .....	xv
 CHAPTER	
1. BACKGROUND: WILDFIRES IN THE NORTHEASTERN UNITED STATES .....	1
1.1 NEUS Ecosystem and Fire Occurrence in the Historical Period .....	2
1.2 A Note on “Fire Risk” .....	3
1.3 Dissertation Layout .....	4
 2. HISTORICAL FIRE RISK IN THE NORTHEASTERN U.S.: EVALUATING FIRE RISK INDICES BY COMPARISON TO METEOROLOGICAL DATA .....	 7
2.1 Introduction .....	7
2.1.1 Fire Index History .....	8
2.1.1.1 Canadian Forest Fire Weather Index System .....	8
2.1.1.2 National Fire Danger Rating System (USA) .....	9
2.1.1.3 Other Fire Risk Indices .....	10
2.2 Methods .....	11
2.3 Results .....	13
2.3.1 Fire Occurrence .....	13
2.3.2 Comparison of Fire Indices to Meteorological Data .....	14
2.3.3 Comparison of Fire Indices to Lagged Meteorological Variables .....	15
2.3.4 Comparison of Fire Indices to Eachother .....	15
2.4 Discussion .....	16
2.4.1 Selection of Fire Risk Indices for Regional Analysis .....	16
2.4.2 Fire Risk vs. Fire Occurrence .....	17
2.5 Conclusions .....	18
 3. MODELING FIRE RISK IN THE NORTHEASTERN UNITED STATES FROM 1950 – 2100 AD: LARGE INCREASES IN FIRE RISK PROJECTED FOR THE NEUS .....	 29
3.1 Introduction .....	29
3.2 Methods and Data Analysis .....	31

3.2.1 Estimating Fire Risk Using the Keetch Byram Drought Index .....	31
3.2.2 Analysis of Climate Model Data.....	32
3.2.2.1 Downscaling Methods .....	32
3.2.2.2 Representative Concentration Pathways (RCPs).....	33
3.2.2.3 Selection of RCMs for Ensemble Model.....	34
3.2.3 Case Study Site Selection .....	36
3.2.4 NEUS Regional Projections.....	37
3.3 Results and Discussion .....	37
3.3.1 Evaluating Model Performance using Case Studies .....	37
3.3.2 Model Reproducibility of Observed Fire Risk.....	38
3.3.2.1 Accuracy of Model Data.....	39
3.3.2.2 Assumptions in the Calculation of the KBDI .....	40
3.3.2.3 Error in Observational Data Measurements.....	42
3.3.3 Northeastern United States Regional KBDI Analysis .....	44
3.3.4 Fire Season Length and Severity – Implications for Fire Management.....	45
3.4 Conclusions.....	47
4. LOCAL AND REGIONAL WILDFIRE ACTIVITY IN CENTRAL MAINE (USA) DURING THE PAST 900 YEARS.....	62
4.1 Abstract.....	63
4.2 Introduction.....	64
4.2.1 Study Location.....	66
4.3 Materials and methods .....	67
4.3.1 Core collection .....	67
4.3.2 Age model.....	68
4.3.3 Organic geochemical analyses.....	68
4.3.4 Charcoal analysis .....	69
4.4 Results.....	70
4.5 Discussion.....	70
4.5.1 Historical wildfire data .....	71
4.5.2 Age model considerations.....	71
4.5.3 The basin pond charcoal record .....	72
4.5.4 Basin pond PAH records.....	74
4.5.5 Comparison of wildfire proxies .....	75
4.5.6 Retene: a proxy for regional wildfire activity? .....	77
4.6 Conclusions.....	77
4.7 Acknowledgements.....	78
5. A 900-YEAR NEW ENGLAND TEMPERATURE RECONSTRUCTION FROM <i>IN SITU</i> SEASONALLY PRODUCED BRANCHED GLYCEROL DIALKYL GLYCEROL TETRAETHERS (BRGDGTS).....	86
5.1 Abstract.....	87
5.2 Introduction.....	88
5.3 Site information and field sampling.....	91
5.3.1 Study Site.....	91

5.3.2 Sediment Coring .....	92
5.3.3 Sediment trap construction, deployment and retrieval .....	92
5.4 Methods.....	93
5.4.1 Sedimentary Age Model .....	93
5.4.2 Laboratory Methods.....	94
5.4.3 brGDGT analysis .....	95
5.4.4 Time Series Analysis .....	96
5.5 Results.....	96
5.5.1 Catchment Soils .....	97
5.5.2 SPM.....	97
5.5.3 Surface sediment samples .....	98
5.5.4 Sediment Core.....	98
5.5.5 BrGDGT isomer ratios.....	99
5.5.6 Algal biomarkers.....	99
5.6 Discussion .....	99
5.6.1 Sources and seasonal production of Basin Pond brGDGTs.....	99
5.6.2 Calibration of the 900 year brGDGT record to temperature.....	102
5.6.3 Comparison to Regional Hydroclimate Records in the NE US.....	104
5.6.4 Comparison with Northern Hemisphere records .....	106
5.6.5 20th Century temperature, brGDGT Reconstructions and Algal Community Shifts .....	108
5.7 Conclusions.....	111
5.8 Data Availability .....	112
5.9 Author Contributions .....	112
5.10 Competing Interests .....	113
5.11 Acknowledgements.....	113
5.12 Supplementary Information .....	113
5.12.1 MBT <sub>5ME</sub> Calibration to Local Temperature.....	113
6. CONCLUSIONS AND FUTURE WORK.....	130
6.1 Future Work .....	131
BIBLIOGRAPHY.....	134

## LIST OF TABLES

Table	Page
Table 1.1: Various definitions of “fire risk” with sources. ....	6
Table 2.1: A list of widely-used fire indices in North America. Primary parameters are the main variables in each index, and include P ( <i>precipitation amount</i> ), T ( <i>temperature</i> ), W ( <i>wind speed/direction</i> ), RH ( <i>relative humidity</i> ), FT ( <i>fuel type</i> ), Veg ( <i>Other vegetation parameters</i> ), Loc ( <i>Other location parameters</i> ), and Atm ( <i>other atmospheric parameters</i> ). ....	26
Table 2.2: List of selected meteorological stations with period of record (POR) length given in years. Locations of each station can be viewed in Figure 2.1. ....	27
Table 2.3: Mean correlations between all fire indices and meteorological variables from April 1 through November 1, as well as the average correlations for each index (based on the absolute value) and for each weather variable. ....	27
Table 2.4: Mean correlations between moving averages of lagged meteorological variables from April 1 - November 1, and daily values of the a) KBDI, b) DMC, and c) DC fire indices. ....	28
Table 2.5: Mean correlations between fire indices from April 1 - November 1. ....	28
Table 3.1: Drought factor table for areas with annual rainfall of 30 – 39”, adapted from Keetch and Byram (1968). The “drought factor” is added to daily KBDI depending on max temperature and previous day’s KBDI as listed in the table. ....	61
Table 4.1: Results of radiocarbon analysis of Basin Pond macrofossils from core BP2014-5D. The laboratories used were the U.S. Geological Survey’s Eastern Geology and Paleoclimate Science Center (USGS), and the Woods Hole Oceanographic Institute NOSAMS Facility (OS). <sup>14</sup> C ages were converted to calibrated ages using the “BChron” package for R (see text for more detail). ....	79
Table 4.2: PAH present in laboratory standards and searched for in Basin Pond sediments, with major ions for each compound. ....	80
Table 5.1: Meteorological data used for calculating MBT’ <sub>5Me</sub> to temperature calibration at Basin Pond, ME from June 2014 through June 2015. ....	128
Table 5.2: Additional information regarding sites discussed in the main text for comparison with the Basin Pond record. ....	129

## LIST OF FIGURES

Figure	Page
Figure 1.1: Northeastern U.S. Forest Cover through time, broken down by state and with region population (red dashed line). .....	6
Figure 2.1: Map of Northeastern U.S. meteorological stations used in this study. A) Bedford, MA; B) Boston, MA; C) Westover, MA; D) Portland, ME; E) Bangor, ME; F) Caribou, ME; G) Concord, NH; H) Pease, NH; I) Burlington, VT; J) New Haven, CT; K) Providence, RI; L) Amherst, MA; and M) Gardiner, ME. More information on each site can be found in table 2.2. ....	20
Figure 2.2: Fire Occurrence Data for the state of Maine from 1900 – 2017. A) number of fires each year, and B) total acres burned each year. ....	21
Figure 2.3: Comparison of max yearly KBDI (green), average yearly KBDI (red), number of fires in the Maine (black), and total acres burned in Maine (Blue). Bolded KBDI lines are 5 year running averages. Note that in extreme years, KBDI tracks fire occurrence data (e.g. early 1970s, mid 1960s) reasonably well. ....	22
Figure 2.4: the “fire season”, as seen from the KBDI throughout the year from 1900 – 2017 from Gardiner, ME. Note the key in the top right corner, indicating the color of the daily KBDI values. A shift in timing of the fire season can be seen from the late 1970’s through present day. ....	23
Figure 3.1: Model Projections for percent changes in precipitation and temperature from historical averages to 2100 averages, using the 5-member ensemble used in this study. Adapted from Karmalkar et al. (2018) under RCP 8.5 scenarios for the NEUS. Due to the fact that the fire season is during the summer/fall months, the June-July-August averages were used to estimate model projections. These 5 models capture the range of uncertainty in model projections for the NEUS. ....	48
Figure 3.2a: Map of the NEUS, with 4 case studies indicated: F) Caribou, Maine, M) Gardiner, Maine, I) Burlington, Vermont, and L) Amherst, Massachusetts. White shaded boxes represent the area used in model projections for comparison to observed station data. ....	49
Figure 3.2b: Map of the NEUS with subregions defined – Southern New England (white), Southern Vermont/New Hampshire (yellow), Northern Vermont/New Hampshire (green), Southern Maine (Red), Central Maine (light blue), and Northern Maine (Brown). ....	50
Figure 3.3: Seasonal average KBDI from historical observations (black dashed line), modeled runs from 1950-2017 (black line), 2018-2058 (red line), and 2059-2099	

(purple line) for selected four case study locations – A) Amherst, MA, B)Gardiner, ME, C)Burlington, VT, and D)Caribou, ME. ....51

Figure 3.4: Anomalies between observed KBDI (solid black line top) and modeled KBDI (dashed line) for the historical period (1950-2017 AD), with difference (blue line) and percent difference (bottom black line) between model and observed KBDI, for the 4 case study locations. Shaded area on each plot represents the “fire season”, where KBDI becomes increasingly significant to fire managers. Note the small differences between modeled and observed KBDI on plots A and B (Amherst and Gardiner), while larger differences occur at C)Burlington and D) Caribou. ....52

Figure 3.5: Modeled KBDI from 1950-2099 at A)Amherst, MA , B)Gardiner, ME, C) Burlington, VT, and D) Caribou, ME, for RCP 8.5. Note scales and color ranges remain constant for each plot: lower KBDI of 0-150 are indicative of little/no fire risk (green), increasing to KBDI values of 150-300 (yellow), 300-450 (orange), 450-600 (red) and then greater than 600 (purple) for maximum KBDI values and extreme fire risk.. ....53

Figure 3.6: Model Ensemble NEUS Climatic Data and KBDI from 1950-2099, under both RCP 8.5 and 4.5. a) Mean annual temperatures (black (RCP 8.5) and grey (RCP 4.5)), b) Annual Precipitation in inches per year (Dark blue (RCP 8.5) and light blue (RCP 4.5)), c) Average annual KBDI (dark red (RCP 8.5) and light red (RCP 4.5)), and d) Maximum annual KBDI (purple (RCP 8.5) and pink (RCP 4.5)). ....54

Figure 3.7: Averaged seasonal KBDI for the NEUS under A) RCP 8.5 and B) RCP 4.5. Averages have been broken into three time periods: 1950-2017 (black line), 2018-2058 (red line), and 2059-2099 (purple line).....55

Figure 3.8: Modeled KBDI from 1950-2099 for the NEUS for a) RCP 8.5 and b) RCP 4.5. Note scales and color ranges remain constant for each plot: lower KBDI are indicated by green, increasing to yellow, orange, red and then purple for maximum KBDI values.....56

Figure 3.9: Averaged seasonal KBDI for subregions under RCPs 8.5 and 4.5: a-b) Southern New England, c-d) central Maine, e-f) southern VT-NH, g-h) Northern Maine, i-j) Southern Maine, and k-l) Northern VT-NH. Averaged time periods include 1950-2017 (black), 2018-2058 (red), and 2059-2099 (purple). ....57

Figure 3.10: Modeled KBDI from 1950-2099 for subregions for RCP 8.5. Color ranges remain constant for each plot.. A) Southern New England, B) South Maine, C) South VT-NH, D) Central Maine, E) Northern Maine, and F) North VT-NH. ....58

Figure 3.11: Modeled KBDI from 1950-2099 for subregions for RCP 4.5. Color ranges remain constant for each plot.. A) Southern New England, B) South Maine, C) South VT-NH, D) Central Maine, E) Northern Maine, and F) North VT-NH. ....59

- Figure 3.12: Comparison of modeled and observed climate data from Caribou, ME.  
 A) Average temperature for observed (black solid line) and modeled (grey dashed line), and B) Annual Precipitation in inches per year for observed (blue solid line) and modeled (blue dashed line). .....60
- Figure 3.13: LANDFIRE Map of fire return intervals in the NEUS, provided by the Northeast Forest and Fire Management LLC (2013). Note that many areas in the southern portion of the NEUS have low return intervals for fire, in some cases lower than 35 years. ....60
- Figure 4.1: Location of Basin Pond, ME and bathymetric map. A) Map of the NEUS with Maine highlighted in gray and Basin Pond indicated by a star. B) Map of Maine with estimated ranges of known large wildfire events (>400km<sup>2</sup> acres burned) from historical records within 100km of Basin Pond, adapted from Coolidge (1963). Shaded locations indicate the fires of 1761-1762 AD (yellow), 1825 AD (blue), and 1947 AD (red). Orange shading indicates regions effected by both the 1761-1762 AD and 1947 AD fires. C) Bathymetric map of Basin Pond.....81
- Figure 4.2: A) Age-depth model for the sedimentary record of Basin Pond, with age measured in Years AD. Black markings indicate dated positions through varve counting (varve counts every 4-cm are marked), radiocarbon dating, and lead-210 dating. Grey shading indicates the 95% confidence interval at any given depth. B) Age model for 1920AD – present day. Gray points indicate <sup>210</sup>Pb dates with associated errors, while black points are varve counts. ....82
- Figure 4.3: Fire reconstructions from the historical period (1725AD to present day). From top to bottom: charcoal counts per cm<sup>3</sup> sediment (red triangles), the retene/(chrysene + retene) ratio (green circles), retene concentrations (black squares), chrysene concentrations (blue diamonds), and the top 5 most abundant PAH (excluding retene and chrysene) measured in the sedimentary record. All PAH concentrations are reported in µg / g sediment extracted. ....84
- Figure 4.4: Fire reconstructions from Basin Pond, ME since 1100 AD; a) charcoal counts per cm<sup>3</sup> sediment (red triangles), b) the retene/(chrysene + retene) ratio (green circles), c-d) retene (black squares and black dashed squares) and e) chrysene concentrations (blue diamonds), measured in µg / g sediment extracted. Due to the drastic increase in retene concentrations in the historic period from background levels, pre-historic retene has been plotted twice (dashed black line) in panels c and d. Note the difference in the y-axis scale between plots c and d and also the scale break in plot d. The retene/(chrysene + retene) ratio, shown in plot b, used as an indicator of PAH combustion source, remains above 0.8 throughout the pre-historic record, while decreasing below 0.8 from regional industrialization marked with several increases to above 0.8 following fire events (0.8 marked by dashed, horizontal line). Fire events of 1761-1762 AD, 1825 AD, and 1947 AD are marked by dashed vertical lines. Increased periods of fire activity outside of those noted in historical records, which are suggested by our data, are shaded in yellow. ....85

- Figure 5.1: Map of Basin Pond. (a) The location of Basin Pond (BP) (white star) in Maine, USA. Locations of three other sites are labelled: Little Pond (LP; Gao et al. 2017), Great Heath Lake (GH; Nichols and Huang, 2012; Clifford and Booth, 2013), and Saco Bog (SB; Clifford and Booth, 2013). (b) Bathymetric profile (6 m contours) of Basin Pond with position of floating sediment traps (circles), surface soil samples (squares), and core BD-2014-5D used for the downcore temperature reconstruction in this study (star). The pond has an area of approximately 0.14 km<sup>2</sup>. (c) Schematic of sediment traps utilized in this study. ....116
- Figure 5.2: Temporal variation of the relative abundance of group I, II and III brGDGTs in SPM (green shaded bars), sediment (black bars), and catchment soil samples (white bars). As in the plot of June SPM, the brGDGT groups III, II, and I, are displayed from left to right for each collection period and sediment and soil samples. Sediment and soil samples were collected in Spring of 2014. Green shaded bars for SPM samples reflect averages for each date samples were collected, measured in July 2014 (lightest green), August 2014, September 2014 and June 2015 (darkest green). For each category, brGDGT groups III, II, and I are shown in that order (left to right). Lines in each bar represent the relative abundance of 5- and 6- methyl brGDGTs, with cross hatching representing 6- methyl abundances.....117
- Figure 5.3: Time series of brGDGT fluxes for each of the sediment traps in Basin Pond. brGDGT fluxes at 6m (a), 12m (b), 18m (c), 24m (d), and 30m (e) are shown. There is no data for trap (e) in July 2014. Note the change of scale for (d) and (e), indicating fluxes an order of magnitude higher for the lowermost traps. Green bars correspond to the time periods in Figure 2. Blue bars correspond to the depth ranges in Figure 5. ....118
- Figure 5.4: Hydrolab-measured temperature and pH profiles for Basin Pond compared with flux weighted average brGDGT-based reconstructions. (a) Fall lake temperature profile, showing the mixed layer extending to ~9 m water depth, followed by the thermocline (9-15 m) and a cold deep layer (15-32 m). (b) Fall pH profile. the pH ranges from ~7.5 at the surface to ~6.2 at depth. (c) Flux weighted average MBT values measured at sediment traps. (d) Flux weighted average CBT values measured at sediment traps. (e) brGDGT fluxes measured at sediment traps. ....119
- Figure 5.5: Spatial variation in the water column of the relative abundance of groups I, II and III brGDGTs in SPM as a function of water depth. As in the plot of June SPM, the brGDGT groups III, II, and I, are displayed from left to right for each collection period and sediment and soil samples. For each group, the relative abundance at depths of 6 m (lightest blue), 12 m, 18 m, 24 m, and 30 m (darkest blue) is plotted next to the average surface sediment (black) and catchment soil (white). For each category, brGDGT groups III, II, and I are shown in that order (left to right). Lines in each bar represent the relative abundance of 5- and 6- methyl brGDGTs, with cross hatching representing 6- methyl abundances.....120

- Figure 5.6: BrGDGT-based proxies measured on surface sediments (black), SPM (gray), and catchment soils (white). (a) Cyclization of Branched Tetraethers (CBT), (b) Methylation of branched tetraethers ( $MBT'_{5ME}$ ), and (c) the Isomer Ratio (IR)....121
- Figure 5.7: Comparison of Basin Pond  $MBT'_{5ME}$  with newly published temperature calibrations. (a) Core BP2014-5D plotted using the African Lakes calibration (Russell et al., 2018), and the (b) Chinese lakes calibration (Dang et al., 2018). (c) Basin Pond  $MBT'_{5ME}$  values. ....122
- Figure 5.8: Ternary diagram of brGDGT distributions of lake sediments (Dang et al., 2018; Russell et al., 2018) and global soils (Peterse et al., 2012) and Basin Pond sediments.....123
- Figure 5.9: The Basin Pond  $MBT'_{5ME}$  record compared with other paleoclimate records from the NE US. (a)  $MBT'_{5ME}$  (this study). Colored bars indicate the three main periods discussed in the text. (b) Pollen-based reconstruction of temperature at Basin Pond (Gajewski, 1988). (c) Deuterium isotope ( $\delta D$ )-based temperature reconstruction at Little Pond (Gao et al., 2017). (d) Great Heath aridity reconstruction based on the *Sphagnum*/Vascular Ratio (SVR) (Nichols and Huang, 2012). (e) Water table reconstruction from Great Heath (Clifford and Booth, 2013). (f) Water table reconstruction from Saco Bog (Clifford and Booth, 2013). (g) Charcoal counts from Basin Pond (Miller et al., 2017).....124
- Figure 5.10: The Basin Pond  $MBT'_{5ME}$  record compared with regional and global records of temperature change. (a) Tree-ring based reconstruction of the AMO Index (Gray et al., 2004). (b) NAO Index reconstruction (Sun et al., 2015). (c–f) Regional temperature stacks based on composite proxy reconstructions for the Arctic (c), Europe (d), and North America (pollen, (e); tree rings, (f)). The records have been standardized to have the same mean (0) and standard deviation (1) from 1190–1970 AD (PAGES2k 2013). (g)  $MBT'_{5ME}$  (this study). ....125
- Figure 5.11: Comparison of historical temperature records for the state of Maine,  $MBT'_{5ME}$  reconstruction, and algal lipid biomarkers in Basin Pond. (a) Relative abundance of four major algal lipids. (b)  $MBT'_{5ME}$  record. (c) Maine state-wide average temperature (NOAA, 2014). The black line indicates the rotenone treatment of the lake in 1955.....126
- Figure 5.12: a) Comparison of  $MBT'_{5ME}$  values from all SPM samples (averaged for each date range) to average air temperatures during each time period. The equation for the plotted linear regression line, along with the correlation coefficient, are shown. b) Downcore reconstructed temperatures (in °C) from the Basin Pond calibration (long dashed line), the Russell et al. 2018 African lakes calibration (short dashed line), and from the Dang et al. 2018 Chinese lakes calibration (solid line).....127

## CHAPTER 1

### **BACKGROUND: WILDFIRES IN THE NORTHEASTERN UNITED STATES**

The overarching question of this dissertation is “How has fire risk in the Northeastern United States fluctuated over time, and how will it continue to evolve with anticipated future climate change?” To answer this question, fire risk was investigated on different timescales using a variety of methods. Lacustrine sedimentary archives from Maine were used to estimate “pre-historic” (prior to 1750AD) fire risk and occurrence on centennial timescales. Meteorological station data from the region were used to estimate fire risk indices from 1900-2018AD throughout the region. Finally, climate model data was utilized to investigate future fire risk in the region through 2100AD.

The Northeastern United States (NEUS) has been home to some of the most infamous and largest historic “megafires” in North America, such as the Miramichi Fire of 1825 and the fires of 1947 (Irland 2013). Although return intervals in most areas of the NEUS are high (hundreds of years), wildfires have played a critical role in ecosystem development and forest structure in the region (Carlson 2013). Therefore, predicting fire occurrence or vulnerability to large wildfires in the NEUS is economically and culturally relevant. However, predicting fire occurrence is not a simple task due to the nature of wildfire activity in the NEUS. While in most regions of the world, natural factors such as lightning are the driving cause of wildfires, it has been estimated that the vast majority (99%) of wildfires in the NEUS are caused by anthropogenic activity and not natural causes (Pyne 1982). Consequently, only studying data associated with fire occurrence (i.e. area burned, number of fires) is likely inadequate for the investigation the region’s fire risk over time.

## **1.1 NEUS Ecosystem and Fire Occurrence in the Historical Period**

The NEUS is a heavily forested region, with approximately 80% forested land cover. The region consists of diverse groups of temperate ecosystems and is a transition zone between the Northern boreal forest and deciduous forest to the south (Davis et al. 2017). Coniferous forests are found to the north and at high altitudes (greater than 900 m), and includes many different dominant species depending on location and altitude (red pine, balsam fir, red spruce, white spruce, jack pine, white pine, paper birch). Northern hardwood forests dominate the mid-latitudes of the NEUS, mixing with the northern coniferous forest at mid-latitudes. Common northern hardwood species include sugar/red maple, beech, hemlock, red oak, and white ash. Finally, northern hardwood forests transitions to primarily oak-hickory forest in the southern NEUS (Davis et al. 2017).

The history of NEUS forests has been studied and documented over the past several decades (Carlson 2013; Pyne 1982; Foster & Aber 2004). Prior to European settlement of the region, Native American communities had a noticeable anthropogenic influence on forests, which included using fire for land clearance practices (Patterson and Sassaman 1988). However, forests in the region have undergone the most drastic changes in recent centuries due to European settlement and human activity. Land clearance peaked in the mid-19<sup>th</sup> century, with a steady recovery of forests across the region over the past century. This was primarily due to increased forest management practices being developed and used throughout the NEUS in recent decades (Carlson 2013). Consequently, the NEUS has one of the most heavily-developed and forested regions in the world, making wildfire risk a noteworthy economic and societal concern.

Due to the vast amounts of forested area and typical meteorological conditions in the NEUS, the region is prone to increased wildfire activity during the spring and fall (Pyne 1982). The vast majority of forests in the NEUS are susceptible to wildfires on some time scale, with fire return intervals varying on sub-decadal to millennial timescales (Carlson 2013). In some communities found on Cape Cod through southern Maine, wildfires are the primary disturbance mechanism and are necessary for stand rejuvenation and health. Therefore, prescribed burning practices have been employed throughout the NEUS to aid in managing forests and providing a safe alternative to natural wildfires in populated forested areas (NWCG 2012; Carlson 2013). This makes future fire risk due to changes in climate and meteorological patterns a relevant, pressing issue for many forest and fire managers in the region.

## **1.2 A Note on “Fire Risk”**

Before proceeding, it is important to define what the term “fire risk” is referring to throughout this dissertation. In the past, fire risk has been defined in numerous ways or with different methods (Table 1.1). Furthermore, fire risk indices have been created to attempt to quantify different aspects of “fire risk”, including rate of fire spread, probability of ignition, fire severity, or the probability of fires affecting humans (Deeming et al. 1972; Van Wagner et al. 1987). One of the primary focuses in this dissertation is the direct effects of climate variability on wildfire regimes and wildfire risk. Therefore, in this dissertation, “fire risk”, or perhaps more accurately termed “climatic fire risk”, will be defined as the risk associated with the direct effects of climate and meteorological patterns on establishing conditions that favour wildfires. As detailed

in chapters 2 and 3, this definition of fire risk will become more specific once certain fire indices are chosen for analysis in this study.

### **1.3 Dissertation Layout**

This dissertation is laid out in six chapters, including this introductory chapter. Chapter 2, entitled “Historical Fire Risk in the Northeastern United States”, focuses on calculating a suite of fire risk indices and performing an analysis developed to aid in interpreting which indices perform best in the NEUS at capturing climatic fire risk. Chapter 3, entitled “Modeling fire risk in the Northeastern United States from 1950-2100”, focuses on using the selected fire risk index from Chapter 2, the Keetch Byram Drought Index (KBDI), to estimate climatic fire risk in the NEUS throughout the 21<sup>st</sup> century using an ensemble of climate models from CMIP5. This study reveals that climatic fire risk is expecting to drastically increase by 2100AD, regardless of regional annual precipitation increases or RCP scenario used. A combination of these chapters is currently in preparation to be submitted for publication in the Journal of Wildland Fire.

Chapter 4, entitled “Local and Regional Wildfire Activity in Central Maine (USA) during the past 900 years”, investigates local and regional fire occurrence from analysis of a sedimentary record from Basin Pond, located in Central Maine. Through a multi-proxy method, including macrocharcoal and Polycyclic Aromatic Hydrocarbon (PAH) analysis, local and regional wildfire outbreaks were noted throughout the sedimentary record, including three known wildfires documented in historical records in 1947, 1825, and 1761-1762 AD. This manuscript was published in the Journal of Paleolimnology (Miller et al. 2017).

Chapter 5, entitled “A 900-year New England temperature reconstruction from in situ seasonally produced branched glycerol diacyl glycerol tetraethers (brGDGTs)”, details a study performed on the Basin Pond sedimentary record, as well its water column and catchment soils, investigating temperature variability over time. Results from this study indicate that downcore sedimentary brGDGTs are likely produced in the water column, as opposed to the catchment soils, with a bloom occurring in September, implying that the temperatures reconstructed from the sedimentary record are likely fall-biased. The Basin Pond temperature record, being the first record of its kind for the region, was compared to other regional hydroclimate paleorecords, as well as other Northern Hemisphere records, to investigate causes of long-term fluctuations in temperatures at Basin Pond. This study was published in the open-access journal *Climate of the Past* (Miller et al. 2018).

The final chapter summarizes the work outlined and discussed in this dissertation, its impacts, and directions for future studies that could advance the work discussed in this thesis.

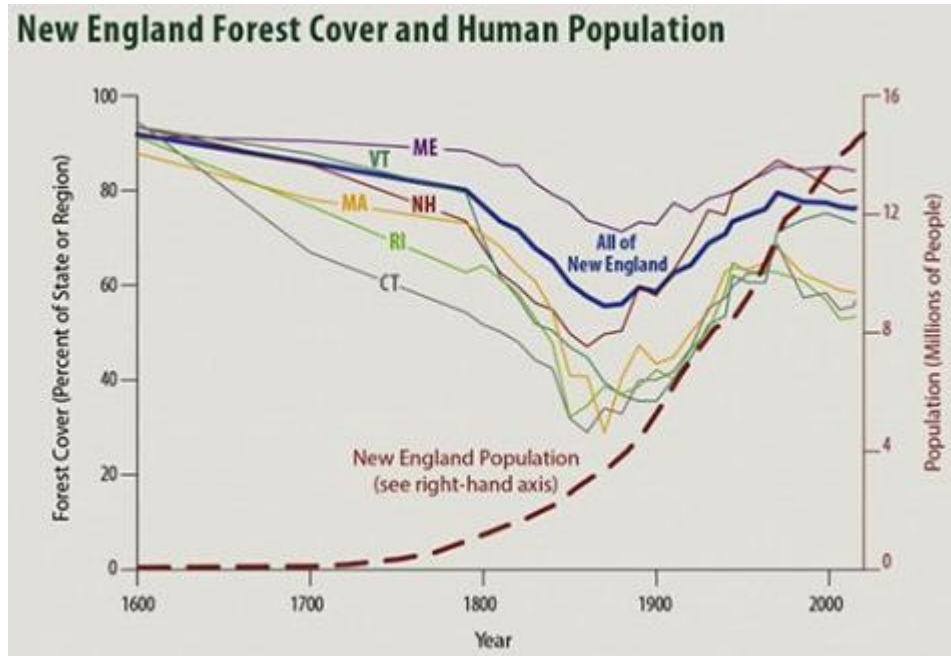


**Figure 1.1: Northeastern U.S. Forest Cover through time, broken down by state and with region population (red dashed line), adapted from Foster and Aber (2004).**

Source	"Fire Risk" Definition
FAD, United Nations (1986)	"The chance of a fire starting as determined by the presence and activity of any causative agent"
San-Miguel-Ayanz et al. (2003)	"the probability of fire initiation"
Canadian Forest Services (1997)	"the potential number of ignition sources"
Chuvieco and Congalton (1989)	"the union of two components: fire hazard and fire ignition"
Bachman and Allgower (2001)	"the probability of a fire to happen and its consequences"

**Table 1.1: Various definitions of "fire risk" with sources.**

## CHAPTER 2

### HISTORICAL FIRE RISK IN THE NORTHEASTERN U.S.: EVALUATING FIRE RISK INDICES BY COMPARISON TO METEOROLOGICAL DATA

#### 2.1 Introduction

Estimating historical fire risk is a complex task, largely due to human disturbance and fire suppression activities taking place throughout the same time period that historical fire records have been kept in the NEUS (i.e., the 20<sup>th</sup> century) (Pyne 1982). These factors influence fire occurrence (i.e. area burned, number of fires) and create a need for an alternative method of investigating the region's fire risk. In light of this, various "fire danger indices" have been introduced in recent decades, with the goal of modeling different aspects of a region's fire risk (table 2.1). These indices range from simple meteorological calculations (i.e. Fosberg 1978) to more complex indices incorporating atmospheric, meteorological, geographical, and ecological parameters (i.e. Deeming et al. 1972). Furthermore, fire risk indices vary on the time-scale of the parameters included in the indices. Short-term indices are based on variables that continuously and rapidly change, which can be useful in estimating daily or sub-daily fluctuations in fire risk. On the other hand, longer-term indices are based on parameters that change little in the short term, and have been used to estimate seasonal or fire risk on longer time scales (San-Miguel-Ayanz et al. 2003).

All of these indices have been utilized by governmental organizations and fire management officials to aid in the prompt dissemination of fire risk among communities are useful in preventing recent large fire outbreaks (Carlson 2013, Irland 2013). While these variables have provided a useful approach for quantifying wildfire risk in recent

decades, little work has been done on reconstructing these indices to assess long-term variations. Consequently, current understanding of the usefulness or accuracy of fire indices in tracking fire risk *in the NEUS*, and how regional fire risk has fluctuated in historical records, is limited. In this study, we address this outstanding issue by performing statistical analysis of fire indices in comparison with meteorological parameters from observation stations located throughout the region, and then compare selected indices to fire occurrence data (i.e., acres burned and total number of fires per year). Through this analysis, we hope to gain a better understanding of which fire index, if any, correlate best with fire occurrence, and which meteorological parameters have the most dominant influence on this selected index or indices.

### **2.1.1 Fire Index History**

#### **2.1.1.1 Canadian Forest Fire Weather Index System**

The first efforts to quantify fire risk through numerical indices began as early as the early 20<sup>th</sup> century. Much of this research was pioneered by Canadian scientists, who developed a preliminary forest fire danger rating system, known as the “Wright system of fire-hazard rating”, in the mid-1920’s (Wright 1937; Beall 1990). Since then, five different fire danger rating systems have been developed and used in Canadian forests. However, the Wright System still forms part of the current Canadian Forest Fire Weather Index System (CFFWIS) and was an essential foundation of Canadian fire research (Beall 1990). Over the past 90 years, the Canadian system for estimating fire risk has built on previous systems using experimental fieldwork and extensive statistical and empirical analysis. Currently, the CFFDRS is the accepted national fire danger rating system for

Canadian forests, and incorporates two modules: the Canadian Forest Fire Behavior Prediction (FPB) System (Taylor et al. 1996) and the Canadian Forest Fire Weather Index System (FWI) (Van Wagner 1987). The latter has been in use since 1970 with minor revisions and updates occurring in 1976, 1978, and 1984.

The FWI system incorporates solely meteorological parameters and does not include differences in other vegetation or “fixed” parameters, such as fuel type or topography (San-Miguel-Ayanz et al. 2003). Six numerical indices are computed in the FWI, and require dry-bulb temperature, relative humidity, wind speed, and daily precipitation totals to calculate. The first three components – the Fine Fuel Moisture Code (FFMC), the Duff Moisture Code (DMC), and the Drought Code (DC) – attempt to quantify fuel moisture that track both short and long-term changes in the moisture content of fuel with varying drying rates. The final three indices – the Initial Spread Index (ISI), Buildup Index (BUI), and the Fire Weather Index (FWI) – all describe potential fire behavior, including the rate of spread, fuel load, and fire intensity (San-Miguel-Ayanz et al. 2003). More information on all six fire indices in the CFFDRS can be found in table 2.1.

#### **2.1.1.2 National Fire Danger Rating System (USA)**

Work on constructing a fire risk index in the United States began in the mid-20<sup>th</sup> century with the development of the National Fire Danger Rating System (NFDRS). First published and applied in 1972, the NFDRS computed three fire behavior indices based on a mathematical fire spread model (Rothermel 1972; Deeming et al. 1972). Unlike its Canadian counterpart, the NFDRS incorporated both meteorological parameters and other aspects of fire risk, including various fuel models, fuel classes and

different slope classes. The NFDRS was updated in 1978 to take into account feedback from users and developments in fire science technology (Deeming et al. 1977). Fire risk indices that were computed in the NFDRS include the Burning Index (BI), Spread Component (SC), Energy Release Component (ERC), and Ignition Component (IC). The NFDRS was updated again in 1988 to calculate fire risk more accurately in the eastern United States (Burgan 1988), a region that is more humid and has different fuel loading than the western U.S. The major addition in this release was the Keetch Byram Drought Index (KBDI), which addresses the effects of long-term drought on fire danger in the eastern U.S., through increasing dead fuel in deep duff layers during times of increased drought (Keetch & Byram 1968). More information on the NFDRS indices, including the KBDI, can be found in table 2.1.

### **2.1.1.3 Other Fire Risk Indices**

Outside of the NFDRS and CFFDRS, a handful of other indices have been developed to estimate different aspects of fire risk. As technology advanced and satellites were developed that capture high resolution images of the earth, fire indices were developed to assess the status of live versus dead vegetation through “greenness” of the vegetation (Burgan et al. 1996). One such index is the Fire Potential Index (FPI), which is a numerical rating of available fuel and susceptibility to ignition based on the proportion of live to dead vegetation and its moisture content (Burgan et al. 1998).

Apart from ecological parameters, various indices have been developed that utilize different atmospheric variables to assess fire risk. The Haines Index (HI), an atmospheric index designed to measure the instability of air in the lower atmosphere, was developed to quantify the probability that land fires will become large and erratic in a

given air mass (Haines 1988). At low elevations, the HI is derived from a lapse rate using 950- to 850 mb temperature differences and a temperature to dew point spread at 850mb. The HI gives higher values when there is a greater lapse rate, or temperature gradient, between isobars, and was found to strongly correlate with fire occurrence (Haines 1988).

Lastly, the Fosberg Fire Weather Index (FFWI) was developed as a simple tool for estimating short term fire potential from meteorological parameters including temperature, wind speed, and relative humidity (Fosberg 1978). An update to this index was made to incorporate “fuel availability”, as seen in the KBDI, to account for precipitation variability (Goodrick 2002). The simplicity of the FFWI is ideal for computing from the output from various meteorological models, as all other factors affecting fire risk are assumed constant (i.e. vegetation type). More information on all fire indices can be found in table 2.1.

## **2.2 Methods**

Fire indices were reconstructed for selected meteorological stations located throughout the NEUS. Automated Surface Observing System (ASOS) stations were the dominant type of station utilized in this study for several reasons (NCDC, 2018). First, in order to produce accurate representations of fire risk, multiple readings per day are needed from each station to capture ‘true’ maximum and minimum daily values of selected meteorological variables. ASOS stations record data as frequently as every 10 minutes to 1 hour, making these datasets ideal. ASOS stations also record meteorological parameters such as wind direction, wind speed, and cloud cover, which are frequently used in fire indices but are not recorded by a vast majority of weather stations. Finally, due to the widespread use of ASOS stations at regional airports and their importance in

providing accurate, real-time data used by the aerospace industry, these stations are normally well-maintained and are in ideal locations for monitoring weather conditions.

Twelve ASOS station datasets were selected based on record length (greater than 50 years) and geographical location (Figure 1, Table 2). One challenge that arose with the ASOS datasets was the completeness of record. Only eight of the selected stations contained >98% of data during the period of record. To fill in missing geographical gaps in the region and to extend records back through the entire 20<sup>th</sup> century, an additional two meteorological stations were selected for analysis. While these stations do not provide multiple observations per day and are missing certain variables (i.e. wind speed, direction, and relative humidity), they do provide maximum, minimum, and average daily temperatures as well as daily precipitation extending over 100 years. Due to the limitations of these two stations, not all fire indices could be reconstructed using these stations. However, as detailed below, this issue was resolved by the selection of specific fire indices.

Fire indices (Table 1) for each station were calculated using FireFamily Plus (FFP) (Bradshaw & McCormick 2013). FFP is software package designed for analyzing daily weather observations and calculating all U.S. National Fire Danger Rating System (NFDRS), the Canadian Fire Danger Rating System (CFDRS) variables, and other widely-used indices such as the Fosberg Fire Weather Index (FFWI) or Keetch-Byram Drought Index (KBDI). FFP also has statistical analysis tools to assess relationships among weather data, fire indices, and fire occurrence. While FFP is generally used by fire management organizations or professionals for short-term forecasting of fire indices, this research utilized the tools found in FFP for analysis of long-term datasets. Datasets were

then compiled, organized, and statistically analyzed using R-studio and the R programming environment.

Fire occurrence parameters (area burned per year, number of fires per year) were obtained from the National Interagency Fire Center. Unfortunately, these parameters only exist for years 2002 – present day for all NEUS states, while records for the state of Maine extend back to 1903 (Patterson, personal communication). The reconstructed fire index datasets were compared to fire occurrence parameters for the region to assess the suitability of each index for the NEUS, as well as to investigate changes in fire risk throughout the period of record.

## **2.3 Results**

### **2.3.1 Fire Occurrence**

Fire occurrence data for the NEUS is unfortunately temporally limited to 2002 AD – present (National Interagency Fire Center, 2018). However, fire occurrence data, while sparse for the entire NEUS, exists for the state of Maine over past 115 years. This dataset contains the number of fires per year and total acres burned per year, and is the longest record of wildfire occurrence in the region. Number of fires per year was lowest in the earliest part of the record (below 100 fires/year) and steadily increased through the early 1940s. From 1945-1955, fire occurrence increased sharply to nearly 1000 fires/year, before decreasing to approximately 400 fires/year through the early 1970s. In 1974, values again increased sharply, and continued to do so until peak values (>1400 fires/year) were reached in the early 1980s. The number of fires then decreased steadily through present day values of 300-500 fires/year (Fig 2.3a).

Total acres burned per year behaves differently than the number of fires per year, with maximum values occurring in the early portion of the record with peaks (>200,000 acres) occurring in 1903 and 1947. Acres burned per year steadily decreased throughout the record, with minimum values (<1,000 acres) occurring from 2006 to present day (Fig 2.3b).

### **2.3.2 Comparison of Fire Indices to Meteorological Data**

The following 13 fire indices were computed from each meteorological station dataset: the Keetch-Byram Drought Index (KBDI), Fosberg Fire Weather Index (FFWI), Spread Component (SC), Burning Index (BI), Energy Release Component (ER), Ignition Component (IC), Fine Fuel Moisture Code (FFMC), Duff Moisture Code (DMC), Drought Code (DC), Initial Spread Index (ISI), Build Up Index (BUI), Initial Rate of Spread (RSI), and the Canadian Fire Weather Index (FWI). Because a majority of these indices incorporate multiple types of parameters (i.e. meteorological, vegetation, and topographical variables) (see Table 2.1 for more information), the first step of this study involved demonstrating which variables are strongly influenced by meteorological parameters in this region. In order to assess if certain meteorological data have a dominant effect on the fire indices, correlations were calculated between each index and the meteorological parameters utilized (temperature, precipitation, wind speed, and humidity) during the fire “season”, April 1 – November 1. Correlation coefficients were computed for each individual station and then compiled into a “mean” correlation table (Table 2.3).

Temperature was positively correlated with all fire indices, while daily precipitation and relative humidity were negatively correlated with each fire index. Wind speed was the

only meteorological parameter that showed mixed correlation between different indices, with some showing strong positive correlation (i.e. the FFWI) and others showing a weak negative correlation (i.e. the KBDI). On average, relative humidity showed the strongest correlation with all fire indices ( $R^2 = -0.37$ ), temperature showed the second strongest correlation ( $R^2 = 0.29$ ), followed by precipitation ( $R^2 = -0.25$ ) and wind speed ( $R^2 = 0.14$ ). Averages of meteorological correlation coefficients (based on absolute values) for each fire index varied from 0.14 (RSI) to 0.44 (FFWI).

### **2.3.3 Comparison of Fire Indices to Lagged Meteorological Variables**

In order to examine any autocorrelations, or “legacy” effects, from meteorological variables on each fire index, indices were compared to meteorological data averaged on different timescales – daily, weekly (7 days), bi-weekly (14 days), and monthly (30 days), and seasonal (90 days) moving averages. Out of the 13 fire indices, three showed any indication of a lag effect on the variable. KBDI, DMC, and DC all demonstrated stronger correlations with temperature and precipitation on monthly to seasonal time scales than on daily to weekly averages (Tables 2.4 a – c). This possibly indicates that longer-term trends in temperature and precipitation have a substantial effect on these three fire indices.

### **2.3.4 Comparison of Fire Indices to Eachother**

Correlations between each fire index was done to demonstrate any “grouping” of fire indices, or if there is any fire index that could be representative of other indices (Table 2.5). Several of the indices – KBDI, DMC, DC, and BUI – are highly correlated

( $R^2 > 0.67$ ), which indicates that these longer-term indices show similar patterns throughout the records.

## **2.4 Discussion**

### **2.4.1 Selection of Fire Risk Indices for Regional Analysis**

One of the primary goals of the work presented in this chapter has been to assess which fire index can best be used to interpret fire risk in the region using meteorological data in recent times, and also using climate model data for extrapolating fire risk throughout the remainder of the 21<sup>st</sup> century (see Chapter 3). To find which fire index could be utilized to interpret regional fire risk, results from the analyses listed above were taken into consideration. First, we can gain insight into which fire indices are best reconstructed using only meteorological data (as opposed to topographical or ecological variables). When correlating temperature, relative humidity, precipitation, and wind speed with each index, the FFWI seems to be most influenced by meteorological parameters ( $R^2 = 0.44$ ). However, it should be noted that while relative humidity and wind speed do influence fire activity and risk, these variables have much larger error in models projecting future activity as opposed to temperature and precipitation trends.

When average correlations are computed without including humidity or wind speed, a handful of fire indices have much higher correlation coefficient values with meteorological parameters. In particular, the five indices with strongest correlation to meteorological data (temperature and precipitation) are the KBDI, BUI, DMC, DC, and FFMC ( $R^2 = 0.54, 0.61, 0.68, 0.68, \text{ and } 0.84$ , respectively). Furthermore, increased understanding of trends in climate model data can be obtained when looking at longer-

term trends (monthly to seasonal) in temperature and precipitation. We find that three indices – the KBDI, DMC, and DC – all increase in correlation strength with longer-term variability in meteorological data. Finally, these three indices seem to track each other as well (Table 2.5), indicating that these all can be used to assess fire risk for the region. In particular, the KBDI will be used in the remainder of this study due to the reasons listed above, the widespread use and popularity of the KBDI in the NEUS and southeastern US (Burgan 1988), and the simplicity of the index (which only includes meteorological variables and assumes all other topographical and ecological parameters are fixed).

#### **2.4.2 Fire Risk vs. Fire Occurrence**

With the selection of the KBDI as a representative fire index based on the previously mentioned work, a comparison can be done to see how “well” the KBDI performs at tracking fire occurrence in the region. Max yearly KBDI and average yearly (April 1 – November 1) KBDI values were reconstructed from the Gardiner, ME station dataset and compared to Maine wildfire data (number of fires per year, acres burned per year) (Figure 2.4). This station was chosen due to the completeness of record, its location within the state of Maine, and its length of record. Both maximum and average KBDI values seem to correlate well with number of fires per year ( $R^2 = 0.26$  and  $0.32$ , respectively), particularly in the “extreme” fire risk years (e.g. the late 1940’s, 1965, and 2016). Weaker correlation exists between acres burned and maximum and average KBDI values, however ( $R^2 = 0.06$  and  $0.13$ ). This difference between acres burned and number of fires per year could likely be caused by human disturbance and fire suppression activities across the state. Regardless, the correlation strength between the KBDI and fire occurrence gives promise for the KBDI being used as a representative index of fire risk in

this study.

Reconstructed KBDI values can also be used to identify any shifts or variability in the fire season throughout the record (Figure 2.5). A shift in the timing of the fire season, beginning approximately in 1980 and continuing through recent years, can be seen superimposed on the annual variability of the record. However, interpretation of this shift is difficult due to the lack of longer-term data sets, which would be necessary to see if this is within the realm of natural variability of the fire season.

## **2.5 Conclusions**

Analysis of a suite of fire risk indices reconstructed from meteorological observations across the NEUS revealed that certain indices performed better at tracking fire risk and fire occurrence in the region than others. In particular, the KBDI was shown to strongly correlate with fire occurrence, particularly in the “extreme” years seen throughout the period of record. Furthermore, the KBDI was shown to be dominantly influenced by precipitation and temperature, as opposed to wind speed, relative humidity, or other ecological and topographical parameters, indicating that this index can be reliably reconstructed using precipitation and temperature data without taking into account variations in other parameters. The fire risk “season”, as reconstructed using the KBDI, fluctuates on multi-year timescales, with certain years (e.g. 1947) having high fire risk late in the season (through October), correlating with large, statewide wildfire outbreaks. Finally, the fire season appears to have shifted earlier throughout the late 20<sup>th</sup> century, with most years having season end dates in late August by the beginning of the 21<sup>st</sup> century (with the exception of the 2 most recent years). Based on the current time

scale of record, it remains unclear if this trend is within the realms of natural variability, or if this trend will continue into the future.

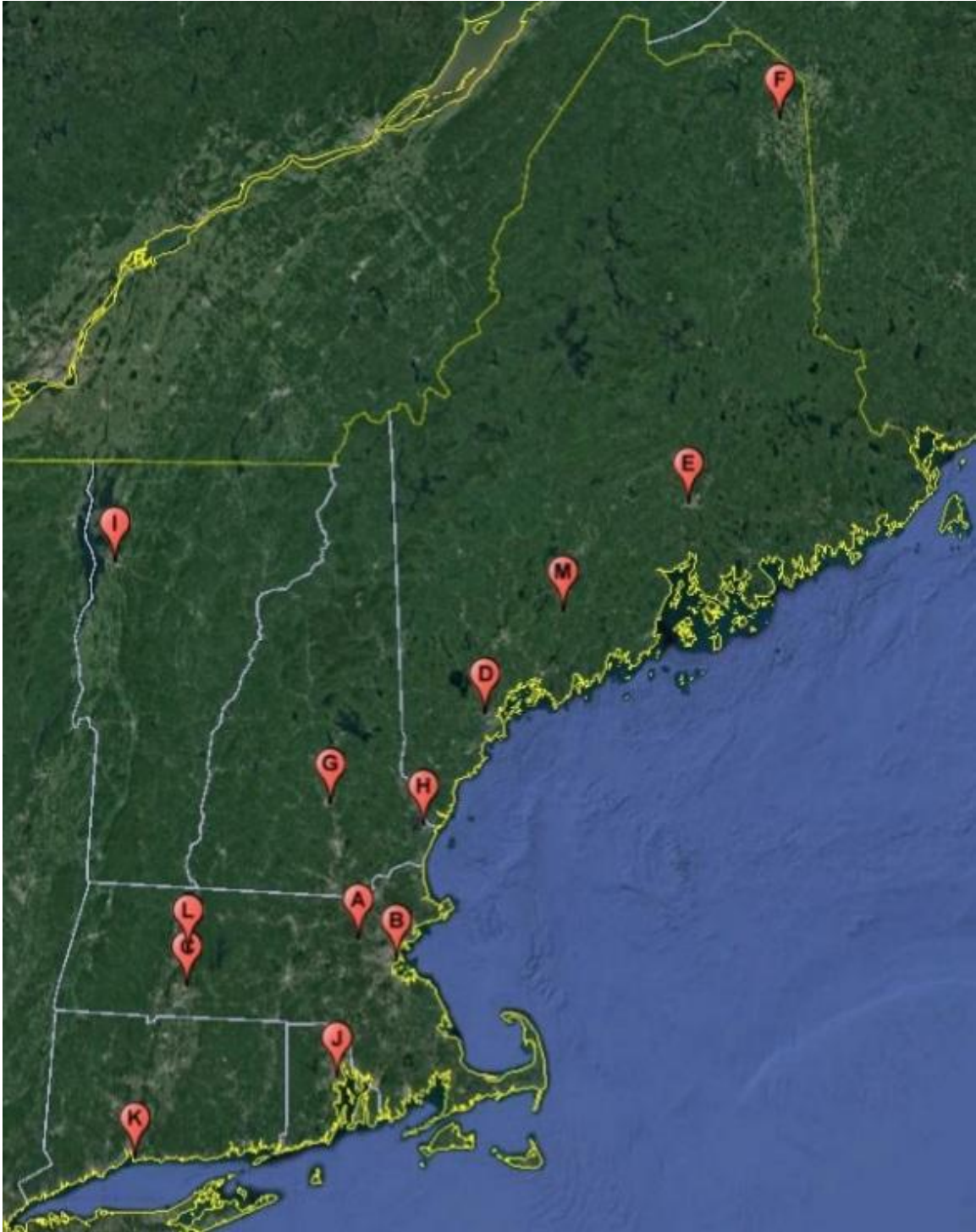


**Figure 2.1: Map of Northeastern U.S. meteorological stations used in this study. A) Bedford, MA; B) Boston, MA; C) Westover, MA; D) Portland, ME; E) Bangor, ME; F) Caribou, ME; G) Concord, NH; H) Pease, NH; I) Burlington, VT; J) New Haven, CT; K) Providence, RI; L) Amherst, MA; and M) Gardiner, ME. More information on each site can be found in table 2.2.**

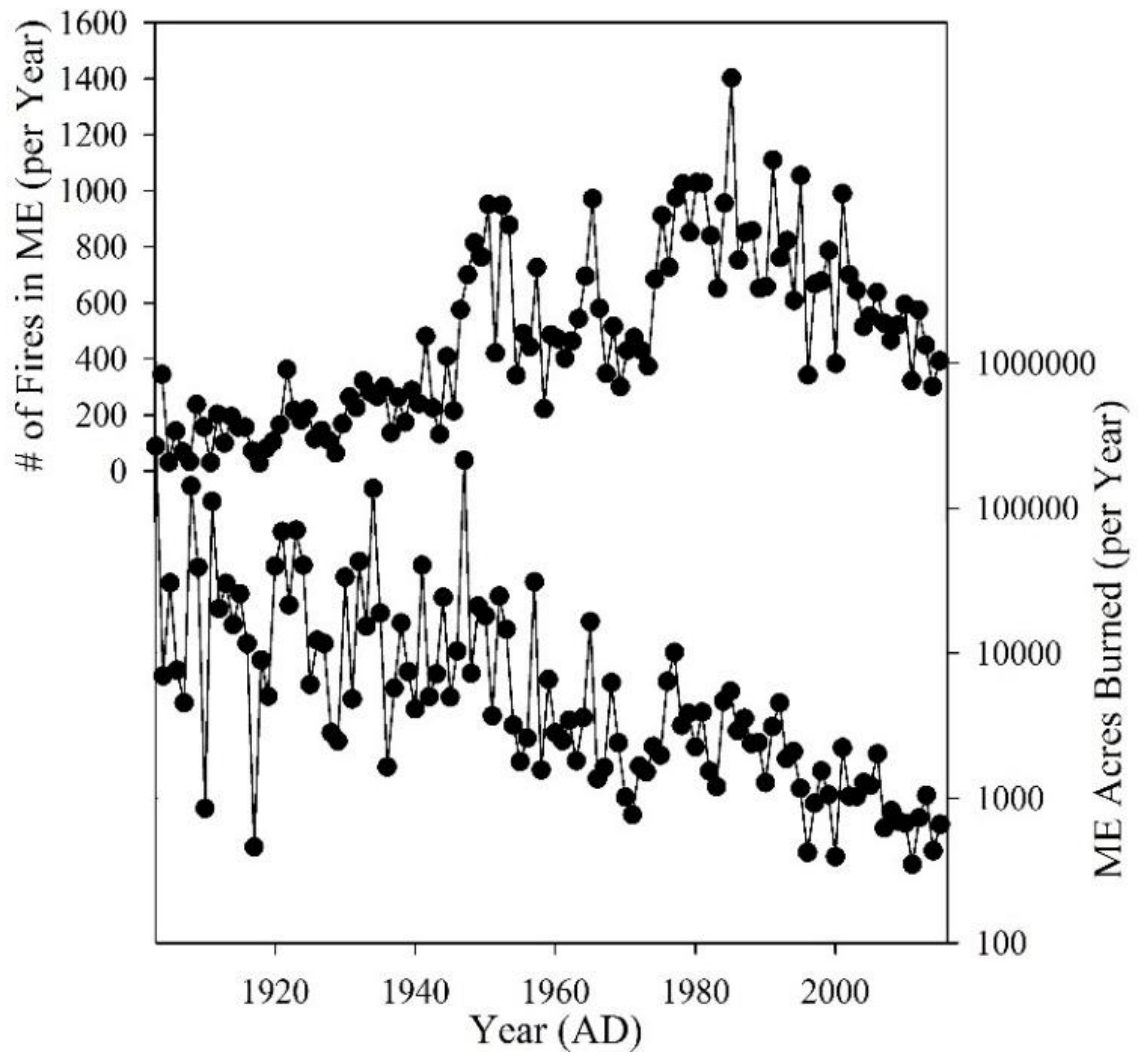


**Figure 2.2: Fire Occurrence Data for the state of Maine from 1900 – 2017. A) number of fires each year, and B) total acres burned each year.**

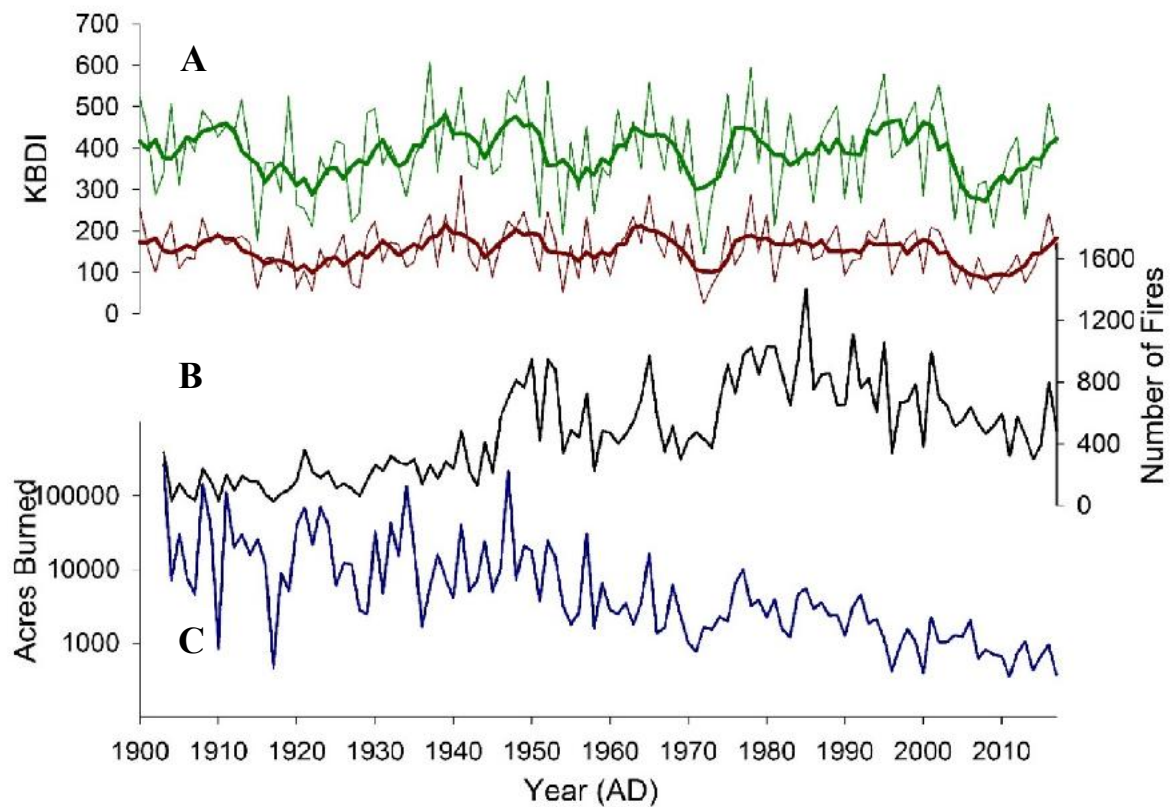


**Figure 2.3: A) Comparison of max yearly KBDI (gray) and average yearly KBDI (red), B) number of fires in the Maine (black), and C) total acres burned in Maine (blue). Bolded KBDI lines are 5 year running averages. Note that in extreme years, KBDI tracks fire occurrence (e.g. early 1970s, mid 1960s) reasonably well.**

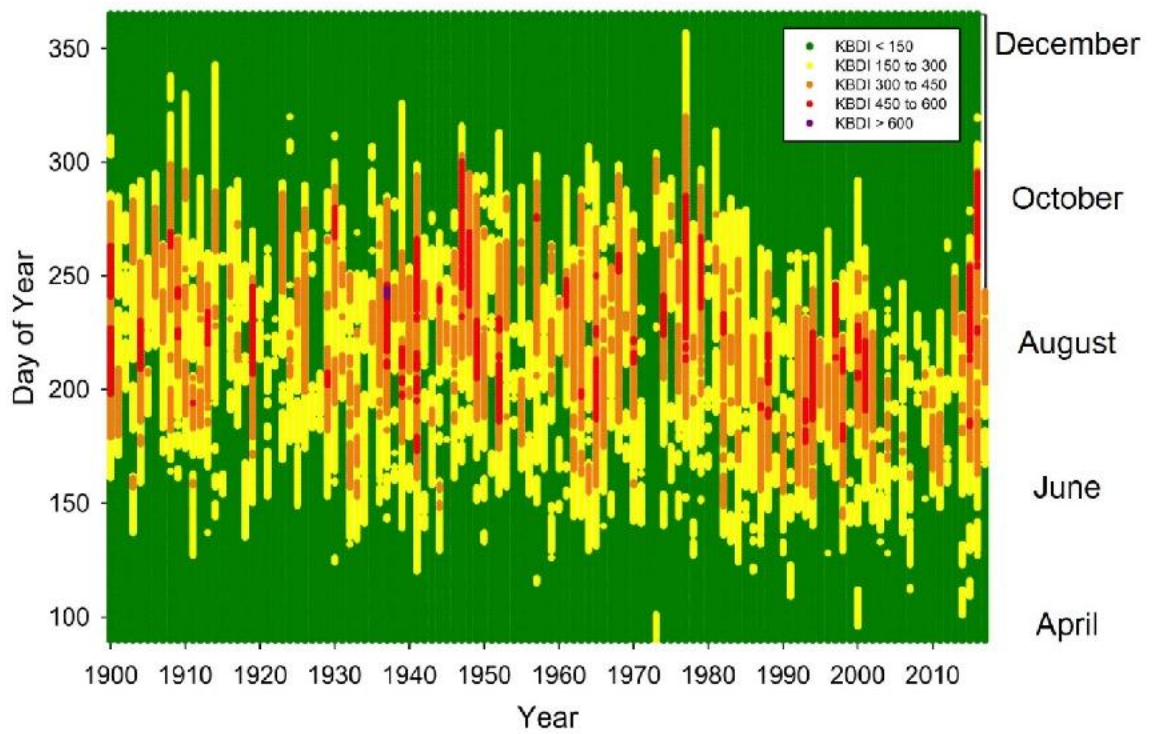


**Figure 2.4: the “fire season”, as seen from the KBDI throughout the year from 1900 – 2017 from Gardiner, ME. Note the key in the top right corner, indicating the color of the daily KBDI values. A shift in timing of the fire season can be seen from the late 1970’s through present day.**

<b>Index</b>	<b>Abbrev.</b>	<b>Parameters</b>	<b>Reference</b>	<b>Summary</b>
Fine Fuel Moisture Code	FFMC	P, W, T, RH	Van Wagner 1985	An index of flammability (as most fires are started in the fine fuels). The FFMC tracks changes in the moisture content of fine-scale fuel, and therefore varies on short time scales.
Duff Moisture Code	DMC	P, T, RH	Van Wagner 1985	Index describing the intensity of a fire already started. Tracks longer-term changes in moisture content of available fuels.
Drought Code	DC	P, T	Van Wagner 1985	Sensitive to seasonal drought, so it becomes an important index which can predict underground (creeping or smoldering) fires.
Fuel Moisture Build-Up Index	BUI	DMC, DC	Van Wagner 1985	Modifies spread rates to account for longer weather time lags than the FFMC (i.e., 10-day time lag).
Initial Spread Index	ISI	FFMC, W	Van Wagner 1985	Incorporates wind speed as a factor into the FFMC to estimate the potential initial spread of a fire.
Fire Weather Index	FWI	FFMC, DMC, DC, ISI, BUI, and FWI	Van Wagner 1985	Incorporates all other CFFWIS indices into one final index to describe a region's fire risk.
Initial Rate of Spread	RSI	ISI, Vegetation	Van Wagner 1987	Similar to the ISI, but includes fuel type into the ISI.
Spread Component	SC	W, Location	Deeming et al. 1972	Index describing the predicted forward rate of spread at head of fire (in feet/min). For example, a SC=30 means that a fire should progress at 30 ft per minute. SC is sensitive to wind speed, and moderately sensitive to slope especially if fuel is dry.
Energy Release Component	ER	P, T, RH, Vegetation	Deeming et al. 1972	Related to the available energy per unit area within the flaming front at the head of the fire. Estimates the amount of heat released from when the head enters and exits a burning area. As live fuels cure and dead fuels dry, the ER increases. This index is essentially a reflection of drought conditions. ER is not affected by wind, so reasonably stable on short timescales.

Burning Index	BI	W,SC,ER, wind	Deeming et al. 1972	<p>Related to the contribution of fire behavior to the effort of containing a fire. Derived from a combination of SC and ER, so strongly effected by wind speed, varies considerably day to day. BI values represent the near upper limit to be expected if a fire occurs in the worst fuel, weather and topo conditions for this fuel type.</p> <p>A rating of the probability that a firebrand will cause a fire requiring suppression. IC ranges from 0 (no firebrand would cause an actionable fire) to 100 (all firebrands would cause an actionable fire if it contacts fuel). IC is the probability of a fire starting and the potential of fire spread.</p>
Ignition Component	IC	P,T,W,RH,FT, SC	Deeming et al. 1972	<p>A drought index specifically designed for fire potential assessment in the eastern US. Can be used to measure the effects of seasonal drought on fire potential.</p> <p>Estimates the net effect of evapotranspiration and precipitation in producing cumulative moisture deficiency in deep duff and upper soil layers, and relates to the flammability of organic material on the ground. In the United States, values range from 0 (soil moisture is high, little to no fire risk) to 800 (severe drought, extreme fire risk; live fuels can be expected to burn actively), measured in hundredths of an inch. This index is especially used in fire control, where flammability of organic rich soils becomes an issue in having successful firelines as an effective barrier for wildfires in the eastern U.S. During extreme drought, this index tracks the intensity of fire if started (i.e., fires may crown more easily). Reduction in index occurs only when rainfall exceeds 0.20 inches. The purpose of the KBDDI is to provide managers with a tool for estimating deep-drying conditions for fire suppression and control practices.</p>
Keetch-Byram Drought Index	KBDDI	P,T, latitude	Keetch & Byram 1968	

Fosberg Fire Weather Index	FFWI	T, W, RH	Fosberg 1978	Simplified fire index based only on equilibrium moisture content and wind speed, transformed to combustion efficiency. Assumes constant fuel (example: vegetation = all grass). Used previously to assess potential for seasonal fire danger forecasting. Max of 100 (moisture=0, wind=>30mph), min of 0.
modified Fosberg Fire Weather Index	FFWIm	FFWLP, KDBI	Goodrick 2002	Updated version of the Fosberg index to include a drought component (KBDD) to look at a "fuel availability factor" (FAF).
Haines Index	HI	T, RH, Atmospheric Parameters	Haines 1988	A lower atmosphere severity index used indicate potential for fire growth by the stability and dryness of the air over a fire. Has been shown to be correlated with large fire growth and on initiating fires where surface winds do not dominate fire behavior. Values range from 2 (moist, stable airmass) to 6 (dry, unstable airmass).
Fire Potential Index	FPI	Vegetation	Burgan 1998	A moisture-based vegetation flammability indicator. The FPI provides relative moisture of fuel flammability for a region, not the chance a large fire occurs. Function of live greenness as a proportion of max greenness.

**Table 2.1: A list of widely-used fire indices in North America. Primary parameters are the main variables in each index, and include P (precipitation amount), T (temperature), W (wind speed/direction), RH (relative humidity), FT (fuel type), Veg (Other vegetation parameters), Loc (Other location parameters), and Atm (other atmospheric parameters).**

	<b>Station Name</b>	<b>State</b>	<b>POR (Yr)</b>
A	Bedford - Hanscom Fld Apt	MA	70
B	Logan International Apt	MA	73
C	Westover Air Force Base	MA	75
D	Portland International Apt	ME	68
E	Bangor International Apt	ME	72
F	Caribou Municipal Apt	ME	68
G	Concord Municipal Apt	NH	67
H	Pease International Tpt	NH	60
I	Burlington International Apt	VT	59
J	Tweed-New Haven Apt	RI	67
K	Providence-Green Apt	CT	64
L	Amherst	MA	124
M	Gardiner	ME	131

**Table 2.2: List of selected meteorological stations with period of record (POR) length given in years. Locations of each station can be viewed in Figure 2.1.**

<b>Index</b>	<b>Temperature</b>	<b>Relative Humidity</b>	<b>Precipitation</b>	<b>Wind Speed</b>	<b>Average</b>
<b>FFWI</b>	0.23	-0.72	-0.18	0.72	0.44
<b>KBDI</b>	0.53	-0.03	-0.33	-0.10	0.25
<b>SC</b>	0.27	-0.41	-0.17	0.42	0.32
<b>ERC</b>	0.08	-0.75	-0.35	0.04	0.33
<b>BI</b>	0.25	-0.52	-0.24	0.20	0.33
<b>IC</b>	0.13	-0.71	-0.25	0.27	0.34
<b>FFMC</b>	0.17	-0.58	-0.67	-0.01	0.36
<b>DMC</b>	0.46	-0.21	-0.22	-0.07	0.22
<b>DC</b>	0.48	-0.03	-0.20	-0.11	0.15
<b>ISI</b>	0.15	-0.31	-0.18	0.41	0.24
<b>BUI</b>	0.38	-0.17	-0.23	-0.09	0.22
<b>RSI</b>	0.32	-0.05	-0.11	-0.08	0.14
<b>FWI</b>	0.29	-0.27	-0.19	0.23	0.24
<b>Average</b>	0.29	-0.37	-0.25	0.14	

**Table 2.3: Mean correlations between all fire indices and meteorological variables from April 1 through November 1, as well as the average correlations for each index (based on the absolute value) and for each weather variable.**

A) KDBI	Daily	7 Day	14 Day	30 Day	90 Day
Temperature	0.529	0.541	0.565	0.590	0.592
Relative Humidity	-0.028	-0.053	-0.051	-0.038	-0.039
Precipitation	-0.329	-0.345	-0.432	-0.478	-0.479
Wind Speed	-0.102	-0.142	-0.152	-0.15	-0.135

A) DMC	Daily	7 Day	14 Day	30 Day	60 Day
Temperature	0.463	0.525	0.556	0.587	0.623
Relative Humidity	-0.213	-0.19	-0.168	-0.139	-0.132
Precipitation	-0.219	-0.38	-0.402	-0.369	-0.414
Wind Speed	-0.074	-0.092	-0.096	-0.087	-0.056

A) DC	Daily	7 Day	14 Day	30 Day	60 Day
Temperature	0.484	0.535	0.617	0.640	0.643
Relative Humidity	0.026	-0.008	-0.002	0.0011	-0.022
Precipitation	-0.204	-0.326	-0.411	-0.469	-0.487
Wind Speed	-0.107	-0.174	-0.124	-0.127	-0.126

Table 2.4: Mean correlations between moving averages of lagged meteorological variables from April 1 - November 1, and daily values of the a) KBDI, b) DMC, and c) DC fire indices.

	SC	ERC	BI	KBDI	IC	FFMC	DMC	DC	ISI	BUI	RSI	FWI
<b>ERC</b>	0.79											
<b>BI</b>	0.96	0.87										
<b>KBDI</b>	0.39	0.41	0.46									
<b>IC</b>	0.80	0.85	0.88	0.31								
<b>FFMC</b>	0.35	0.63	0.46	0.34	0.48							
<b>DMC</b>	0.43	0.52	0.50	0.67	0.40	0.44						
<b>DC</b>	0.40	0.41	0.46	0.95	0.30	0.29	0.68					
<b>ISI</b>	0.14	0.10	0.12	0.04	0.15	0.13	0.07	0.02				
<b>BUI</b>	0.44	0.51	0.51	0.77	0.39	0.42	0.98	0.79	0.06			
<b>RSI</b>	0.41	0.42	0.42	0.33	0.43	0.41	0.48	0.30	0.83	0.46		
<b>FWI</b>	0.19	0.12	0.15	0.10	0.17	0.10	0.14	0.07	0.93	0.13	0.86	
<b>FFWI</b>	0.48	0.54	0.49	-0.02	0.61	0.44	0.13	0.02	0.49	0.08	0.61	0.44

Table 2.5: Mean correlations between fire indices from April 1 - November 1.

## CHAPTER 3

### MODELING FIRE RISK IN THE NORTHEASTERN UNITED STATES FROM 1950 – 2100 AD: LARGE INCREASES IN FIRE RISK PROJECTED FOR THE NEUS

#### 3.1 Introduction

Understanding how future fire risk will change with respect to anthropogenic global warming is a critical question for the fire-science community. Furthermore, anticipated changes with fire risk pose both social and economic risk in heavily populated regions of the world such as the Northeastern United States (NEUS), with direct (infrastructure, property, and loss of life) and indirect (forest composition, ecosystem impacts, and carbon sequestration) consequences occurring with increased wildfire activity (Gould et al., 2013; Hunter-Kerr & DeGaetano, 2018). Therefore, it is imperative to accurately assess various aspects of fire risk with anticipated climate change. Past research has primarily focused on seasonal to multi-seasonal forecasts of fire risk in select regions of the world (i.e. the Western U.S.) (Roads et al. 2005). Recent studies are projecting fire risk trends into the future through the use of Regional Climate Models (RCMs) and General Circulation Models (GCMs) (Liu et al 2013). However, these studies primarily focus on current fire-prone regions like the Western U.S. or on global scales (Scholze et al., 2006; Krawchuk et al., 2009; Liu et al., 2010; Moritz et al., 2012; Tang et al., 2015; Wang et al., 2015), and have only been conducted in the NEUS over the past year (Hunter-Kerr & DeGaetano, 2018).

One common theme in these studies is the approach in which future fire trends are projected. The most popular methods used include (1) predicting fire occurrence through statistical relationships between historical fire variables and atmospheric conditions (Liu

et al. 2013) and (2) through vegetation modeling using dynamic global vegetation models (DGVMs) (Levis et al. 2004, Tian et al. 2010). Another approach to predicting fire trends into the future is utilizing fire indices to quantify fire risk, such as the Haines Index (Tang et al., 2015), and the Canadian Forest Fire Weather Index System (CFFWIS) (Wang et al., 2015; Hunter-Kerr & DeGaetano, 2017). However, most of these past studies have been focused on the U.S. as a whole (Tang et al. 2015) and have been performed using coarse model resolution (Wang et al. 2015). In a study by Hunter Kerr and DeGaetano (2017), fire risk was estimated using the CFFWIS for the NEUS through employing regional climate models dynamically downscaled from the Coupled Model Intercomparison Project (CMIP5). This study found that overall fire risk, as estimated from the FWI of the CFFWIS, will increase in the NEUS throughout the 21<sup>st</sup> century. However, there are several limitations to the CFFWIS. This index in particular was developed and tested in regions dominated by boreal forest ecosystems, making its application to the NEUS questionable, as this region is comprised of several forest types and ecosystems. Due to inherent differences in fire risk indices and their outputs (see Chapter 2 for more detailed descriptions), selecting appropriate indices is a necessary step to accurately quantify and interpret regional fire risk into the future. Furthermore, few of these studies attempted to calibrate their modeled fire risk using historical data to see how accurately (or inaccurately) fire indices can be estimated using climate model output. Overall, little work has been done to understand trends in fire risk in the NEUS over the remainder of the 21<sup>st</sup> century through the use of fire risk indices estimated from downscaled climate data.

This study employs the Keetch Byram Drought Index (KBDI) to assess climatic fire risk in the NEUS. Quantification of the KBDI was performed using the most recent set of coordinated climate model intercomparison experiments (CMIP5), relying on the Coordinated Regional Climate Downscaling Experiment (CORDEX) to provide dynamically downscaled regional scenarios for the NEUS (Giorgi et al., 2009). Prior to regional analysis, four case studies were chosen throughout the region in order to assess the accuracy of the modeled versus observed KBDI at different locations with varying climate averages and historically normal ranges of KBDI. Finally, projected changes in fire risk for the region were estimated throughout the 21<sup>st</sup> century using the KBDI and compared to results from past studies (Hunter-Kerr & DeGaetano, 2018).

## **3.2 Methods and Data Analysis**

### **3.2.1 Estimating Fire Risk Using the Keetch Byram Drought Index**

Daily fire risk for the NEUS was calculated using the Keetch Byram Drought Index (KBDI), a numerical index for estimating the moisture content of upper soils (i.e., litter and duff) (Keetch and Byram, 1968). In locations with deep upper soil layers, such as the NEUS, the dryness of these fuels in the upper layers is an important factor in fire risk and suppression activities. When dry (i.e., a high KBDI), these fuels can make fire suppression extremely difficult, as fire lines tend to fail more readily and creeping fires are difficult to extinguish (Keetch and Byram, 1968). Furthermore, under times of extreme drought, high KBDI values are correlated with increased risk in fires with increased severity and in crowning fires (Keetch and Byram, 1968; see Chapter 2 for more details). Therefore, in the NEUS where deep duff layers dominate the landscape,

the KBDI can be an important tool used by fire managers in planning fire suppression activities.

### **3.2.2 Analysis of Climate Model Data**

Similar to methods used by Hunter Kerr & DeGaetano (2018), fire risk was estimated in this study using climate data obtained from Localized Constructed Analogs (LOCA)-derived daily RCMs that have been dynamically downscaled by a subset of GCMs from Phase 5 of the Coupled Model Intercomparison Project (CMIP5) (Taylor et al., 2011; Pierce et al., 2014).

#### **3.2.2.1 Downscaling Methods**

Downscaling, which is a method for taking information at large scales (i.e. global scale) and forecasting at small scales (i.e. local scales), can be done with either a dynamical or statistical downscaling approach. Statistical downscaling, which finds statistical relationships between climate variables and atmospheric conditions and applies them to GCM outputs, often fail to capture daily ranges or extremes in climate variables (Karmalkar, personal communication). Dynamical downscaling using high-resolution climate models on a regional scale, then “fine tunes” the output using observational data or low resolution climate model output as boundary conditions (UCAR, 2016). While more computationally extensive than statistical downscaling, studies have typically used dynamical downscaling as the method to extract sub-regional climate data for future fire trend analysis (Liu et al. 2013). Models used in this study were downscaled using the LOCA technique, developed to help address some of the issues that arise with statistical downscaling (Pierce et al., 2014). LOCA-derived climate data is available for the

continental US at a higher resolution (1/16 degree grid box) and on a daily time scale for scenarios incorporating RCP 4.5 and 8.5 (Pierce et al. 2014) Finally, the COordinated Regional Climate Downscaling EXperiment (CORDEX) provides dynamically downscaled reanalyses, historical simulations, and future projections of regional climate scenarios for North America (Giorgi et al., 2009).

### **3.2.2.2 Representative Concentration Pathways (RCPs)**

To better understand the complex interactions between climate, ecosystems, human activities, and nature, different future scenarios have been developed to provide possible portrayals of how the future climate might change. These scenarios help evaluate how future climate may vary given uncertainty in human activities, levels of future emissions, and mitigation efforts of emission reduction (Moss et al., 2010). Past sets of scenarios, such as IS92 scenarios (Leggett et al., 1992) and SRES (Nakicenovic et al., 2000) have been utilized for this purpose, but did not explore the adoption of various climate policies in the future (Moss et al., 2010). Therefore, the most recent set of scenarios – the Representative Concentration Pathways (RCPs) – were developed to address this issue, and provide four possible emission trajectories with different end-of-century (2100 AD) radiative forcing target levels (van Vuuren et al., 2011).

The four scenarios developed include one pathway with maximum mitigation efforts, resulting in very low radiative forcing by 2100 AD (RCP 2.6), two medium (emission stabilization) scenarios (RCP 4.5 and RCP 6), and one high emission scenario where emission production continues as-is through the 21<sup>st</sup> century (RCP 8.5) (van Vuuren et al., 2011).

In this study, RCP 4.5 and 8.5 were used to capture a range of future regional fire risk in the NEUS under different emission and mitigation pathways. Traditionally, only RCP 8.5 has been utilized in studies quantifying future fire risk, due to the fact that current trends in global emissions show yearly increases similar to those estimated in RCP 8.5 (i.e. Le Goff et al., 2009; Clarke et al., 2011; Hunter Kerr and DeGaetano, 2018). However, in order to capture a better range of climate uncertainty and to estimate if fire risk changes with different variations in climate, climate data run under RCP 4.5 emissions was also used in KBDI calculations.

### **3.2.2.3 Selection of RCMs for Ensemble Model**

Generally, one of the biggest issues in climate change impact studies at the regional (or sub-regional) level is the computational time and cost of utilizing the large number of available GCMs (Karmalkar et al., 2018). Therefore, selecting a subset of models that accurately captures the variability in uncertainty in the climate projections and that perform well in the region is an important first step in regional climate impact assessments (Barsugli et al., 2013; Snover et al., 2013; Karmalkar et al., 2018).

Selecting a subset of climate models for analysis is not a straightforward process, due to the fact that GCM accuracy varies by region (Mason and Knutti, 2011) and that a selected subset might reduce the range of uncertainty seen in the model ensemble (Weigel et al., 2010). While past studies selected subsets of GCMs through assessing their accuracy in reconstructing historical climate variability (McSweeney et al., 2015; Monerie et al., 2017), recent work has attempted to develop a process-based methodology to identify which models accurately capture circulation features that drive changes in climate, so that subsets of GCMs can be identified that are credible and diverse by region

(Karmalkar et al., 2018). In a study by Karmalkar and colleagues (2018), this methodology was employed on the 36 model simulations that were used in the CMIP5 for the NEUS. Overall, 22 of the 36 models were eliminated from the ensemble without reducing model performance or the range of uncertainty in projections. The authors concluded that the subset selection process of these remaining 14 models must focus on retaining the amount of uncertainty sampled in the 36 model ensemble while still providing diverse climate scenarios (Karmalkar et al., 2018).

This study utilizes 5 of the 14 CMIP5 models found to be “best performing” by Karmalkar et al. (2018): (1)bcc-csm1-1, (2)GFDL-ESM2M, (3)GISS-E2-R, (4)HadGEM2-CC, and (5)HadGEM2-ES (Karmalkar et al. 2018). These five models were chosen for this analysis for several reasons. First, these models capture the range of uncertainty of the ensemble for the NEUS in both temperature and precipitation variability (Figure 3.1). For bcc-csm1-1 and GFDL-ESM2M, these were both found to have “good” overall performance (models that ranked in the top half of the 36 models for all 4 sets of performance metrics utilized by Karmalkar and colleagues) and essential for capturing the range of uncertainty (Karmalkar et al. 2018). GISS-E2-R and HadGEM2-CC are “mixed” in performance, but are essential due to the range of uncertainty of projections in the ensemble model. For instance, HadGEM2-CC projects large increases in temperature and precipitation in all seasons. Finally, HadGEM2-ES, while having “mixed” performance, is designated essential due to its pre-existing use and downscaling in the CORDEX project (Karmalkar et al., 2018).

It is important to note that in an ideal world, all 14 models deemed “essential” would be retained and used in the ensemble. However, due to time constraints and costs,

the 5 models listed above were selected in order to accurately estimate future climate projections for the NEUS, while preserving the range of uncertainty in the 36 model ensemble of the original CMIP5 project. Nevertheless, this methodology of using a 5 model ensemble was tested for a small region of the NEUS against using the 14 member ensemble found to be essential in Karmalkar and colleagues (2018). Both the 5- and 14-member ensembles were extremely similar with minimal differences in projected changes. Therefore, the 5-model ensemble has been utilized to estimate fire risk for the NEUS.

### **3.2.3 Case Study Site Selection**

In order to assess the accuracy of the model ensemble for the NEUS, four locations were chosen for analysis prior to investigating regional changes in the future. This preliminary analysis reconstructed KBDI from the modeled historical period (1950-2017 AD) and compared it to observed KBDI values for the same time period from meteorological stations (see Chapter 2). The four locations – (1)Amherst, MA, (2)Gardiner, ME, (3)Burlington, VT, and (4)Caribou, ME – were chosen to capture the range of latitudes and ecosystems found in the region. Furthermore, these locations all have virtually complete, long records (see Chapter 2 for more details), with daily records going back well prior to the start of model runs in 1950 AD. Climate data from model runs were taken at a 4x4 1/16<sup>th</sup> degree grid box centered around each meteorological station (Figure 3.2) and averaged for the gridded area prior to KBDI calculation.

### **3.2.4 NEUS Regional Projections**

Regional analysis was performed for the entire NEUS, using the methods detailed above, for the time periods 1950-2017, 2018-2058, and 2059-2099. Due to the large variability in climate and in KBDI ranges throughout the region, fire risk was also evaluated six “sub-regions” in the NEUS – Southern New England (consisting of Connecticut, Rhode Island, and Massachusetts), Vermont, New Hampshire, Southern Maine, Central Maine and Northern Maine.

## **3.3 Results and Discussion**

### **3.3.1 Evaluating Model Performance using Case Studies**

Generally, observational KBDI ( $KBDI_{obs}$ ) and modeled KBDI values ( $KBDI_{mod}$ ) for the historical period (1950-2017 AD) follow a seasonal cycle, with peak KBDI occurring in August – September (Figure 3.3a-h). Severity of the seasonal KBDI cycle increases to the south, with Amherst, MA and Caribou, ME having the highest (~300) and lowest (~100) peak KBDI values of the four studies, respectively.  $KBDI_{mod}$  consistently underestimates  $KBDI_{obs}$  at all case study sites, with the biggest discrepancy at the northern/inland sites (Burlington and Caribou). At these sites, the percent difference between modeled and observed values are as high as 50% during times with maximum KBDI values (Figure 3.4 c-d). However, at Amherst and Gardiner, the discrepancy between modeled and observed values is minimal, particularly during the NEUS “fire season” (April 1 – October 31), where percent difference stay well below 10% for the majority of the time period (Figure 3.4 a-b).

KBDI<sub>mod</sub> has a mixed performance at capturing known severe droughts in the observational records. For instance, increases in KBDI<sub>mod</sub> values at Amherst, MA, can be seen during times of severe drought including the early 1980s, 2003-2004, and 2015-2016. However, other times of known severe drought, such as the 1960's, are not apparent in the KBDI<sub>mod</sub> record (Figure 3.5a). The same holds true for Gardiner, ME, where notable severe droughts occurred in 1995, 1978, and the mid 1980s and are seen in the KBDI record (Figure 3.5b). However, at the northern stations, KBDI<sub>mod</sub> struggles to capture any historical droughts using typical KBDI scales (Figure 3.5 c-d).

All case studies show increases in average seasonal KBDI values from historical levels using both RCP 4.5 and 8.5, with the largest increases occurring in the latter half of the 21<sup>st</sup> century under RCP 8.5 (Fig 3.3 a-h). Furthermore, maximum KBDI values for all case studies increase exponentially towards the latter portion of the 21<sup>st</sup> century under RCP 8.5, while increasing linearly under RCP 4.5.

### **3.3.2 Model Reproducibility of Observed Fire Risk**

In order to interpret future regional fire risk using the KBDI with confidence, it is important to assess the accuracy of the KBDI reconstructed from the model ensemble in comparison to observed KBDI values from throughout the NEUS. While the two case studies in the southern NEUS (Amherst, MA and Gardiner, ME) seem to reproduce average seasonal observed KBDI values with precision, northern case studies from Burlington, VT and Caribou, ME have substantially underestimated KBDI values from the model ensemble (Fig 3.3). This could be caused by a variety of reasons, including (1) the accuracy of climate data obtained at high spatial resolution from the climate models,

(2) assumptions within the calculation of the KBDI, and (3) issues with observational data and measurements of climatic parameters made at meteorological stations.

### **3.3.2.1 Accuracy of Model Data**

One issue that arises in any study of future climate scenarios is how the range of uncertainty associated with the climate models is propagated throughout the data analysis. While temperature predictions can be made with more accuracy, precipitation varies much more widely among models, and is therefore more difficult to estimate with confidence (Pierce et al. 2014). One way that the modeled KBDI values are consistently underestimated in comparison to observed KBDI could be that the downscaling methods used to obtain highly resolved data for the region overpredicted precipitation. While choosing a downscaling method can be somewhat subjective, LOCA derived data reproduce absolute and relative changes in precipitation that have much smaller error (approx. 20 times smaller) than other popular downscaling methods (i.e., BCCA) (Pierce et al. 2014). Therefore, LOCA provides downscaled, highly resolved, daily climatic data with minimal error. However, it should be noted that LOCA has trouble reproducing precipitation in regions that experience very little rainfall or in mountainous regions (Pierce et al. 2014).

To test the accuracy of the LOCA downscaled precipitation and temperature, observed climate data from Caribou, ME (daily precipitation and temperature) was compared to the model ensemble and revealed that the models capture yearly historical trends reasonably well (Figure 3.12). While the ensemble fails to capture the “extreme” years, it accurately follows the multi-year trends in both precipitation and temperature,

and gives us confidence in the reproducibility of historical climate using the model ensemble.

### **3.3.2.2 Assumptions in the Calculation of the KBDI**

Several issues that are potentially producing bias in the modeled KBDI records lie within the calculation of the KBDI itself, including (1) multi-day precipitation events, (2) average annual precipitation, and (3) effects of low vs. high daily max temperatures. The first issue involves how to account for multi-day precipitation events in the KBDI. Originally, the KBDI would only be reduced when when the consecutive 2-day total precipitation exceeded 0.2 inches (Keetch and Byram, 1968). However, calculating the index becomes murkier when considering multi-day rainfall events. For example, if there are eight consecutive days of rainfall, with no 2-day totals over 0.2 inches, would this result in a reduction to the KBDI? While some managers have rightfully taken this into account and have included multi-day precipitation in the KBDI (as was done in this study), some have not (FireFamilyPlus 2016), which can lead to overestimated KBDI values. Furthermore, climate model data can exacerbate this issue, as a “drizzle effect” is a common issue with model data, where many days are estimated to have small but measurable rainfall (Pierce et al. 2014).

To test for this issue, observed and modeled daily rainfall were compared from the Caribou, ME case study. It was found that while the number of days with rainfall exceeding 0.2 inches were very similar between modeled and observed datasets (3,451 and 3,880 days, respectively), the modeled dataset had drastically more days with any measurable rainfall compared to the observed dataset (24,471 and 10,893 days, respectively). However, while this could be the reason why modeled KBDI is much

lower than observed KBDI, this same test was also performed on the Gardiner, ME case study, where modeled and observed KBDI are much closer in value. Similar results to the Caribou case study were found, indicating that this “drizzle effect”, if significant enough to cause the discrepancy between modeled and observed KBDI, would be a regional signal and not localized to the northern areas of the NEUS.

Another issue with KBDI calculations is the bracketing of “drought factors” in the KBDI into tables using average annual precipitation. The drought factor, which is how much KBDI on a given day increases due to temperature and previous day KBDI, is broken up into 5 tables based on annual precipitation – 10-19”, 20-29”, 30-39”, 40-59”, and 60+” per year (Keetch and Byram, 1968). Both northern case studies at Burlington, VT and Caribou, ME, have average annual precipitation of 36.79” and 38.54”, respectively (US Climate Data, accessed 2018). This puts these locations on the high-end of the 30-39” table, while the southern areas fall within the 40-59” table. While this could be causing the discrepancy in northern KBDI values, it is potentially problematic when looking into future scenarios where both of these cities cross the 40” per year barrier, moving them to the next bracket for calculating the KBDI. To account for this, KBDI values were reconstructed for both Burlington and Caribou using both the 30-39” and 40-59” tables. Fortunately, the effects of changing brackets were insignificant, with only a 2-3% increase in reconstructed values at each location. Nevertheless, this could be a contributing factor to the north-south discrepancy in modeled and observed KBDI and should not be overlooked.

Finally, a potentially more promising explanation for the discrepancy in the KBDI occurs when maximum daily temperatures are cooler, such as in the northern regions.

Traditionally, the KBDI is not changed when temperatures are below 50° F (i.e., “drought factor” = 0 for days with max temperature below 50° F). Furthermore, daily increases in KBDI due to high maximum temperatures are not linear, as seen in the original drought factor tables from Keetch and Byram (1968) (Table 3.1). For example, at max temperatures of 90°F, additions to the KBDI can be from 0-16, depending on the previous day’s KBDI. However, at max temperatures of 70°F, this addition reduces in range from 0-5. Due to the lower temperatures observed in the northern regions of the NEUS, this issue could be potentially important and have a substantial impact on the modeled KBDI, as the model ensemble tends to miss “extreme” years of higher temperatures when compared to the observed dataset (Fig 3.12).

### **3.3.2.3 Error in Observational Data Measurements**

When comparing modeled KBDI to observed KBDI, caution must be taken in assuming observed KBDI was calculated perfectly and methods of data measurement (i.e., max temperature) remained unchanged throughout the period of record (POR). In reality, many long-term weather stations in the NEUS have been relocated at least once during their POR, with most moves including significant changes in elevation, sun cover, or height of measurements off of the ground. The type of thermometer used has become increasingly of concern to the calculation of the KBDI. Mercury thermometers and newer thermocouple thermometers produce temperature differences of 5°F, further exacerbated by whether or not the thermometer was exposed or encased in some protective surround (Patterson, personal communication). Finally, time of daily observation has a significant effect on KBDI, as max daily temperatures are used in the calculation. While new ASOS stations record and update conditions rapidly,

measurements at old weather stations were done manually, and the timing of observations could change daily. For instance, if one observation was made at 4pm daily, “max temperature” would be listed as the temperature at 4pm, which may not necessarily be accurate.

Unfortunately, station metadata does not always reflect these changes in measurement method or relocations, concealing any apparent changes in the meteorological data due to measurement methods or station movement. At Burlington and Caribou, station movement has been well documented, and show that both stations have been relocated several times throughout their POR, sometimes up to miles in distance (NCDC, accessed 2018). However, datasets were supposedly “corrected” for these changes in location or elevation, but how they were corrected remains unknown. Furthermore, prior to ASOS station implementation at these locations, it is unknown what time measurements were taken each day. All of these factors could be contributing to bias in the observed KBDI at each location. However, it should be noted that such issues are common at many locations and not just at Burlington and Caribou, and any implications associated with observed measurements need to be considered on a case-by-case basis for the entire NEUS.

To summarize, despite these issues listed above and discrepancies between modeled and observed KBDI in the northern NEUS, modeled KBDI appears successful at reproducing average seasonal variability for most locations in the NEUS. Results from four case studies tell us that models capture observed data in all locations, and show similar trends across models and time frame, indicating a regional response in fire risk

into the future, and allow us to look at regional averages and future changes with more confidence.

### **3.3.3 Northeastern United States Regional KBDI Analysis**

Regardless of discrepancies between modeled and observed historical KBDI in northern areas of the NEUS, the overall trends in KBDI over time are the same throughout the region. Regional analysis of the entire NEUS reveals similar results to those seen in the case studies. Ensemble model runs estimate that NEUS temperature is projected to increase by 6 – 10 degrees F, while average annual precipitation increases approximately 5 inches per year (Fig 3.6). Using RCP 8.5, a 500% increase from historical levels is expected in average annual KBDI values which approach 150 by 2099 (Figure 3.6). Furthermore, a 300% increase is expected in maximum annual KBDI, with end-of-century KBDI between 400-500. Under RCP 4.5, these increases are lessened but still prominent, with 50-100% increases from historical levels for both average and maximum KBDI (Figure 3.6).

The NEUS “fire season” is also expected to substantially lengthen. Increases in KBDI are expected throughout the fire season in both RCP scenarios, with 2059-2099 September peak KBDI increasing by 300% and 100% from historical levels under RCP 8.5 and 4.5, respectively (Figure 3.7 a-b). By 2100, the region is expected to see KBDI values above historical peak KBDI for 141 days (RCP 8.5) and 90 days (RCP 4.5) (Figure 3.7). Seasonal timing of peak KBDI does not substantially change in either RCP 8.5 or 4.5 in the NEUS. Finally, year-to-year fluctuations in regional KBDI are present throughout the 1950-2099 time period (Figure 3.8a-b). However, these fluctuations grow

in severity and magnitude towards the end of the 21<sup>st</sup> century, particularly in scenarios under RCP 8.5 (Figure 8b).

Sub-regional analysis reveals a wide range of seasonal KBDI values, with highest KBDI occurring in Southern Maine and Southern New England (CT, RI, and MA), and lowest KBDI occurring in Northern Maine and Northern Vermont/New Hampshire (Figure 3.9, a-l). Furthermore, year-to-year variations in the KBDI are highly variable among sub-regions, with large-scale droughts featured in the southern sub-regions (i.e., Southern New England, Southern Maine) and almost no droughts observed in the northern region (i.e. Northern Maine) under normal KBDI ranges (Figures 10 and 11).

### **3.3.4 Fire Season Length and Severity – Implications for Fire Management**

While interpreting fire risk for the NEUS on a whole is important, sub-regional analysis highlights how variable fire risk and climate is within the NEUS. Many “fire-prone” areas exist throughout the southern NEUS and in southern Maine, with fire return intervals of less than 35 years (Figure 3.13) (LANDFIRE and MassGIS, 2013). In these locations, a regional analysis of the entire NEUS may underestimate the magnitude of change in fire risk associated with climate change, making a sub-regional analysis even more important for management decisions. Furthermore, changes in KBDI between sub-regions are on different scales, indicating the need for sub-regional analysis and interpretation.

In fire-prone areas such as southern Maine and Southern New England (CT, RI, and MA), KBDI is widespread, severe fire risk is modeled to not only appear, but become a reoccurring phenomenon in the late 21<sup>st</sup> century (Figure 10). Under RCP 8.5, these areas can expect KBDI to regularly exceed values of greater than 600 for weeks to

months from 2059-2099, conditions that are unheard of under present conditions and similar to present-day KBDI values seen in the southeastern United States under drought conditions. The “fire season” will also lengthen by months in these areas. Average KBDI is expected to stay above the maximum historical average KBDI in southern New England and Southern Maine for approximately 4 months in each location. Analysis of the entire NEUS reveals similar trends to the sub-regional analysis of the southern areas detailed above, with large increases in average KBDI towards the end of the 21<sup>st</sup> century (Figures 3.7 and 3.8). This signal has been somewhat muted by the lower KBDI averages of the northern areas, but is still a noteworthy response of fire risk to anthropogenic climate change.

It is important to note that there are limitations with using the KBDI as an indicator of fire risk. This study only focuses on *climatic fire risk* – the vulnerability of the region to wildfire due to climatic variables (i.e., temperature and precipitation). Due to the complex nature of wildfire, there are many other aspects of fire risk that are not accounted for. The KBDI does not capture the “spring” fire season, which is driven by wind, dryness, warmth, and availability of fuel, as vegetation has greened early in the year. Other fire risk factors, such as spread rates, ignition vulnerability of available fuels, or variability in fuel loads and vegetation, are not considered by the KBDI, and thus cannot be estimated in this study. However, prior studies investigating future fire risk in the NEUS have used indices attempting to incorporate these factors (i.e. Hunter-Kerr and DeGaetano, 2017), and have found similar results to this study, indicating a future increase in severity and length of the fire season in the NEUS.

In terms of fire management and suppression practices in the fire-prone sub-regions of the NEUS, increases in fire risk of this magnitude will need to be taken into account in the near future. Due to the nature of fire suppression activities (i.e. controlled burns) in these areas, fire managers will need to seriously adjust their “season” of controlled burns to address the lengthening and increased severity they will likely see in the fire season. Furthermore, as KBDI indicates the dryness of upper soil and therefore is associated with the estimated difficulty at suppressing fires already started, increases in fire suppression costs will likely go hand in hand with increases in fire risk quantified using the KBDI.

### **3.4 Conclusions**

Understanding how future fire risk will change with respect to anthropogenic global warming in heavily populated regions is a critical question for the fire-science community. Projected changes in the KBDI in the NEUS indicate that climatic fire risk will increase drastically, with end-of-century annual average and maximum KBDI values 300% and 500% above historical levels. The fire season is expected to considerably lengthen and increase in severity compared to historical levels in all locations of the NEUS, especially in the southern areas of the region. Interestingly, this substantial rise in regional fire risk is accompanied by moderate increases in annual precipitation, indicating that even with generally “wetter” conditions, evapotranspiration processes across the NEUS will grow more negative over time due to large increases in temperature. Results from this study demonstrate the likely changes that will occur with the wildfire season, requiring increased attention for both forest management and wildfire suppression activities throughout the remainder of the 21<sup>st</sup> century.

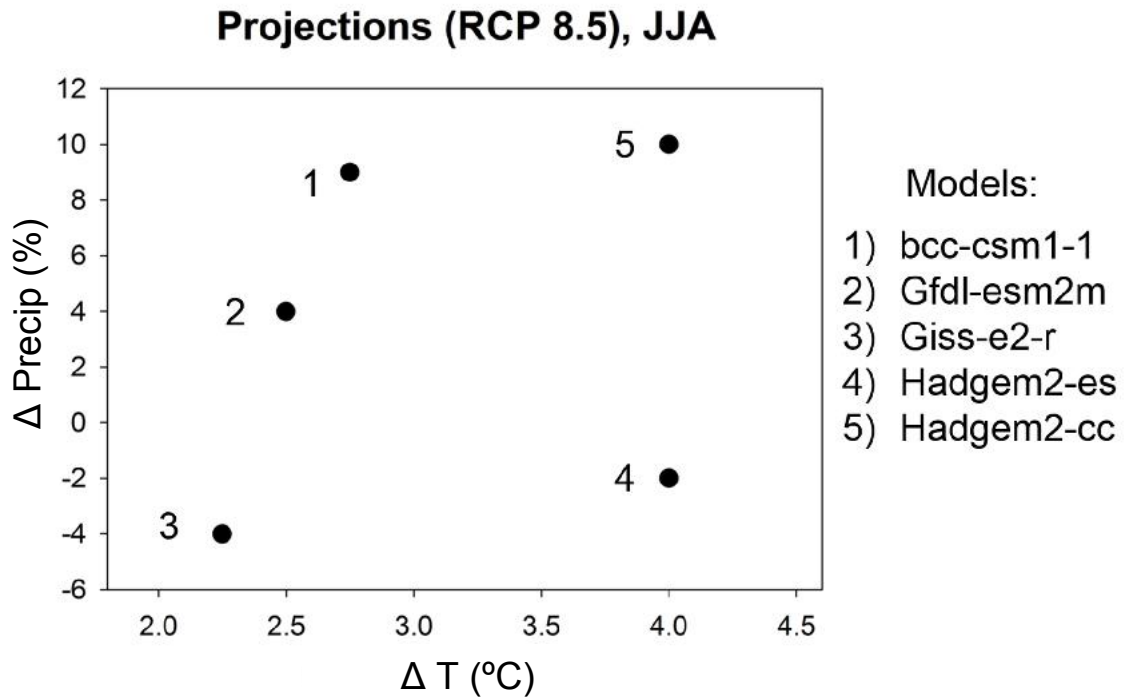


**Figure 3.1: Model Projections for percent changes in precipitation and temperature from historical averages to 2100 averages, using the 5-member ensemble used in this study. Adapted from Karmalkar et al. (2018) under RCP 8.5 scenarios for the NEUS. Due to the fact that the fire season is during the summer/fall months, the June-July-August averages were used to estimate model projections. These 5 models capture the range of uncertainty in model projections for the NEUS.**

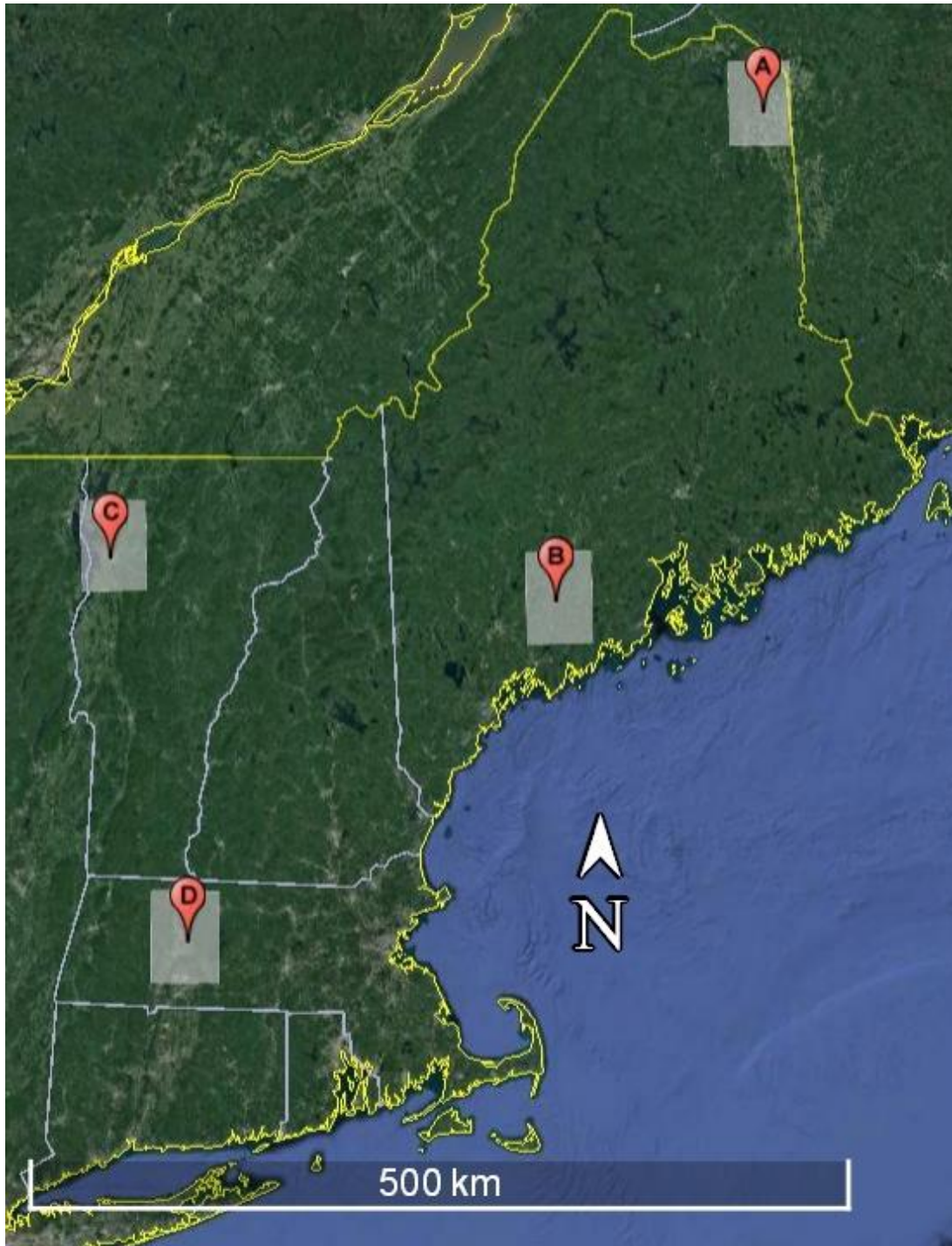


**Figure 3.2a: Map of the NEUS, with 4 case studies indicated: A) Caribou, Maine, B) Gardiner, Maine, C) Burlington, Vermont, and D) Amherst, Massachusetts. White shaded boxes represent the area used in model projections for comparison to observed station data.**

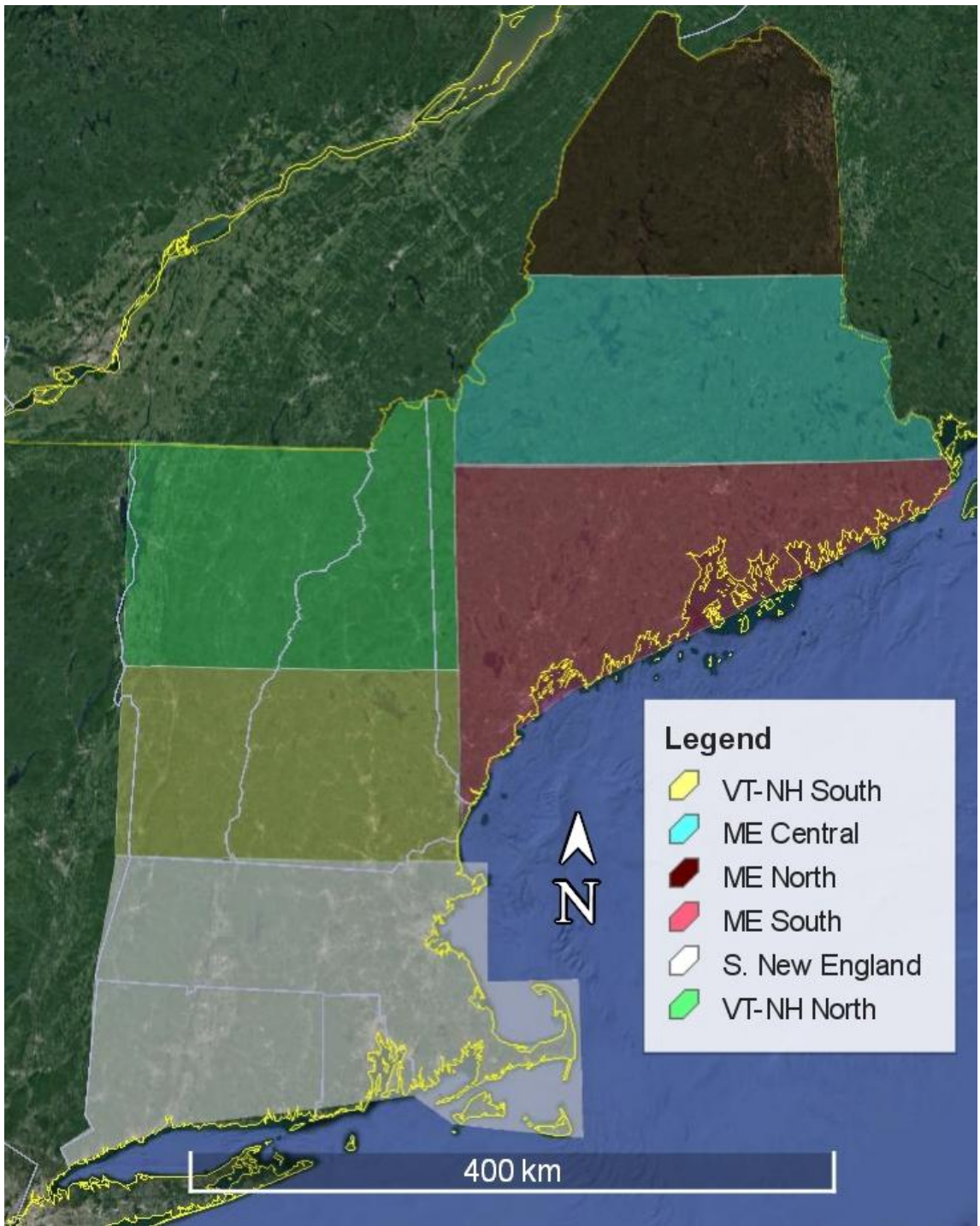


**Figure 2b: Map of the NEUS with subregions defined – Southern New England (white), Southern Vermont/New Hampshire (yellow), Northern Vermont/New Hampshire (green), Southern Maine (Red), Central Maine (light blue), and Northern Maine (Brown).**

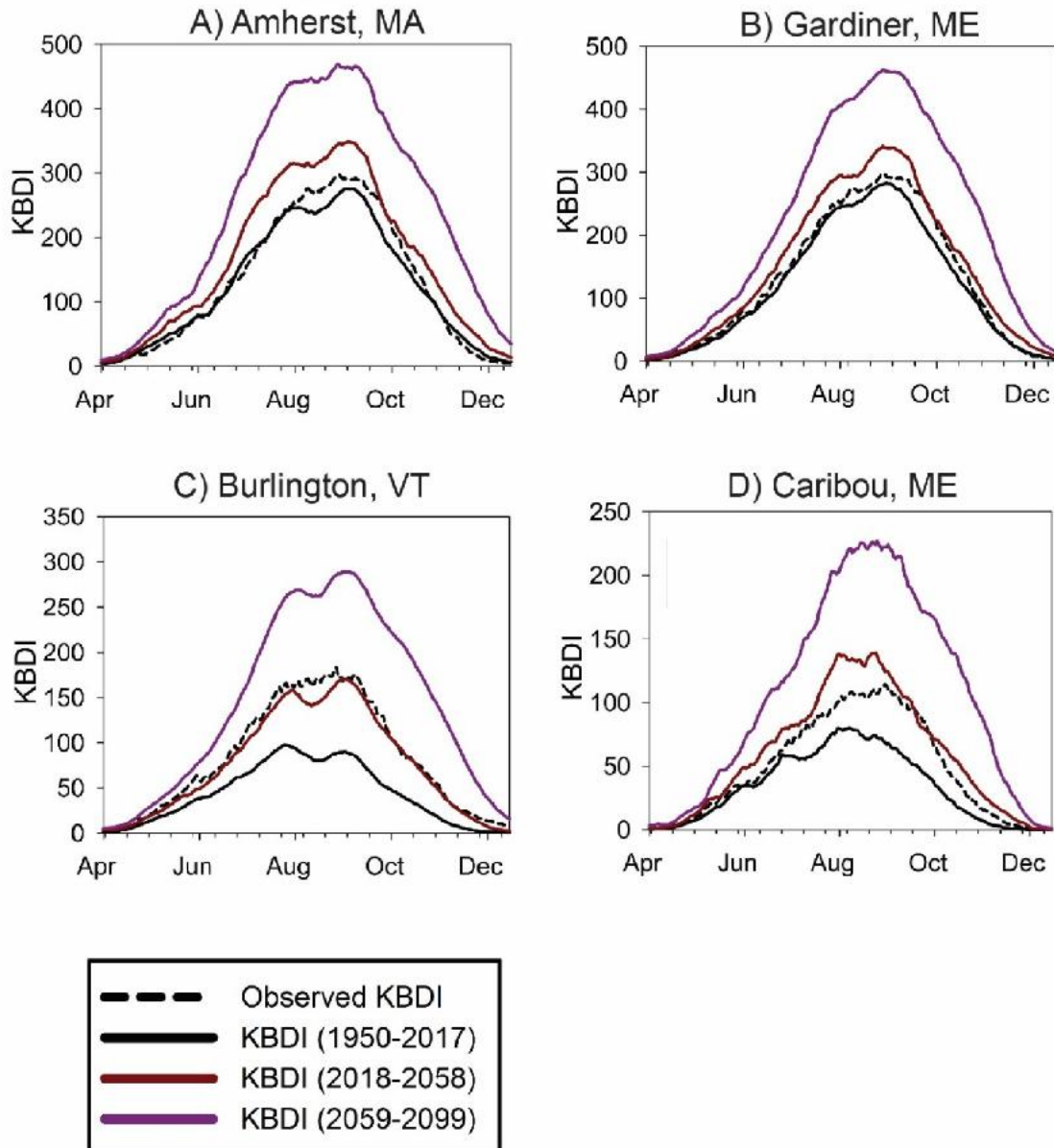


**Figure 3.3: Seasonal average KBDI from historical observations (black dashed line), modeled runs from 1950-2017 (black line), 2018-2058 (red line), and 2059-2099 (purple line) for selected four case study locations – A) Amherst, MA, B)Gardiner, ME, C)Burlington, VT, and D)Caribou, ME.**

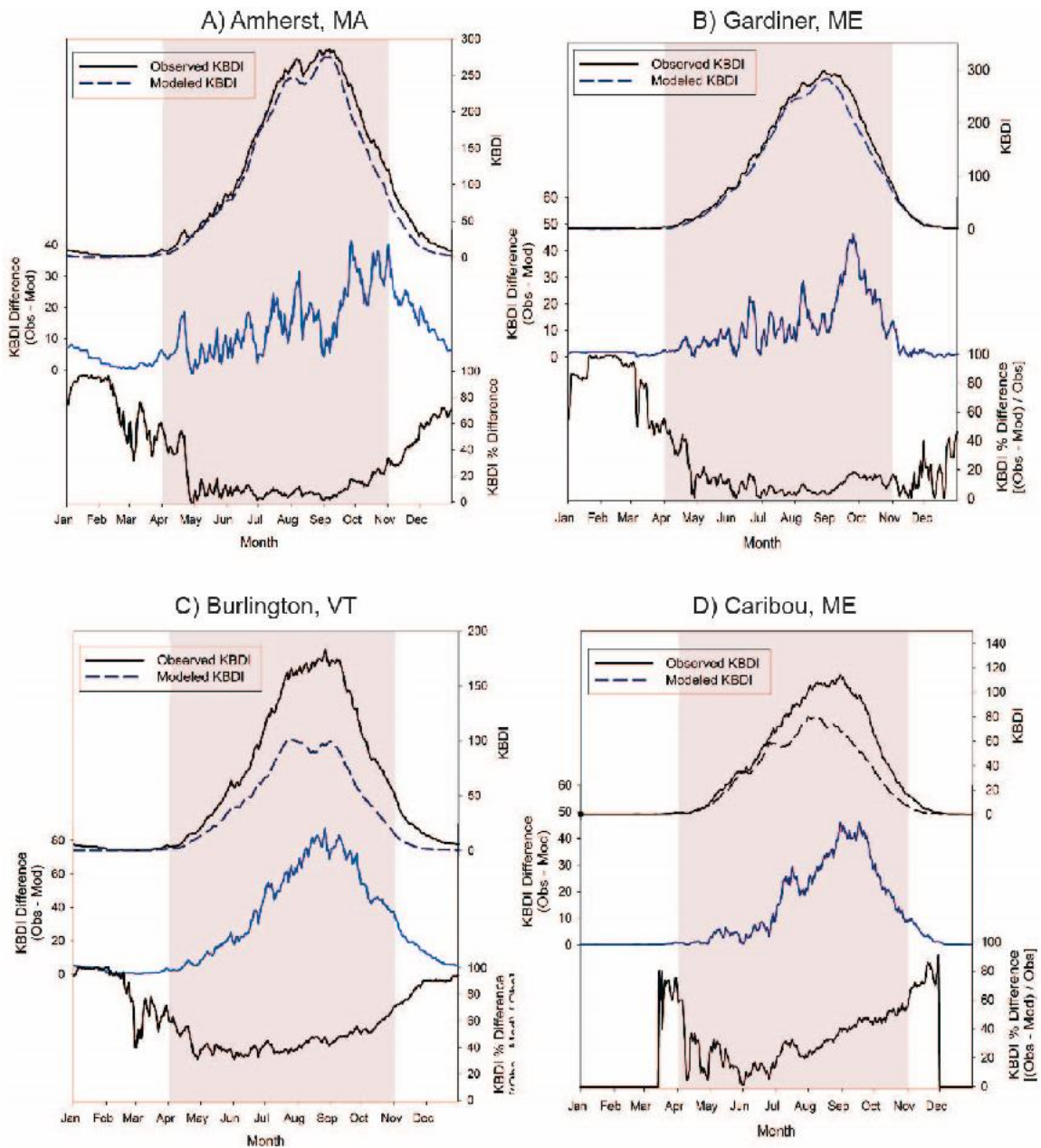


**Figure 3.4: Anomalies between observed KBDI (solid black line top) and modeled KBDI (dashed line) for the historical period (1950-2017 AD), with difference (blue line) and percent difference (bottom black line) between model and observed KBDI, for the 4 case study locations. Shaded area on each plot represents the “fire season”, where KBDI becomes increasingly significant to fire managers. Note the small differences between modeled and observed KBDI on plots A and B (Amherst and Gardiner), while larger differences occur at C) Burlington and D) Caribou.**

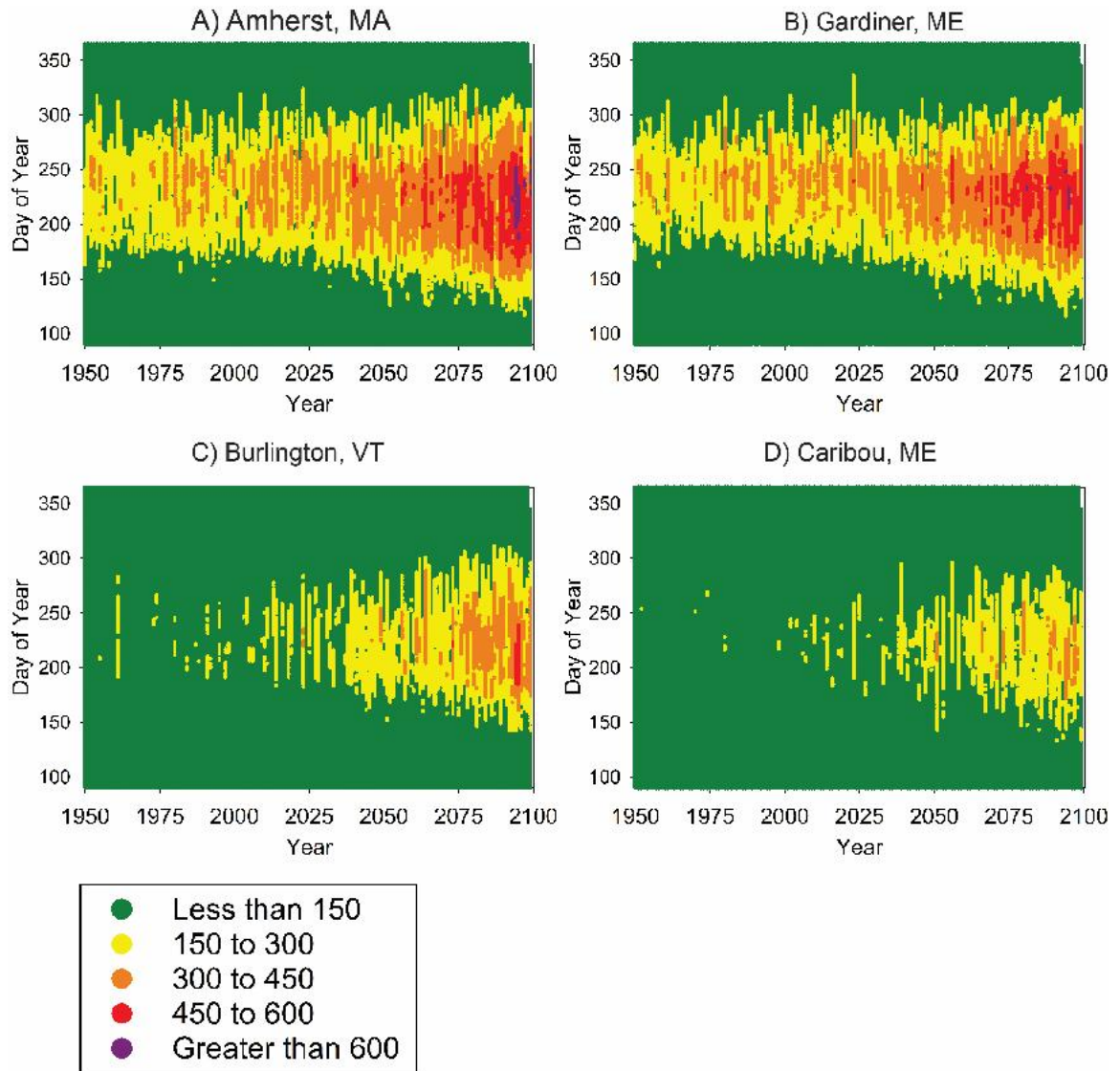


**Figure 3.5: Modeled KBDI from 1950-2099 at A)Amherst, MA , B)Gardiner, ME, C) Burlington, VT, and D) Caribou, ME, for RCP 8.5. Note scales and color ranges remain constant for each plot: low KBDI values of 0-150 are indicative of little/no fire risk (green), increasing to KBDI values of 150-300 (yellow), 300-450 (orange), 450-600 (red) and then greater than 600 (purple) for maximum KBDI values and extreme fire risk.**

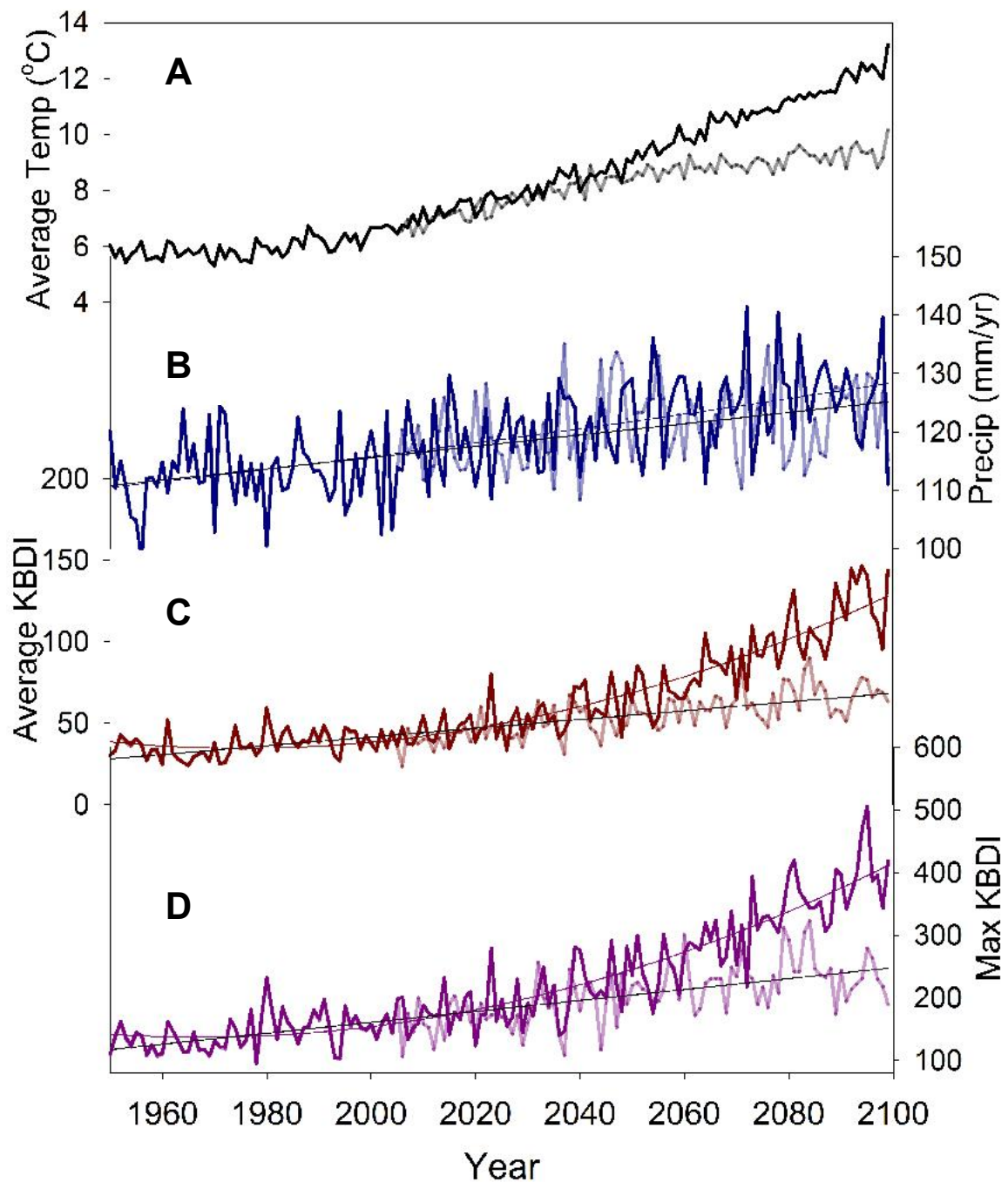


**Figure 3.6: Model Ensemble NEUS Climatic Data and KBDI from 1950-2099, under both RCP 8.5 and 4.5. a) Mean annual temperatures (black (RCP 8.5) and grey (RCP 4.5)), b) Annual Precipitation in inches per year (Dark blue (RCP 8.5) and light blue (RCP 4.5)), c) Average annual KBDI (dark red (RCP 8.5) and light red (RCP 4.5)), and d) Maximum annual KBDI (purple (RCP 8.5) and pink (RCP 4.5)).**

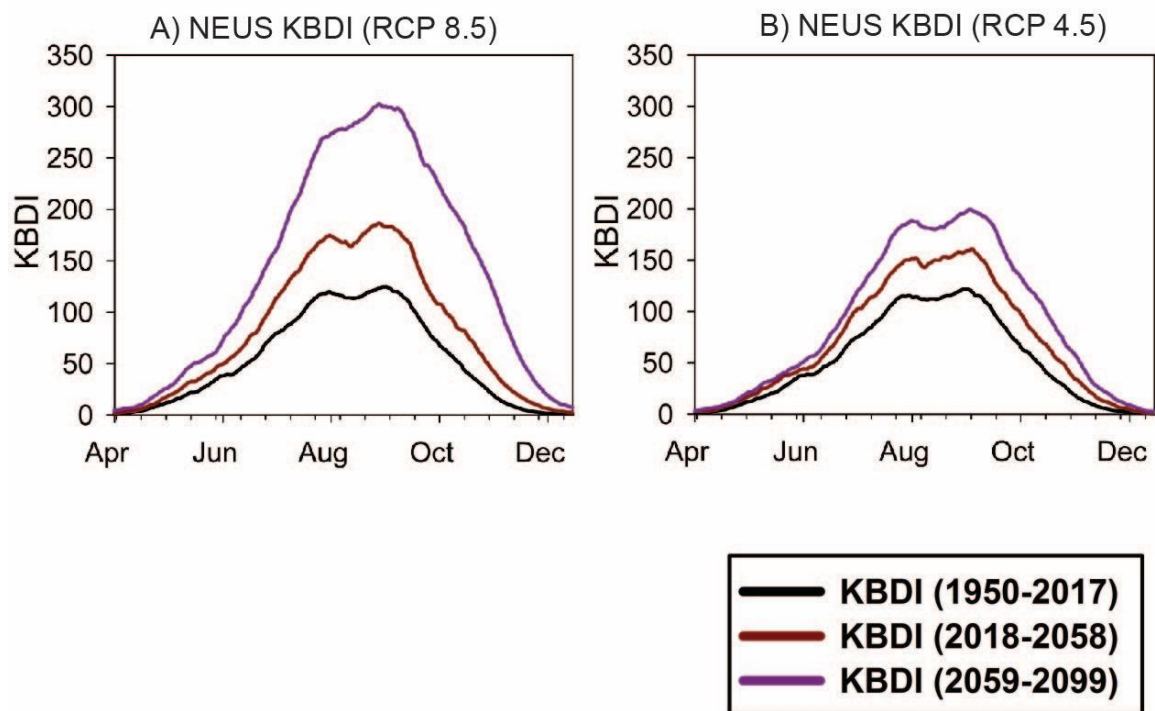


**Figure 3.7: Averaged seasonal KBDI for the NEUS under A) RCP 8.5 and B) RCP 4.5. Averages have been broken into three time periods: 1950-2017 (black line), 2018-2058 (red line), and 2059-2099 (purple line).**

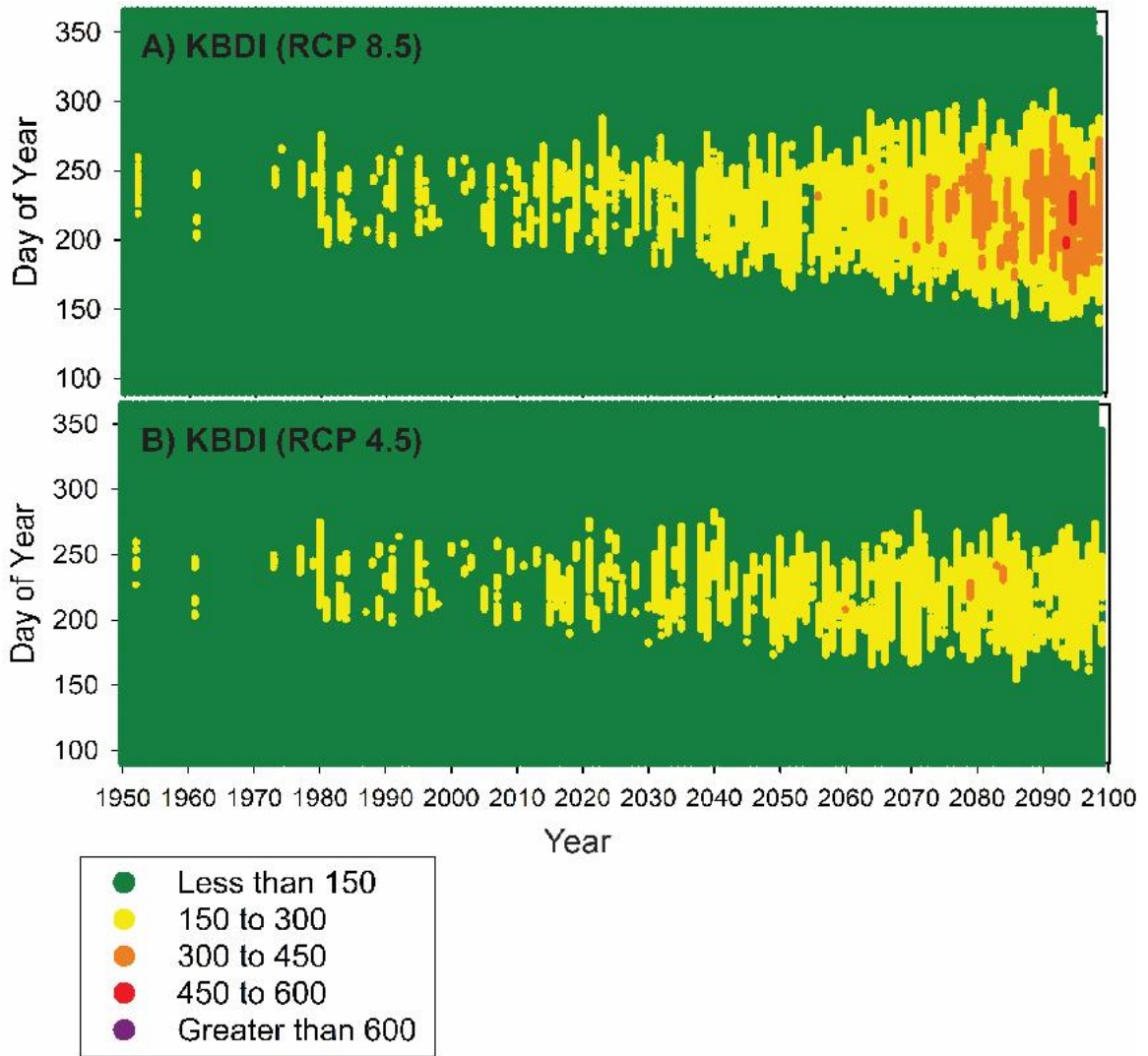


**Figure 3.8: Modeled KBDI from 1950-2099 for the NEUS for a) RCP 8.5 and b) RCP 4.5. Note scales and color ranges remain constant for each plot: lower KBDI are indicated by green, increasing to yellow, orange, red and then purple for maximum KBDI values.**

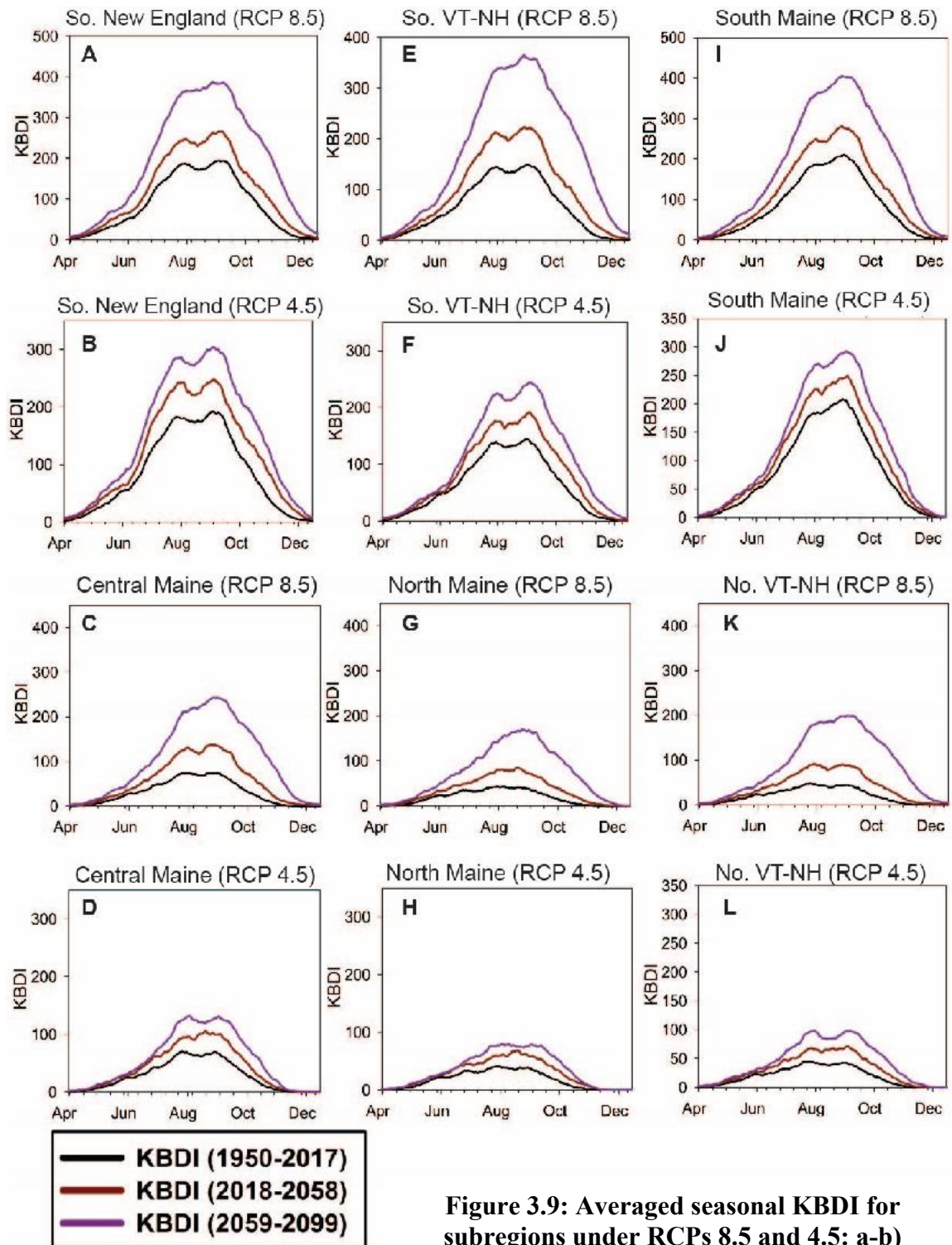


**Figure 3.9: Averaged seasonal KBDI for subregions under RCPs 8.5 and 4.5: a-b) Southern New England, c-d) central Maine, e-f) southern VT-NH, g-h) Northern Maine, i-j) Southern Maine, and k-l) Northern VT-NH. Averaged time periods include 1950-2017 (black), 2018-2058 (red), and 2059-2099 (purple).**

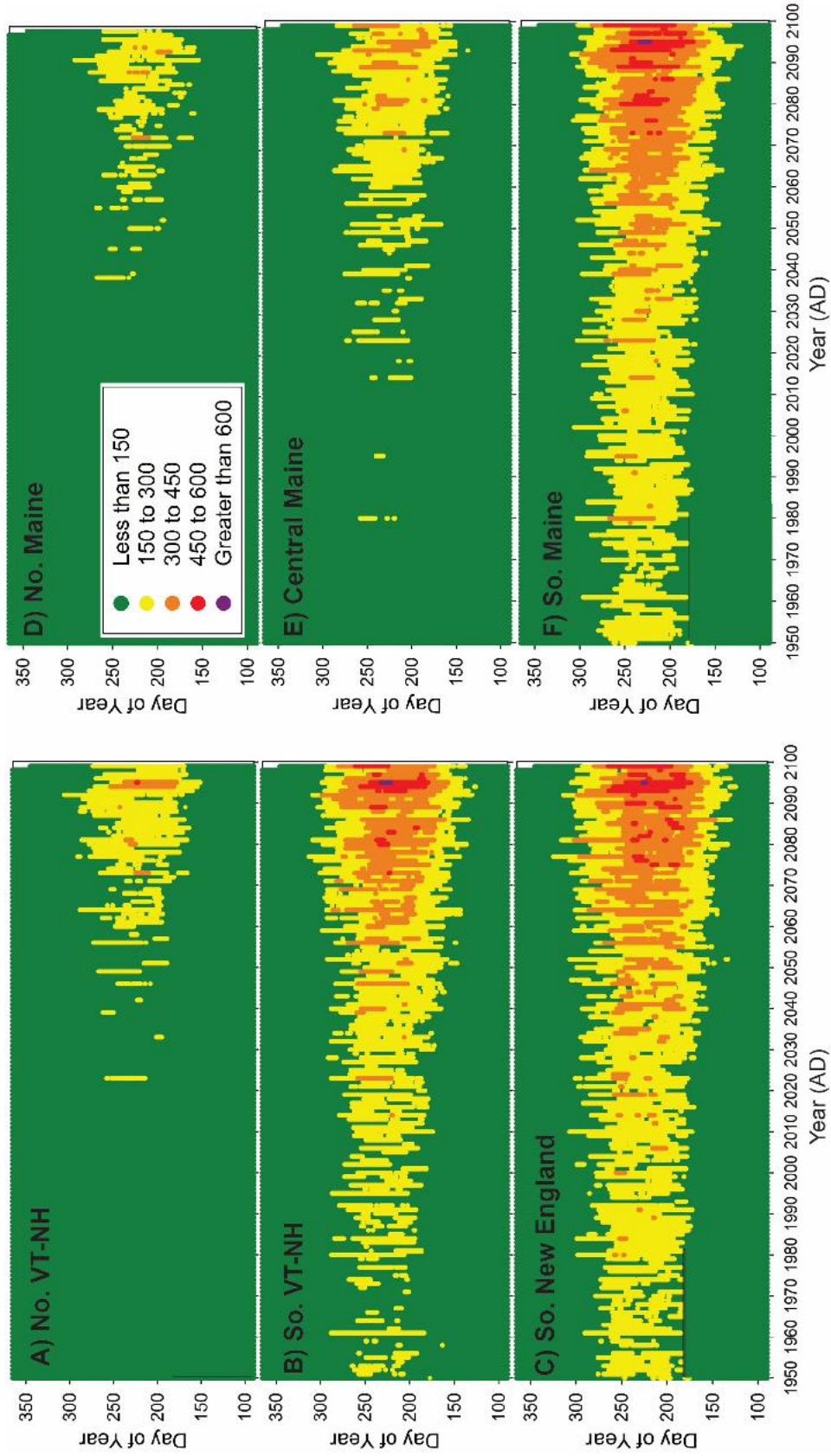


**Figure 3.10: Modeled KBDI from 1950-2099 for subregions for RCP 8.5. Color ranges remain constant for each plot.. A) Southern New England, B) South Maine, C) South VT-NH, D) Central Maine, E) Northern Maine, and F) North VT-NH.**

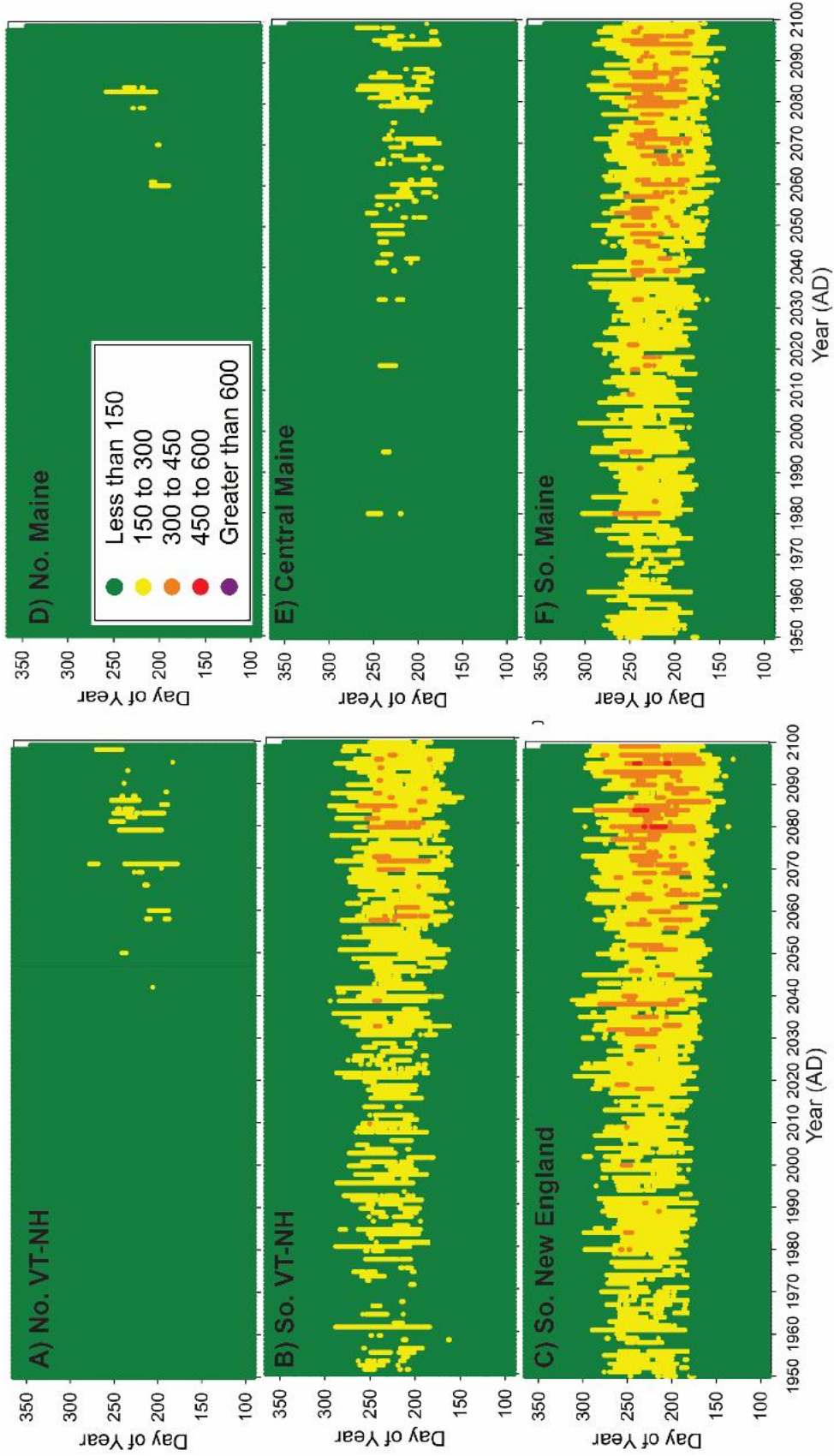


**Figure 3.11: Modeled KBDDI from 1950–2099 for subregions for RCP 4.5. Color ranges remain constant for each plot.. A) Southern New England, B) South Maine, C) South VT-NH, D) Central Maine, E) Northern Maine, and F) North VT-NH.**

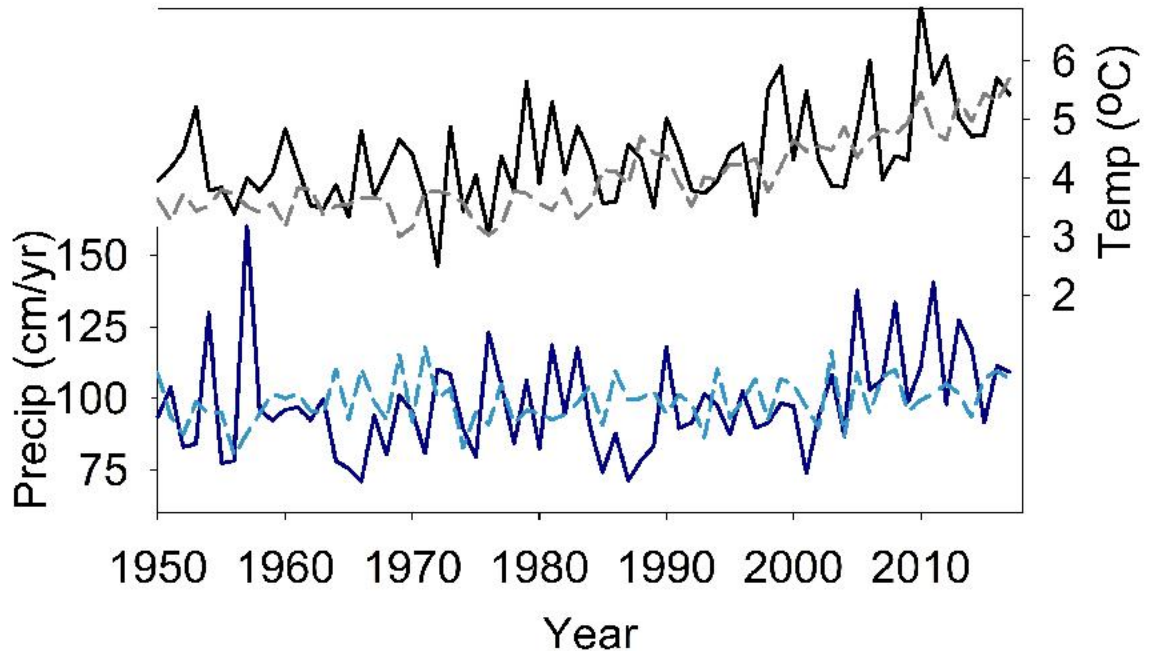


**Figure 3.12: Comparison of modeled and observed climate data from Caribou, ME.**  
**A) Average temperature for observed (black solid line) and modeled (grey dashed line), and B) Annual Precipitation in inches per year for observed (blue solid line) and modeled (blue dashed line).**

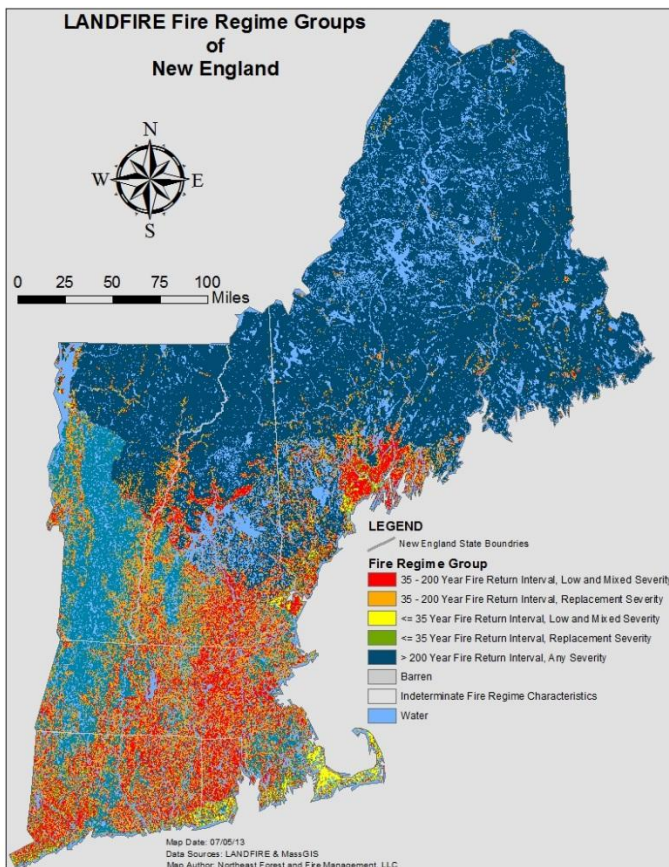


**Figure 3.13: LANDFIRE Map of fire return intervals in the NEUS, provided by the Northeast Forest and Fire Management LLC (2013).**  
**Note that many areas in the southern portion of the NEUS have low return intervals for fire, in some cases lower than 35 years.**

Temperature (deg F)	KBDI for Yesterday																Drought Factor
	0 to 49	50 to 99	100 to 149	150 to 199	200 to 249	250 to 299	300 to 349	350 to 399	400 to 449	450 to 499	500 to 549	550 to 639	640 to 699	700 to 759	760 to 799	800	
107+	41	38	36	33	30	28	25	23	20	17	15	11	6	4	1	0	
104-106	35	33	31	28	26	24	22	19	17	15	13	9	5	3	1	0	
101-103	30	28	26	24	22	20	19	17	15	13	11	8	5	3	1	0	
98-100	26	24	23	21	19	18	16	14	13	11	9	7	4	2	1	0	
95-97	22	21	19	18	16	15	14	12	11	9	8	6	3	2	1	0	
92-94	19	18	16	15	14	13	12	10	9	8	7	5	3	2	1	0	
89-91	16	15	14	13	12	11	10	9	8	7	6	4	3	1	1	0	
86-88	14	13	12	11	10	9	8	7	6	5	4	4	2	1	1	0	
83-85	11	11	10	9	9	8	7	6	5	4	3	3	2	1	1	0	
80-82	10	9	8	8	7	7	6	5	4	3	3	3	2	1	0	0	
77-79	8	8	7	7	6	6	5	4	4	3	3	2	1	1	0	0	
74-76	7	6	6	5	5	5	4	4	3	3	2	2	1	1	0	0	
71-73	6	5	5	5	4	4	3	3	3	2	2	2	1	1	0	0	
68-70	5	4	4	4	3	3	3	3	2	2	2	1	1	1	0	0	
65-67	4	3	3	3	3	3	2	2	2	2	1	1	1	1	0	0	
62-64	3	3	3	2	2	2	2	2	1	1	1	1	1	1	0	0	
59-61	2	2	2	2	2	2	1	1	1	1	1	1	1	0	0	0	
56-58	2	2	2	1	1	1	1	1	1	1	1	1	1	0	0	0	
53-55	1	1	1	1	1	1	1	1	1	1	1	1	0	0	0	0	
50-52	1	1	1	1	1	1	1	1	1	1	1	0	0	0	0	0	

**Table 3.1: Drought factor table for areas with annual rainfall of 30 – 39”, adapted from Keetch and Byram (1968). The “drought factor” is added to daily KBDI depending on max temperature and previous day’s KBDI as listed in the table.**

## CHAPTER 4

### LOCAL AND REGIONAL WILDFIRE ACTIVITY IN CENTRAL MAINE (USA) DURING THE PAST 900 YEARS

Miller, Daniel R.<sup>1,2\*</sup>, Isla S. Castañeda<sup>1</sup>, Raymond S. Bradley<sup>1,2</sup>, and Dana MacDonald<sup>1</sup>

1. Department of Geosciences, University of Massachusetts Amherst, Amherst, MA,  
01003, USA

2. Northeast Climate Science Center, University of Massachusetts Amherst, Amherst,  
MA 01003, USA

\*Corresponding Author Email: [dmiller@geo.umass.edu](mailto:dmiller@geo.umass.edu)

Keywords: Varve, Wildfire, PAH, Retene, Charcoal, New England

AS SUBMITTED, ACCEPTED, AND PUBLISHED  
IN THE JOURNAL OF PALEOLIMNOLOGY

CITATION:

Miller, D.R., Castañeda, I.S., Bradley, R.S., MacDonald, D., 2017. Local and regional wildfire activity in central Maine (USA) during the past 900 years. *Journal of Paleolimnology* 58, 455–466.

## 4.1 Abstract

Climatic and environmental change has a direct effect on wildfire frequencies and distributions throughout many regions of the world. Reconstructions from natural archives such as lake sediments can extend temporally limited historical records of regional wildfire activity over longer timescales through sedimentary charcoal analysis or examining polycyclic aromatic hydrocarbon (PAH) concentrations. To date, little work has been completed on sedimentary PAH distributions from lacustrine records in the Northeastern United States (NEUS), making it difficult to assess how accurately PAHs trace fire activity in the region, the spatial scope of the signal (local versus regional), or if certain compounds do a more adequate job of tracking fire than others. In this study, we examine PAHs and macrocharcoal from a varved sedimentary record from Basin Pond, Fayette, Maine (USA). We find that a drastic increase in the concentrations of 17 measured PAHs occurred during the 19<sup>th</sup>-20<sup>th</sup> centuries due to industrialization of the region. Additionally, elevated concentrations of the PAH retene were found to be highly correlated with known large-scale regional wildfire events that occurred in 1761-1762, 1825, and 1947 (A.D.). To distinguish between biomass burning and anthropogenic combustion sources, we examined the ratio of the PAHs retene and chrysene. Our new Basin Pond PAH records, along with a local signal of fire occurrence from charcoal analysis, offers the prospect of using this multi-proxy approach as a method for examining long-term wildfire frequency at both the local and regional scale in the NEUS.

## 4.2 Introduction

Wildfires are an important consequence of global climatic and environmental change. Understanding fire frequency and anthropogenic impacts on wildfires is critical in the context of climate change because they directly impact atmospheric composition, ecosystem diversity, and land management practices (Clark and Royall 1995; Gill and Bradstock 1995; Werf et al. 2004; Denis et al. 2012; Kirchgeorg et al. 2014). Fire frequency is expected to increase in most global warming scenarios, and costs relating to wildfire management and damage have been increasing in recent years (U.S. Forest Service 2015; National Interagency Fire Center 2016). Furthermore, there is uncertainty about how human disturbance, particularly in the Northeastern United States (NEUS), has affected natural burning patterns due to our lack of continuous fire history records for pre-settlement times (Clark and Royall 1995). Therefore, long term wildfire reconstructions are a major factor in understanding climate-wildfire feedbacks and how climate influences natural wildfire regimes (Denis et al. 2012).

While wildfires are a less common phenomena in the NEUS than in other regions of the world, large events can occur and significantly impact the landscape. Due to limited historical wildfire records in the region, reconstructions from natural archives including lake sediments and tree rings are needed to extend fire history over longer timescales. In the NEUS, tree-ring studies are temporally limited due to human disturbance on forest ecosystems and land clearance practices (Lorimer 1977; Parshall et al. 2003; Barton et al. 2012). Therefore, most wildfire reconstructions are based on macrocharcoal distributions in lacustrine sediments (Swain 1973; Fahey and Reiners 1981; Clark and Royall 1995; Clark et al. 1996; Parshall et al. 2003; Pederson et al.

2005). Although this method has greatly increased our knowledge of past wildfire activity, there are some limitations. Charcoal analysis can require large volumes of sediment depending on sediment composition and charcoal abundance (Whitlock and Larsen 2001; Denis et al. 2012). Furthermore, many existing charcoal records in the NEUS are poorly resolved, not continuously sampled, and only provide a local signal of burning (Marlon et al. 2009; Zennaro et al. 2015), making determining a regional signal of fire activity difficult.

Molecular compounds that can be used as markers of burning have become increasingly studied in paleoenvironmental reconstructions of wildfire activity (Yunker et al. 2002; Denis et al. 2012; Kirchgeorg et al. 2014). One such compound class is polycyclic aromatic hydrocarbons (PAHs). PAHs, produced through natural and anthropogenic processes, were first found in soils and have since been studied across different ecosystems and environments, including lakes (Blumer 1961; Grimalt et al. 2004; Bianchi and Canuel 2011). Pyrogenic PAHs are made through the incomplete combustion of organic material (Page et al. 1999), and can be used to trace regional combustion processes such as fossil fuel burning or forest fire activity (Page et al. 1999; Yunker et al. 2002; Denis et al. 2012). Therefore, the historical record of certain PAHs, or groups of PAHs, in sediment cores can be used as proxies for the frequency and size of wildfires in pre-industrial times (Musa Bandowe et al. 2014). However, interpreting PAH abundances as proxies for wildfires becomes more complicated when moving into modern (post-industrialization) time periods. Industrialization and widespread use of fossil fuels has caused increases in concentrations of most PAHs. Fortunately, different combustion sources, such as combustion from fossil fuels or biomass combustion, can be

distinguished by the ratios of specific PAHs, such as retene/(chrysene + retene) and anthracene/(anthracene + phenanthrene) (Yunker et al. 2002; Yan et al. 2005; Kuo et al. 2011; Denis et al. 2012). However, to our knowledge, little work on PAH distributions from lacustrine sedimentary records have been completed at high-resolution in the NEUS, making it difficult to assess how accurately PAHs trace fire activity in the region, the spatial scope of the signal (local versus regional), and if certain compounds do a better job of capturing fire history than others.

To address these issues, we present an organic geochemical analysis of a 900-year sedimentary record with sub-decadal resolution from Basin Pond, Maine, USA. Past studies of Basin Pond have focused on paleoenvironmental reconstructions using pollen and charcoal, as well as sedimentological analyses spanning the Holocene (Gajewski et al. 1987; Gajewski 1988; Doner 1990; Clark and Royall 1994, 1996; Clark et al. 1996; Frost 2005). The goal of this study was to reconstruct a continuous, highly-resolved record of local and regional wildfire activity from the NEUS and to better understand differences in fire history recorded in lacustrine sediments by PAHs and macrocharcoal. We compare our reconstructions with historical records of large regional fires to assess the accuracy of the sediment records as wildfire proxies.

#### **4.2.1 Study Location**

Basin Pond is a small (0.14km<sup>2</sup> area) lake with a maximum depth of 32.6m located in Fayette, ME (44°28'N, 70°03'W) at an elevation of 124m above sea level (Figure 1) (Gajewski et al., 1987; Frost 2005). Basin Pond has no fluvial inlets, with the main sources of water from groundwater and precipitation. The sole outlet is a small, dammed stream running westward into the adjacent David Pond (Frost 2005). Most of the

0.53km<sup>2</sup> catchment area is located within the “Basin Pond Conservation Area” with one residential building in the watershed (Frost 2005). The catchment is dominated by a well-developed forest of deciduous hardwoods and evergreen trees, with hemlock being the most abundant species (Frost 2005).

Basin Pond is unique in that the sedimentary record is comprised of annual laminations, or varves, due to a permanent meromictic water column (Wetzel 1983; Frost 2005). A persistent chemocline was found throughout the year to be sufficient to prevent turnover of the water column during the breakdown of thermal stratification during the early spring and late fall. This chemical stratification aids in the permanent anoxic conditions at depth, allowing for the preservation of annual couplets in the sedimentary record (O’Sullivan 1983). The Basin Pond varves are biogenic in nature, with couplets being comprised of a lighter, diatom-rich layer and a darker, humus layer (Frost 2005).

## **4.3 Materials and methods**

### **4.3.1 Core collection**

Primary field work at Basin Pond was conducted in March 2014. Sediment coring was performed from ice in the deepest part of the lake at 32m (44° 27' 27" N, 70° 03' 09" W) using a UWITEC gravity coring system. Core BP2014-3D (52 cm), captured an undisturbed sediment-water interface, and was subsampled in the field at 0.5 cm resolution for radioisotopic dating. Core BP2014-5D (174 cm) was taken and immediately capped. In the Department of Geosciences at University of Massachusetts Amherst, cores were split, photographed, and subjected to non-destructive down-core logging using an Itrax XRF core scanner at 100- $\mu$ m resolution.

### **4.3.2 Age model**

The age model for Basin Pond core BP2014-5D is primarily based on a varve count chronology of the uppermost 80-cm confirmed through radioisotopic dating of the upper sediments and radiocarbon dating of plant macrofossil samples (Figure 2; Table 1). Varve counts were completed using X-Ray radiograph images with 100- $\mu$ m resolution. Laminations in the upper 80-cm of the sediment record appear continuous with no apparent hiatuses, and were counted three times for the creation of the varve count chronology with minimal error. The upper 15-cm of sediment were also dated using radioisotopic analysis. Subsamples from core BP2014-3D were freeze dried, homogenized, and measured for  $^{210}\text{Pb}$  activity on a Canberra GL2020R Low Energy Germanium Detector, following the methods detailed by Woodruff et al. 2013. Ages for  $^{210}\text{Pb}$  measurements were estimated assuming a constant rate of supply of unsupported  $^{210}\text{Pb}$  activity (Appleby and Oldfield 1978). In addition, radiocarbon dating of 5 discrete samples were conducted on terrestrial macrofossils (Table 1; Figure 2). Radiocarbon age estimates were calibrated using the “IntCal13” calibration to years before present in the ‘R’ program ‘BChron’(Parnell 2016). No corrections for ‘old’ carbon were made on these terrestrial macrofossils.

### **4.3.3 Organic geochemical analyses**

One-hundred and thirty-six discrete samples were extracted from core BP2014-5D at 0.5-cm resolution, continuously from the sediment water interface to 68-cm depth. After freeze drying, samples were homogenized and extracted using a Dionex accelerated solvent extractor (ASE 200) with a solvent mixture of dichloromethane(DCM) and methanol (MeOH) (9:1, v/v). The resulting total lipid extract was then separated into

apolar (9:1 hexane:DCM v/v), ketone (1:1 hexane:DCM v/v), and polar (1:1 DCM:MeOH v/v) fractions using alumina oxide column chromatography.

PAHs were identified and quantified on a Hewlett Packard 6890 series gas chromatograph coupled to an Agilent 5973 mass spectrometer (GC-MS) using a Restek Rtx-5ms column (60-m x 250- $\mu$ m x 0.25- $\mu$ m). Samples were run in Selected Ion Monitoring (SIM) mode, where ion masses of 17 PAHs were targeted (Table 2). Sixteen PAHs were identified from a RESTEK SV Calibration Mix PAH Standard, while an additional PAH was identified from a CHIRON AS standard (Table 2). External calibration curves were created for all 17 PAHs based on varying injection concentrations and were used to calculate PAH concentrations in core BP2014-5D. Sedimentary compounds were identified by interpretation of characteristic mass spectra fragmentation patterns, relative retention times, and by comparison with the PAH standards and the literature. Levoglucosan, an organic biomarker that is commonly used to trace vegetation burning in sedimentary records (Fabbri et al. 2002; Lopes dos Santos et al. 2013; Shanahan et al. 2016), was searched for but not detected in the Basin Pond sediments.

#### **4.3.4 Charcoal analysis**

Macroscopic charcoal analysis was analyzed on the same core and at the same intervals as for organic geochemical analyses. 1-cm<sup>3</sup> of wet sediment were taken and soaked in a solution of 10% potassium hydroxide (KOH) solution for 2 weeks to oxidize non-charcoal organic matter, and then sieved over a 125- $\mu$ m mesh (Enache and Cumming 2006; Schlachter and Horn 2010). Charcoal pieces per sample were counted using a microscope at 40x magnification. Charcoal classification was determined based on three criteria: the macrocharcoal in question had to have been completely black and reflective,

breakable upon touch, and have organized plant cellular structure (Whitlock and Larsen 2001).

#### **4.4 Results**

Out of the 17 PAHs (Table 2) we searched for, 5 were not present in most samples, including naphthalene, acenaphthene, anthracene, indeno(1,2,3-cd) pyrene, and dibenz(ah)anthracene. Four PAH were found in most samples throughout the record (benzo(b)fluoranthene, pyrene, retene, and chrysene). The remaining 8 compounds (phenanthrene, fluoranthene, benzo(k)fluoranthene, benzo(a)anthracene, acenaphthylene, benzo(a)pyrene, benzo[ghi]perylene, and fluorene) searched were mainly only found in the upper 15-cm of sediment. PAH concentrations were calculated for each of the 12 detectible compounds. With the exception of retene, all of the PAH distributions are extremely similar, varying from 0-1.6 $\mu\text{g/g}$  in the upper 15-cm of sediment. Retene was the most abundant PAH present and varied in concentration from 0.1-10 $\mu\text{g/g}$  sed throughout the record. Charcoal counts varied from 20-250 pieces per  $\text{cm}^3$  (cc), with the highest peak occurring in the upper 5-cm of sediment.

#### **4.5 Discussion**

Here we examine how local and regional fire history can be recorded in NEUS lacustrine sediment records by organic biomarkers in comparison with sedimentary charcoal counts. We first examine the known historical wildfire data and subsequently provide an in-depth comparison of the Basin Pond macrocharcoal and PAH records. In the following discussion, we divide our records into three main periods: pre-historic

(1100 AD to 1750 AD), historic (1750 AD to 1950 AD), and modern times (1950 AD to present day).

#### **4.5.1 Historical wildfire data**

In Maine, historical records document several large wildfire events ( $> 400\text{km}^2$ ) dating back to the mid-18<sup>th</sup> century (Coolidge 1963). While these have occurred throughout the state, we will focus on large wildfires estimated to have occurred within 80km of Basin Pond. The most recent outbreak in October 1947AD saw numerous fires burn over  $800\text{km}^2$  acres across southern Maine over a week, and became known as “The Week Maine Burned” (Butler 1979). The largest estimated wildfire during the historical period occurred in 1825AD and became known as the “Miramichi Fire” (Butler 2014). During this event, an estimated  $12,000\text{ km}^2$  of land was burned throughout Maine and New Brunswick, with roughly  $3,350\text{ km}^2$  of land burned in central Maine; this was one of the largest wildfires in North American history (Coolidge 1963; Butler 2014). The earliest known large wildfire events, noted in historical records, occurred in 1761-1762 AD throughout southern Maine. The estimated extent of these fire events is less well-constrained, as maps of the burn regions and historical accounts from individual towns do not all agree (Coolidge 1963). Nonetheless, the fires of 1761-1762 AD burned across much of the same areas that were burned during the 1947 AD fire outbreak (Figure 1).

#### **4.5.2 Age model considerations**

A robust chronology is essential to compare the proxy records developed here with those of historical fires. While it appears that the varve chronology of Basin Pond is continuous, and the varve counts are in good agreement with the  $^{210}\text{Pb}$  ages (Figure 2),

we note some differences with the radiocarbon ages. Four of the 5 radiocarbon dates trend slightly younger than the varve count chronology (Figure 2), with 2 samples (BPR-022 and BPR-026) having calibrated ages and associated errors that fall entirely outside the varve count chronology (by 15 years and 65 years, respectively). The most plausible explanation for the discrepancy involves the isotopic fractionation correction. Generally, in order to remove the effects of isotopic fractionation in radiocarbon analysis, the modern fraction of macrofossils is corrected to the value it would have if its original  $\delta^{13}\text{C}$  were -25‰, unless measured on each macrofossil sample. In laboratory analysis,  $\delta^{13}\text{C}$  was unreported for all samples, so the fraction modern in each sample was corrected for isotopic fractionation using an estimated base value of -25‰. With the exception of the basal sample, the Basin Pond macrofossils selected for analysis were eastern hemlock needles, which have  $\delta^{13}\text{C}$  values of -29 to -30‰ (Domec et al. 2013). This difference can produce calibrated ages skewed younger by several decades. Other possible explanations for younger radiocarbon ages include slight error in the varve chronology or the minor inclusion of modern carbon during sample processing. With these issues in mind, we use the varve count chronology as the age model; we note that the varve chronology is in good agreement with the  $^{210}\text{Pb}$  ages and that past studies of Basin Pond also utilized the varve chronology as an acceptable age model (Gajewski 1987, 1988; Clark 1996; Frost 2005).

#### **4.5.3 The basin pond charcoal record**

Macroscopic charcoal analysis has commonly been employed in recent decades as an indicator of local fire activity (Whitlock 2001). Wildfire characteristics, such as size and intensity, have large influences on charcoal production, distribution, and deposition

in lacustrine sediment records. Other factors affecting charcoal transport and deposition in lakes include atmospheric patterns at the time of the fire (Gardner and Whitlock 2001) and distance from the lake. In light of these complex factors affecting charcoal abundance in lacustrine sediments, past studies have generally found that while large charcoal particles ( $>1000\text{-}\mu\text{m}$ ) tend to be deposited near a lake (Clark and Patterson 1997), smaller particles can be transported much greater distances. In large fires (with convective columns  $>1000\text{m}$ ), charcoal particles  $<200\text{-}\mu\text{m}$  can be transported tens of kilometers (Clark 1988; Whitlock 2001). Despite this, there have been instances where charcoal analysis fails to detect either known fire events or events detected in other natural archives such as tree rings (Holz et al. 2012).

The Basin Pond charcoal record demonstrates large peaks occurring after both the 1947 AD and 1825 AD fire events (Figure 3), even though the estimated ranges of burned area are thought to be outside the normally accepted range of macrocharcoal distribution. The most likely explanation is that the burn area estimates for the historical fire events, while reasonably accurate, do not represent all fires that took place in the region during those time periods. Importantly, these fire events were not one large fire, but were comprised of numerous smaller fires taking place at the same time (Coolidge 1963). The estimated burn areas of each are likely not all-inclusive, making it possible that the 1947 AD and 1825 AD fires could have been within range of Basin Pond for a charcoal signal to be recorded. In the pre-historic record, elevated charcoal abundances occur during a period from 1510-1630 AD, indicating a possible time of increased local fire activity (Figure 4).

#### 4.5.4 Basin pond PAH records

A major feature of the Basin Pond record is a dramatic increase in all PAH concentrations between pre-historic and historic times (Figure 3, 4), which is related to increased population and industrialization of the region. Industrialization is likely the driving factor of the simultaneous increases in all PAHs in the mid-19<sup>th</sup> century (Figure 3), as coal and other fossil fuels were increasingly used in the region. Furthermore, population increases led to more wood being used as a heat source during winter months, which possibly also led to higher PAH concentrations. It is important to note, however, that retene shows a slightly different distribution than the other PAHs.

Retene is produced from the breakdown of abietic acid, which is prevalent in conifer tree resin (Ramdahl 1983; Ahad et al. 2015). Here we interpret retene as an indicator of biomass burning because conifers, specifically hemlock, are an important part of the ecosystem in northern New England and the Basin Pond region (Ramdahl 1983; Denis et al. 2012). The retene record exhibits several sharp increases in concentration superimposed on the overall increasing trend following the fire outbreaks of 1761-1762 AD, 1825 AD, and 1947 AD (Figure 4).

One issue that arises with interpreting PAH distributions in relation to biomass burning is that PAHs can be produced by multiple sources (biomass burning or fossil fuel combustion). The retene/(chrysene+retene) ratio (hereafter R/C+R) aids in delineating between combustion sources and can also be a more robust indicator of past fire history than individual PAH concentrations alone, which can show greater variability due to multiple sources (Yan et al. 2005; Kuo et al. 2011). The R/C+R ratio has been used by past studies to distinguish the sources of PAHs, as lower values (0.15 to 0.5) tend to

indicate fossil fuel combustion source while higher values ( $>0.8$ ) indicate a soft-wood combustion source (Yan et al. 2005; Kuo et al. 2011; Denis et al. 2012). All Basin Pond pre-historic samples have R/C+R ratios above 0.8, indicating that PAHs largely derive from biomass burning (Figure 4). Entering the historic period, the ratio shows a steady decrease in the mid-19<sup>th</sup> century from pre-historic levels (0.95-0.99) to  $<0.6$ , only disrupted by a sharp increase to above 0.95 after the 1825 AD fire. Values drop drastically as industrialization of the region accelerated, and remained lower than 0.8 in all but one sample through the rest of the historic period and modern times (Figure 3). The sampling following the 1947 AD fire is the only sample in modern times to reach above 0.8. Therefore, the R/C+R ratio appears to track wildfire activity in the region quite well during the historical and modern periods and results are consistent with wildfire events noted by retene concentrations.

#### **4.5.5 Comparison of wildfire proxies**

Two of three known regional wildfire events (the 1825 AD and 1947 AD fires) are evident in the Basin Pond retene and charcoal records. The 1761-1762 AD fires, while evident in the retene record, are not apparent in the charcoal record (Figure 4). The 1761-1762 AD event is the earliest known wildfire outbreak in the region, and information on the estimated range and magnitude of the fires is limited (Coolidge 1963). If the 1761-1762 AD event was of smaller magnitude or farther from the site than historical records indicate, distribution of charcoal would be limited.

The macrocharcoal and retene concentrations show a strong similarity throughout time, with both records suggesting coeval periods of increased fire activity (Figure 4). However, one noticeable difference is that the retene record shows more variability,

supporting the idea that each proxy is tracking wildfires on different spatial scales. PAH signals can be indicative of regional events, as PAHs can be moved much greater distances through aeolian transport than macroscopic charcoal (Page et al 1999). Therefore, it is likely that retene is tracking regional fire events, while charcoal is primarily tracking fires closer to Basin Pond. The best example of this discrepancy between records occurs during the period of increased fire activity from 1510-1630 AD, where several peaks in the charcoal record indicate increased burning whereas in the retene record, the timing of this increase is slightly longer (Figure 4). The period of increased fire activity in the retene record is evident from 1470-1640 AD, beginning almost 40 years prior and ending slightly earlier to that indicated by the charcoal record. This suggests that while local burning began roughly 500 years ago, regional events had been occurring for several decades prior. Furthermore, another increased period of fire activity is present in the retene record from 1240-1320 AD, but is not present in the charcoal record (Figure 4), indicating that while there were regional fires during this period, there was seemingly no local fire activity.

One interesting difference between the two proxies is the lag of the charcoal peaks in comparison to retene after the 1825 AD and 1947 AD fire events. In both fire events, retene concentrations exhibit maximum values 4 years and 9 years after the fire, respectively. However, in the charcoal record, this peak is delayed to 20 years and 17 years, respectively. Since all charcoal and PAH samples were from the same depths, this suggests that these offsets are real. We hypothesize that this is caused by charcoal and PAH having differing transport and environmental residence times. Lag times associated with charcoal deposition in sedimentary records are a common occurrence, with lags on

the order of several years (Whitlock and Millspaugh 1996, Duffin et al. 2007) to several decades (Patterson 1987). In Basin Pond sediments, retene demonstrates sharp increases in activity almost immediately after the wildfire events, while charcoal shows a more gradual increase over several samples, suggesting that retene is a more rapid indicator of wildfires in a sedimentary record than charcoal.

#### **4.5.6 Retene: a proxy for regional wildfire activity?**

Our data support that retene concentrations are a useful proxy for wildfire activity in the Basin Pond record over the past 900 years, yet caution must be taken when applying this proxy to longer time scales due to the nature of PAH production. PAH profiles are specific to the type of organic matter being combusted (Yang et al. 2007). In the case of retene, a large shift in regional forest composition over time may impact the PAHs produced from biomass burning. In the NEUS, large shifts in forest composition have occurred throughout the Holocene, including regional hemlock declines (Foster et al. 2006) or European deforestation in recent centuries (Foster and O’Keefe 2000). These shifts may alter the sedimentary PAH profiles and thus influence how PAHs trace fire activity in the region. Therefore, we suggest more research should be done on PAHs in lacustrine records in the NEUS over longer time scales to investigate how large-scale vegetation changes over time may alter sedimentary PAH distributions and the effects on how wildfire histories are recorded.

#### **4.6 Conclusions**

Our analysis of the varved Basin Pond sedimentary record reveals generally good agreement between charcoal counts and retene concentrations with historical records of

past large fire events occurring in 1761-1762 AD, 1825 AD, and 1947 AD in central and southern Maine. We find that retene tracks regional fire activity while macrocharcoal counts track localized burning. A dramatic increase in PAH concentrations is seen coincidentally with industrialization of the region in the historic period (1750AD – present day). To distinguish between PAH sources, the retene/(chrysene + retene) ratio allowed for the distinction of regional fire events from fossil fuel combustion. Although there are differences between the timing of fire events indicated by the retene and charcoal records, overall similarities between these records highlight the potential of using retene as a proxy for wildfire activity in the NEUS. Furthermore, the use of retene and the retene/(chrysene + retene) ratio is a novel method to tracking wildfires in the NEUS, and should be investigated in more detail in future wildfire studies in this region, focusing on longer timescales and different ecosystems.

#### **4.7 Acknowledgements**

We thank Jeff Salacup and the UMass Biogeochemistry group for laboratory assistance and helpful discussions. Thanks to Neil Patel for programming assistance and in the creation of bathymetric maps. The research was supported by Grant No. G12AC00001 from the United States Geological Survey. Results are solely the responsibility of the authors and do not necessarily represent the views of the Northeast Climate Science Center or the USGS. D. Miller was supported by a Department of the Interior Northeast Climate Science Center graduate fellowship. Special thanks to Dr. Debra Willard, coordinator of the Climate and Land Use Change Research and Development Program at the USGS, for providing funding for radiocarbon analysis.

Sample Depth (cm)	Description	Lab ID	$^{14}\text{C}$ Age	Calibrated Age Range (yrs BP(1950))		Median Age (cal yr BP (1950))
				(1 $\sigma$ )	(2 $\sigma$ )	
11.5	Hemlock Needle	OS-117501	95 $\pm$ 20	49–236	33–253	106
19	Hemlock Needle	OS-117502	205 $\pm$ 25	19–282	1–295	170
40	Hemlock Needle	OS-117504	310 $\pm$ 35	321–431	303–468	384
68	Hemlock Needle	OS-107506	835 $\pm$ 20	715–764	700–781	740
123	wood	USGS-9906	1700 $\pm$ 35	1569–1673	1546–1694	1603

**Table 4.1: Results of radiocarbon analysis of Basin Pond macrofossils from core BP2014-5D. The laboratories used were the U.S. Geological Survey’s Eastern Geology and Paleoclimate Science Center (USGS), and the Woods Hole Oceanographic Institute NOSAMS Facility (OS).  $^{14}\text{C}$  ages were converted to calibrated ages using the “BChron” package for R (see text for more detail).**

<b>Retention Order</b>	<b>Compound</b>	<b>Major Ion</b>	<b>Standard Used</b>
I	naphthalene	128	Restek
II	acenaphthylene	152	Restek
III	acenaphthene	153	Restek
IV	fluorene	166	Restek
V	phenanthrene	178	Restek
VI	anthracene	178	Restek
VII	fluoranthene	202	Restek
VIII	pyrene	202	Restek
IX	retene	219	Chiron
X	benzo(a)anthracene	228	Restek
XI	chrysene	228	Restek
XII	benzo(b)fluoranthene	252	Restek
XIII	benzo(k)fluoranthene	252	Restek
XIV	benzo(a)pyrene	252	Restek
XV	indeno(1,2,3-cd)pyrene	276	Restek
XVII	dibenz(a,h)anthracene	278	Restek
XVI	benzo[g,h,i]perylene	276	Restek

**Table 4.2: PAH present in laboratory standards and searched for in Basin Pond sediments, with major ions for each compound.**

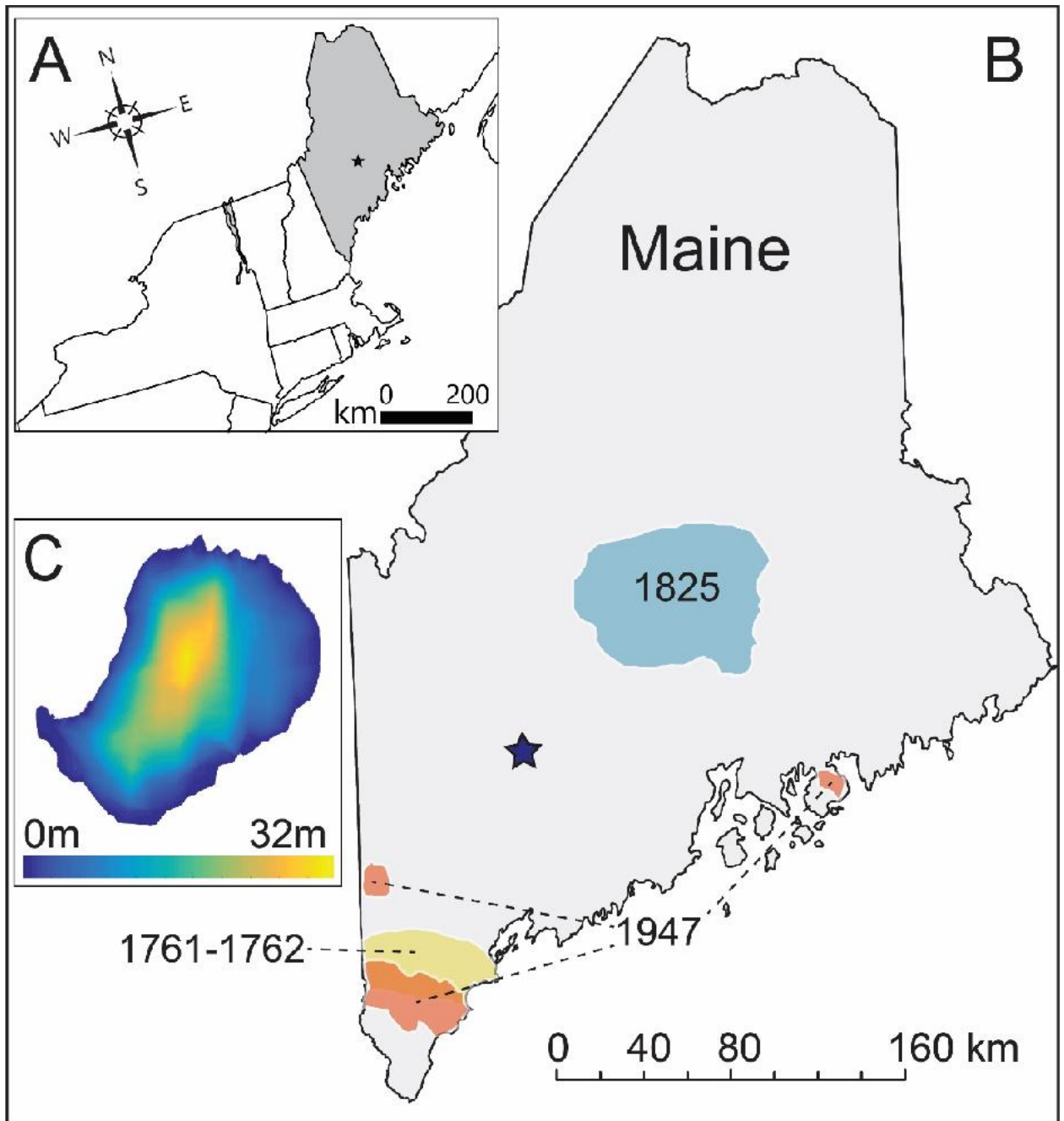


**Figure 4.1: Location of Basin Pond, ME and bathymetric map. A) Map of the NEUS with Maine highlighted in gray and Basin Pond indicated by a star. B) Map of Maine with estimated ranges of known large wildfire events (>400km<sup>2</sup> acres burned) from historical records within 100km of Basin Pond, adapted from Coolidge (1963). Shaded locations indicate the fires of 1761-1762 AD (yellow), 1825 AD (blue), and 1947 AD (red). Orange shading indicates regions effected by both the 1761-1762 AD and 1947 AD fires. C) Bathymetric map of Basin Pond.**

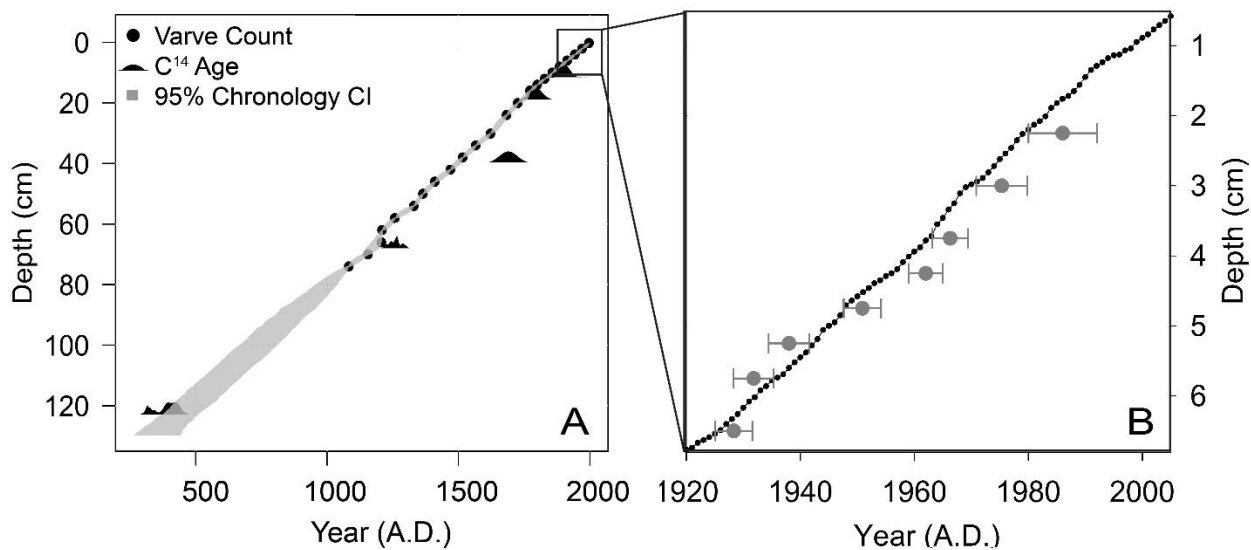


**Figure 4.2: A) Age-depth model for the sedimentary record of Basin Pond, with age measured in Years AD. Black markings indicate dated positions through varve counting (varve counts every 4-cm are marked), radiocarbon dating, and lead-210 dating. Grey shading indicates the 95% confidence interval at any given depth. B) Age model for 1920AD – present day. Gray points indicate <sup>210</sup>Pb dates with associated errors, while black points are varve counts.**

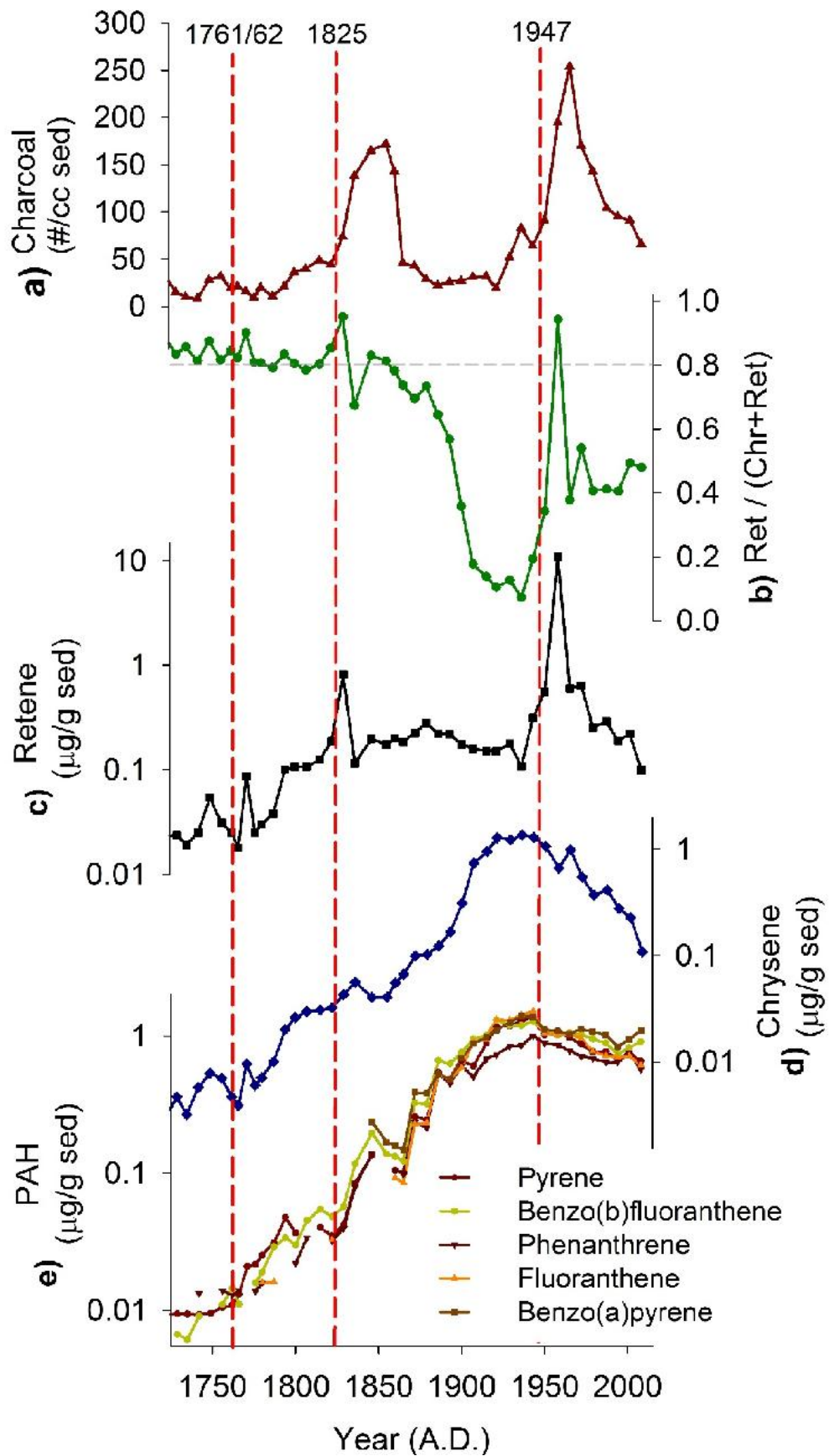


**Figure 4.3: Fire reconstructions from the historical period (1725AD to present day).  
From top to bottom: charcoal counts per cm<sup>3</sup> sediment (red triangles), the  
retene/(chrysene + retene) ratio (green circles), retene concentrations (black  
squares), chrysene concentrations (blue diamonds), and the top 5 most abundant  
PAH (excluding retene and chrysene) measured in the sedimentary record. All PAH  
concentrations are reported in µg / g sediment extracted.**

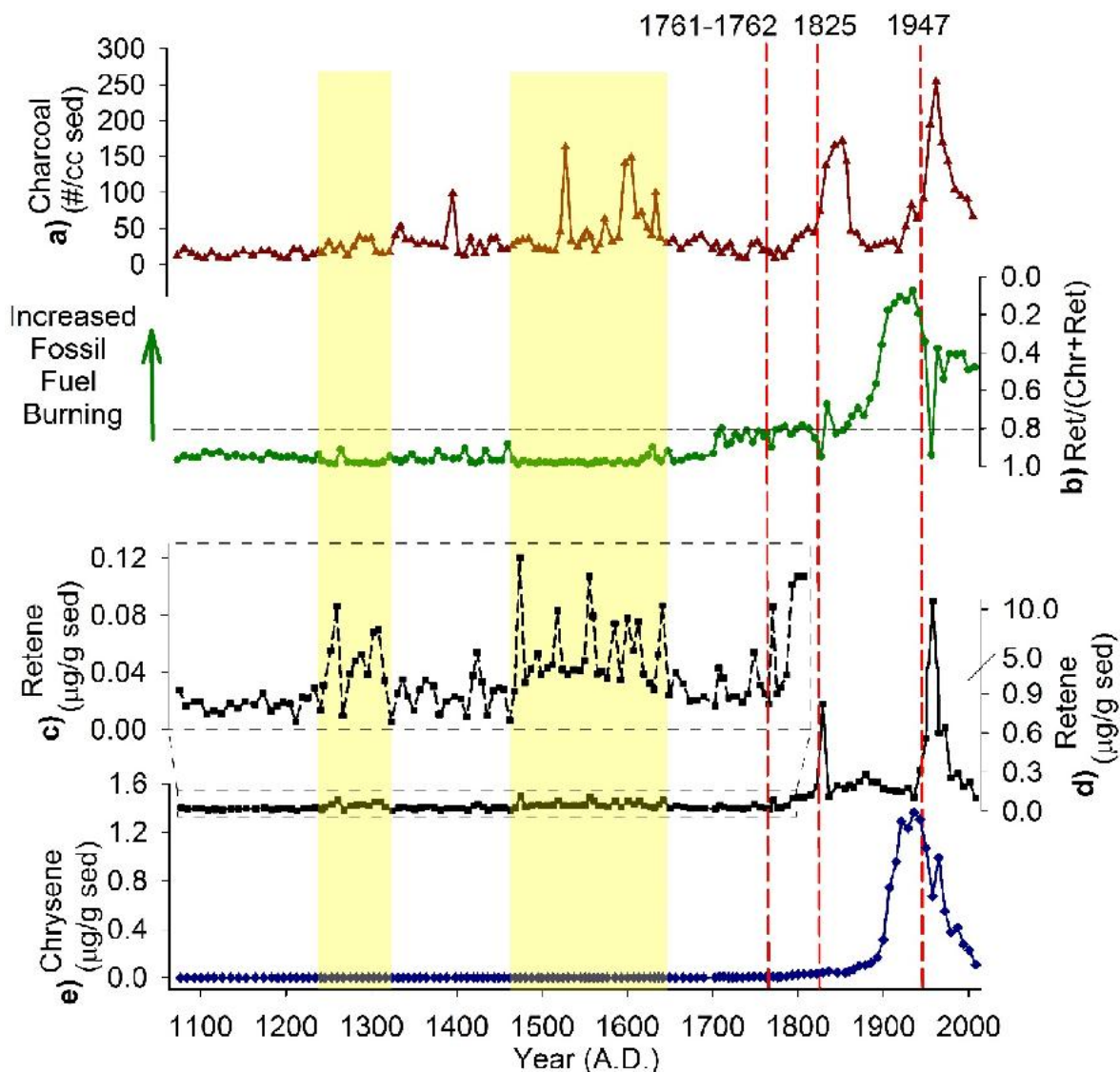


**Figure 4.4: Fire reconstructions from Basin Pond, ME since 1100 AD; a) charcoal counts per  $\text{cm}^3$  sediment (red triangles), b) the retene/(chrysene + retene) ratio (green circles), c-d) retene (black squares and black dashed squares) and e) chrysene concentrations (blue diamonds), measured in  $\mu\text{g} / \text{g}$  sediment extracted.**

Due to the drastic increase in retene concentrations in the historic period from background levels, pre-historic retene has been plotted twice (dashed black line) in panels c and d. Note the difference in the y-axis scale between plots c and d and also the scale break in plot d. The retene/(chrysene + retene) ratio, shown in plot b, used as an indicator of PAH combustion source, remains above 0.8 throughout the pre-historic record, while decreasing below 0.8 from regional industrialization marked with several increases to above 0.8 following fire events (0.8 marked by dashed, horizontal line). Fire events of 1761-1762 AD, 1825 AD, and 1947 AD are marked by dashed vertical lines. Increased periods of fire activity outside of those noted in historical records, which are suggested by our data, are shaded in yellow.

## CHAPTER 5

# A 900-YEAR NEW ENGLAND TEMPERATURE RECONSTRUCTION FROM *IN SITU* SEASONALLY PRODUCED BRANCHED GLYCEROL DIALKYL GLYCEROL TETRAETHERS (BRGDGTS)

Daniel R. Miller<sup>1,2</sup>, M. Helen Habicht<sup>2</sup>, Benjamin A. Keisling<sup>2</sup>, Isla S. Castañeda<sup>2</sup>,  
Raymond S. Bradley<sup>1,2</sup>

<sup>1</sup>Northeast Climate Adaptation Science Center, University of Massachusetts Amherst,  
Amherst, MA 01003, United States

<sup>2</sup>Climate System Research Center, Department of Geosciences, University of  
Massachusetts Amherst, Amherst, MA 01003, United States

*Correspondence to:* Daniel R. Miller (dmiller@geo.umass.edu)

AS SUBMITTED, ACCEPTED, AND PUBLISHED  
IN THE JOURNAL CLIMATE OF THE PAST

### CITATION:

Miller, D.R., Habicht, M.H., Keisling, B.A., Castañeda, I.S., Bradley, R.S., 2018. A 900-year New England Temperature Reconstruction from In Situ Seasonally Produced Branched Glycerol Dialkyl Glycerol Tetraethers (brGDGTs). *Climate of the Past*, 14, 1653-1667, <https://doi.org/10.5194/cp-14-1653-2018>.

## 5.1 Abstract

Paleotemperature reconstructions are essential for distinguishing anthropogenic climate change from natural variability. An emerging method in paleolimnology is the use of branched glycerol dialkyl glycerol tetraethers (brGDGTs) in sediments to reconstruct temperature but their application is hindered by a limited understanding of their sources, seasonal production, and transport. Here, we report seasonally resolved measurements of brGDGT production in the water column, in catchment soils, and in a sediment core from Basin Pond, a small, deep inland lake in Maine, USA. We find similar brGDGT distributions in both water column and lake sediment samples but the catchment soils have distinct brGDGT distributions suggesting that (1) brGDGTs are produced within the lake and (2) this in situ production dominates the downcore sedimentary signal. Seasonally, depth-resolved measurements indicate that most brGDGT production occurs in late fall, and at intermediate depths (18-30 meters) in the water column. We utilize these observations to help interpret a Basin Pond brGDGT-based temperature reconstruction spanning the past 900 years. This record exhibits similar trends to a pollen record from the same site and also to regional and global syntheses of terrestrial temperatures over the last millennium. However, the Basin Pond temperature record shows higher-frequency variability than has previously been captured by such an archive in the Northeastern United States, potentially attributed to the North Atlantic Oscillation and volcanic or solar activity. This first brGDGT-based multi-centennial paleo-reconstruction from this region contributes to our understanding of the production and fate of brGDGTs in lacustrine systems.

## 5.2 Introduction

Anthropogenic climate change is one of the most complex and challenging issues facing the world today and its impacts will likely be exacerbated in heavily populated areas, such as the Northeastern United States (NE US) (Fig. 1), a region comprised of communities that have been historically susceptible to climate change (Horton et al., 2014). Here, over the past 120 years average temperatures have increased by  $\sim 1^{\circ}\text{C}$ , precipitation has increased by 10%, and sea levels have risen by  $\sim 40$  cm (Kunkel, 2013; NOAA, 2014). While historical records document the temperature increase of the past century, they are not long enough to capture the underlying variability of the pre-anthropogenic period. Therefore, high-resolution paleotemperature records, such as those developed from lacustrine sedimentary sequences, are needed to investigate how current climate change compares to long-term natural variability. A regional synthesis of NE US late Holocene climate variability by Marlon et al. (2017) reviews temperature reconstructions from terrestrial sediment records using methods such as pollen (Gajewski, 1987; Webb et al., 2003; Oswald et al., 2007), testate amoeba (Clifford and Booth, 2013), and leaf wax hydrogen isotopic ratios (Huang et al., 2004, Shuman et al., 2006; Gao et al., 2017). However, these climate proxies may also reflect changes in parameters other than temperature (i.e., precipitation, humidity, evapotranspiration, and vegetation) (Gajewski, 1988; Hou et al., 2008; Marlon et al., 2017). Therefore, additional quantitative paleotemperature records are needed to accurately assess past temperature variability in the NE US (Marlon et al., 2017).

Branched glycerol dialkyl glycerol tetraethers (brGDGTs), found globally in lakes, soils, rivers, and peats, provide an independent terrestrial paleothermometer well-

suited to this task (e.g. Weijers et al., 2007; Peterse et al., 2012; De Jonge et al., 2013; Buckles et al., 2014; De Jonge et al., 2015). BrGDGTs are comprised of two ether-linked dialkyl chains containing zero to two methyl branches (prefixes I, II, and III) and zero to two cyclopentane moieties (suffixes a, b, and c) (Sinninghe Damsté et al., 2000). Although the source organisms are unknown, these compounds are thought to be produced by Acidobacteria (e.g., Sinninghe Damsté et al., 2011; Sinninghe Damsté et al., 2018). Noting a strong correlation between mean annual air temperature (MAAT) and the degree of methylation of brGDGTs in global soils, Weijers et al. (2007) proposed that sedimentary brGDGTs could be used as a proxy for past soil temperature, which in many cases is similar to mean annual air temperature. This motivated the development and later refinement of two indices, based on the degree of methylation and cyclization of brGDGTs (MBT and CBT), which were correlated to temperature and pH, respectively (e.g. Weijers et al., 2007; Peterse et al., 2012; De Jonge et al., 2014a).

More recently, improved chromatographic separation techniques for brGDGTs have been developed and indicated the presence of 5- and 6-methyl brGDGT isomers (De Jonge et al., 2013; De Jonge et al., 2014; Hopmans et al., 2016). The 6-methyl isomers may be abundant in environmental samples (De Jonge et al., 2014b), and failure to account for the presence of these compounds can have a significant influence on reconstructed temperatures (De Jonge et al., 2013; De Jonge et al., 2014a). Importantly, De Jonge et al. (2014a) demonstrated that soil pH (CBT) does not have an influence on the degree of methylation (MBT) and that earlier observations suggesting an influence of pH on methylation (Weijers et al., 2007) were the result of incomplete isomer separation. A new index based on the 5-methyl brGDGTs (MBT<sub>5ME</sub>) was developed and calibrated

to temperature using a global soils dataset (De Jonge et al., 2014). MBT'<sub>5ME</sub> and 5-methyl fractional abundances have recently been calibrated for temperature reconstruction in lakes from East Africa (Russell et al., 2018) and China (Dang et al., 2018), respectively.

Initially, brGDGTs were presumed to be exclusively produced in soils, and subsequently washed into lakes or marine environments via erosion by rivers and streams (Hopmans et al., 2004). Further research demonstrated these compounds are also produced *in situ* in lakes and rivers (e.g. Tierney and Russell, 2009; Bechtel et al., 2010; Tierney et al., 2010; Zhu et al., 2011; Loomis et al., 2012; Schoon et al., 2013; Zell et al., 2013). Although some studies suggest that distinct brGDGTs are produced within the water column of lakes (Colcord et al., 2015; Weber et al., 2015) and show that their production is seasonally biased (e.g. Buckles et al., 2014; Loomis et al., 2014), relatively limited work has been done to understand their in-situ production and its consequences for the sedimentary brGDGT record (Zhang et al., 2016). Knowledge of brGDGT production and seasonality is important for appropriately calibrating and interpreting downcore records, yet few studies have combined modern observations of brGDGT distributions in the environment with a paleoclimate reconstruction for a temperate lake system.

Here we examine brGDGT abundances and distributions in catchment soil samples and at varying depths in the water column throughout the year at an inland lake in the NE US (Fig. 1). We collected samples from 2014–2015 to assess the seasonality and location of brGDGT production in and around Basin Pond, ME. We then use our observations to help interpret a 900 year-long relative temperature record, providing the

first decadal-resolved brGDGT-derived lacustrine paleoclimate reconstruction for this region.

### **5.3 Site information and field sampling**

#### **5.3.1 Study Site**

Basin Pond, located in Fayette, ME (44° 28' N, 70° 03' W, elevation 124 m above sea level), is a small, deep lake with an area of 0.14 km<sup>2</sup> and a maximum depth of 32.6 m (Fig. 1). Basin Pond is fed from groundwater and precipitation, with one small, dammed, outlet stream running westward into the adjacent David Pond (Frost, 2005). Most of the 0.53 km<sup>2</sup> catchment area is dominated by a well-developed deciduous hardwood and evergreen forest, with only one residential building. Mean annual air temperature at Basin Pond is ~5.9°C and average annual precipitation is ~1150 mm (NOAA, 2014).

Basin Pond contains a unique sedimentary sequence comprised of annual laminations (varves) due to permanent water column stratification (Wetzel, 1983; Frost, 2005) resulting from a persistent thermocline. This stratification causes permanent bottom water anoxia, which enhances the preservation of annual laminations throughout the record (O'Sullivan, 1983). The Basin Pond varves are biogenic, with couplets comprised of a lighter, diatom-rich summer layer and a darker, humic winter layer (Frost, 2005).

The extent of anthropogenic impacts to Basin Pond and its catchment area have varied over the study interval. Although people were certainly present in Maine for the past 900 years, European-settler land clearance did not begin until the mid-1700s (Foster and Aber, 2004). It is uncertain whether the Basin Pond catchment was affected by this

process. Due to its relatively remote location in New England, Maine experienced substantially less deforestation compared with the other NE US states (Foster and Aber, 2004). However, polycyclic aromatic hydrocarbons (PAHs) reflecting regional anthropogenic activity indicate that industrialization is notable in the Basin Pond sedimentary record (Miller et al., 2017). Furthermore, the lake's natural chemistry was disrupted in the 1950s, when Basin Pond was treated with a chemical piscicide, Rotenone (United States Geological Survey, 1996). Today, the lake is lightly used for recreation by members of the Basin-David-Tilton Ponds Association.

### **5.3.2 Sediment Coring**

Sediment coring was performed from ice in March 2014, in the deepest part of the lake at 32 m (44° 27' 27" N, 70° 03' 09" W), using a UWITEC gravity coring system. Core BP2014-3D (52 cm) captured an undisturbed sediment-water interface and was subsampled in the field at 0.5 cm resolution for radioisotopic dating. Core BP2014-5D (174 cm) was immediately capped upon retrieval. Cores were split, photographed, and non-destructive down-core logging was performed using an Itrax XRF core scanner with a Molybdenum tube at 100  $\mu$ m resolution in the Department of Geosciences at University of Massachusetts Amherst. Cores were kept refrigerated for one month prior to subsampling. Subsamples were stored frozen in WhirlPak bags until extraction.

### **5.3.3 Sediment trap construction, deployment and retrieval**

Sediment traps were designed and constructed at University of Massachusetts Amherst. Sediment trap collection cones were made of high density polyethylene (HDPE) with a diameter of ~1 m (Fig. 1) and attached to 4L bottles for settling

particulate matter (SPM) collection (Fig. 1). Note that our definition of SPM includes both material suspended in the water column and settling into the traps. Five sediment traps were deployed on May 27, 2014 at 6, 12, 18, 24, and 30 meter depth (Fig. 2). SPM was collected from all traps on 7/2/14, 8/16/14, 9/14/14 and 6/5/15. Each trap continuously accumulated SPM from deployment until collection and therefore each sample represents material collected over 36, 40, 28, and 264 days, respectively. The length of the last sampling period of 264 days was due to ice cover at the lake; sediment trap recovery was not possible until ice out. SPM labels on Figures 2, 3, & 5 and throughout the discussion are referred to by the month that was the midpoint of each collection period. Thus, the four sampling periods listed above are referred to respectively as June, July, September, and January SPM. Catchment soil samples were also collected around the perimeter of the lake at the time of initial trap deployment. All soil and water SPM samples were kept frozen until analysis.

## **5.4 Methods**

### **5.4.1 Sedimentary Age Model**

Subsamples for past climate reconstruction were taken every 0.5 cm from the uppermost 68 cm of core BP2014-5D. The age model for Basin Pond is based on  $^{210}\text{Pb}$ , varve counts, and five  $^{14}\text{C}$  dates and was previously published by Miller et al., (2017). The sediment examined here ranges in age from modern to ~1100 BP, with a sampling resolution of 4 to 13 years (median: 7) (Miller et al., 2017).

### 5.4.2 Laboratory Methods

Overall, 10 catchment soil, 19 SPM sediment trap samples, and 136 sediment core samples were analyzed. Soil and lake sediment samples were freeze-dried and homogenized prior to extraction. For SPM samples, water from each collection bottle was filtered through a 47mm, 0.3- $\mu\text{m}$  combusted Sterlitech glass fiber membrane filter, and dried prior to extraction. For most samples, a total lipid extract (TLE) was obtained using a Dionex Accelerated Solvent Extractor (ASE 200) with a mixture of dichloromethane (DCM)/ methanol (MeOH) (9:1, v/v). For four SPM samples, plastic filters were washed and sonicated with HPLC-grade water, which was subsequently extracted with DCM three times. TLEs from SPM and catchment soil samples were separated into apolar (9:1 DCM/hexane v/v) and polar (1:1 DCM/MeOH v/v) fractions, while the lake sediment samples were separated into apolar, ketone (1:1 hexane/DCM) and polar fractions using alumina oxide column chromatography. For all samples, one half of each polar fraction was filtered through 0.45 $\mu\text{m}$  PTFE syringe filters using 99:1 hexane/isopropanol (v/v). 0.1  $\mu\text{g}$  of  $\text{C}_{46}$  GDGT internal standard was added to each polar fraction prior to analysis. The other half of each polar fraction was derivatized using bistrimethylsilyltrifluoroacetamide (BSTFA), and algal biomarkers were identified with a Hewlett-Packard 6890 Series gas chromatograph coupled to an Agilent 5973 mass spectrometer (GC-MS) using a Restek Rtx-5ms (60m x 250 $\mu\text{m}$  x 0.25  $\mu\text{m}$ ) column. Algal biomarkers, (iso)loliolide,  $\text{C}_{30}$  1, 13 *n*-alkyl diol, dinosterol/stanol, and  $\beta$ -sitosterol/stanol, were quantified with an Agilent 7890A dual gas chromatograph-flame ionization detector (GC-FID) equipped with two Agilent 7693 autosamplers and two identical columns (Agilent 19091J-416: 325  $^{\circ}\text{C}$ : 60m x 320 $\mu\text{m}$  x 0.25  $\mu\text{m}$ , HP-5 5% Phenyl Methyl

Siloxan). For both the GC-MS and GC-FID, helium was used as the carrier gas. The ovens began at a temperature of 70 °C, increased at 10 °C min<sup>-1</sup> to 130 °C, increased again at 4 °C min<sup>-1</sup> to 320 °C, and then held for 10 minutes. The GCs were run in splitless mode. Compounds were quantified using an external calibration curve where squalane was injected at multiple concentrations ranging from 2 to 100 ng/μl; r<sup>2</sup> values for linearity tests were >0.99.

### 5.4.3 brGDGT analysis

Polar fractions were analyzed on an Agilent 1260 high performance liquid chromatograph (HPLC) coupled to an Agilent 6120 Quadrupole mass selective detector (MSD). Compound separation was achieved using the method of Hopmans et al. (2016). The technique uses two Waters UHPLC columns in series (150 mm × 2.1 mm × 1.7 μm) and isocratically elutes brGDGTs using a mixture of hexane (solvent A) and hexane: isopropanol (9:1, v:v, solvent B) in the following sequence: 18% B (25 minutes), linear increase to 35% B (25 minutes), linear increase to 100% B (30 minutes). Mass scanning was performed in selected ion monitoring (SIM) mode. brGDGTs were quantified with respect to the C<sub>46</sub> standard, assuming equal ionization efficiency for all compounds. For calculation of MBT'<sub>5ME</sub>, CBT'<sub>5ME</sub>, and the Isomer Ratio (IR), the following equations were used from De Jonge et al. (2014a&b):

$$\text{MBT}'_{5ME} = \frac{\text{Ia}+\text{Ib}+\text{Ic}}{\text{IIa}+\text{IIa}+\text{IIb}+\text{IIc}+\text{Ia}+\text{Ib}+\text{Ic}} \quad \text{Eq. (1)}$$

$$\text{CBT}'_{5ME} = -\log\left(\frac{\text{Ib}+\text{IIb}}{\text{Ia}+\text{IIa}}\right) \quad \text{Eq. (2)}$$

$$IR = \frac{IIa' + IIb' + IIc' + IIIa' + IIIb' + IIIc'}{IIa + IIa' + IIb + IIb' + IIc + IIc' + IIIa + IIIa' + IIIb + IIIb' + IIIc + IIIc'} \quad \text{Eq. (3)}$$

For samples measured in duplicate (n=32), the maximum MBT'<sub>5ME</sub> difference was < 0.01, while the maximum CBT'<sub>5ME</sub> was 0.01; thus analytical error associated with proxy application is insignificant.

#### 5.4.4 Time Series Analysis

To analyze the variance in the data presented here, we used the *Astrochron R* package (Meyers, 2012). Pre-processing of the data was kept to a minimum to avoid introducing spurious signals. The downcore brGDGT reconstruction was re-interpolated to 7-yr resolution (equivalent to median resolution of the raw data, see results) prior to spectral analysis. The published PAGES2k datasets were analyzed with their published chronologies, which is 1 year resolution for most regions and 10 years for the North American tree-ring based reconstruction (PAGES2k, 2013). Each of these reconstructions were smoothed to 7 year averages for easier comparison to our record.

#### 5.5 Results

BrGDGTs were present in all soil, SPM and sediment core samples analyzed. In contrast, isoprenoid GDGTs, on which the TEX<sub>86</sub> temperature proxy is based (Schouten et al., 2002), were absent in a majority of samples or present in very low abundances compared to the brGDGTs. Therefore, TEX<sub>86</sub> could not be utilized as a temperature proxy at Basin Pond.

### 5.5.1 Catchment Soils

BrGDGTs Ia and IIa dominated distributions in the catchment soil samples, with relative abundances of  $65\% \pm 13\%$  and  $28\% \pm 7\%$ , respectively (Fig. 2). The next largest relative abundances were IIIa and Ib, comprising  $3\% \pm 6\%$  and  $3\% \pm 1\%$ , respectively (Fig. 2). Total brGDGT concentrations in soils ranged from 1.5 to 7.3 (median = 2.2)  $\mu\text{g}\text{sed}^{-1}$ .

### 5.5.2 SPM

BrGDGTs Ia, IIa and IIIa dominated distributions in the SPM samples, with relative abundances of  $28\% \pm 8\%$ ,  $37\% \pm 7\%$ , and  $30\% \pm 8\%$ , respectively (Fig. 2). The next largest relative abundances were Ib and IIb, each comprising  $2\% \pm <1\%$ . In June and July 2014, group I brGDGTs were the most abundant, whereas in September 2014 and January 2015 reductions in group I brGDGTs were accompanied by increases in group III brGDGTs (Fig. 2). Overall, fluxes of brGDGTs were highest in September 2014 (ranging from 0.36 to 15.2  $\text{ng m}^2 \text{day}^{-1}$  at different depths) (Fig. 3). In June and July 2014, total brGDGT fluxes at various depths ranged from 0.009 to 0.04  $\text{ng m}^2 \text{day}^{-1}$  and 0.04 to 0.14  $\text{ng m}^2 \text{day}^{-1}$ , respectively (Fig. 3).

BrGDGT fluxes and distributions also varied as a function of depth (Fig. 3,4, 5). In general, summed brGDGT fluxes increase with depth, with up to an order of magnitude higher fluxes at 30 m compared to 6 m for all dates (Fig. 3). BrGDGT fluxes in the upper and lower water column peaked in September with fluxes of 0.4 to 0.6  $\text{ng m}^2 \text{day}^{-1}$  and 7 to 16  $\text{ng m}^2 \text{day}^{-1}$ , respectively. The average distributions also changed as a function of depth. Group I brGDGTs comprised 30% of the distributions at all depths. Group II brGDGTs had the greatest abundance at 12 and 18 m water depth (Fig. 5),

comprising up to 50% of the distribution. Group III brGDGTs comprised an average of 30% with a peak of 35% at 30 m, and a minimum at 18 m of <20%. These distributions lead to variations in  $MBT'_{5ME}$  and  $CBT'_{5ME}$  indices as a function of depth (Fig. 5).  $MBT'_{5ME}$  varied from 0.34 to 0.46, and peaked at 24 m water depth (Fig. 4).  $CBT'_{5ME}$  varied from 1.1 to 1.6, peaked at 12 m and then decreased with depth (Fig. 4).

### 5.5.3 Surface sediment samples

To represent surface sediments, we averaged the measurements from the uppermost 5 cm of Core BP2014-5D, corresponding to approximately 70 years (Miller et al., 2017). BrGDGTs Ia, IIa, and IIIa dominate the distribution, with relative abundances of 27%, 32%, and 33%, respectively (Fig. 3). The next largest relative abundances are IIb, Ib, and IIIb (3%, 2%, and 1%, respectively).  $MBT'_{5ME}$  values in surface sediments range from 0.35 to 0.45 (Fig. 6).

### 5.5.4 Sediment Core

BrGDGT concentrations in these samples ranged from 1.2 to 21.1 (median: 8.09)  $\mu\text{g gsed}^{-1}$ .  $MBT'_{5ME}$  ranged from 0.34 to 0.50 (median: 0.39).  $MBT'_{5ME}$  values fluctuate around a stable mean from 1100-1400 AD, then broadly decrease from ~1400 AD until the present day (Fig. 7). Decadal variability is superimposed on the long-term decreasing trend (Fig. 7). Prominent, multi-decadal low-  $MBT'_{5ME}$  value events are apparent from 1420–1444, 1500–1520, 1593–1627, 1762-1829, and 1908–1950 AD (Fig. 7). Multidecadal high-  $MBT'_{5ME}$  events are observed from 1261–1283, 1317–1351, 1556–1583, 1632–1657, 1829–1846 and 1958–1987 AD (Fig. 7). The brGDGT concentrations in the core range from 1.2-21.1  $\mu\text{g gsed}^{-1}$ , with a median of 8.2  $\mu\text{g gsed}^{-1}$ .

### 5.5.5 BrGDGT isomer ratios

The UHPLC method we utilized for brGDGT analysis (Hopmans et al., 2016) allows for the separation of 5- and 6-methyl brGDGT isomers (DeJonge et al., 2013; DeJonge et al., 2014). Analysis of the relative abundances of these isomers has also been used to identify different production sources of brGDGTs (e.g. soils vs. water column; DeJonge et al., 2014; Weber et al., 2015). The summed IR (equation 3) for soils, lake water and sediments at Basin Pond are significantly different. The IR value for soils is very low and averages 0.03, while the water samples and sediments are higher and average 0.26 and 0.30, respectively (Fig. 6).

### 5.5.6 Algal biomarkers

Samples in the upper 17cm of the sediment core were analyzed for the following algal lipid biomarkers: (iso)loliolide, C<sub>30</sub> 1, 13 *n*-alkyl diol, dinosterol/stanol, and  $\beta$ -sitosterol/stanol. Concentrations of (iso)loliolide ranged from 31-426  $\mu\text{g g sed}^{-1}$  (median=171). C<sub>30</sub> 1, 13 *n*-alkyl diol concentrations ranged from 8-1378  $\mu\text{g g sed}^{-1}$  (median=475). Dinosterol/stanol concentrations ranged from 12-5663  $\mu\text{g g sed}^{-1}$  (median= 1384). Concentrations of  $\beta$ -sitosterol/stanol concentrations ranged from 3-7955  $\mu\text{g g sed}^{-1}$ (median=1465).

## 5.6 Discussion

### 5.6.1 Sources and seasonal production of Basin Pond brGDGTs

It is important to constrain brGDGT sources before interpreting lacustrine sedimentary records. Multiple lines of evidence suggest brGDGTs deposited in Basin Pond sediments are predominantly produced within the water column, in agreement with

prior studies (e.g. Tierney and Russell, 2009; Buckles et al., 2014; Loomis et al., 2014). First, we observe significant differences in the fractional abundances of brGDGTs between soil, SPM and lake sediments (Figs. 2, 5), suggesting *in situ* production occurs in both soil and lacustrine environments, but that soil-derived brGDGTs do not exert a large influence on the Basin Pond sedimentary record. Average distributions of brGDGTs reveal that lake sediments and SPM are similar in group I and III content, while the soils differ substantially (Figs 2, 5). The relative amounts of 5- and 6-methyl brGDGTs also differs between soils and lake water and sediment (Figs 2, 5), and as seen in the average IR values (Fig. 6). MBT'<sub>5ME</sub> and CBT'<sub>5ME</sub> values for lake sediment and soils are distinct, while SPM samples are similar to lake sediment samples, consistent with *in situ* brGDGT production within Basin Pond (Fig. 6). The degree of cyclization (mean CBT'<sub>5ME</sub> = 1.2) is significantly lower in lake sediments than in soil samples (mean CBT'<sub>5ME</sub> = 1.5) (p value = 0.021 from two-tailed t-test), and brGDGTs are more methylated (p value = 0.003) in lake sediments (mean MBT'<sub>5ME</sub> = 0.38) than in soils (mean MBT'<sub>5ME</sub> = 0.7) (Fig. 6). This agrees with differences in brGDGT distributions recorded in other temperate (Tierney et al., 2012; Wang et al., 2012; Loomis et al., 2014) and tropical (Tierney and Russell, 2009; Loomis et al., 2012; Buckles et al., 2014) lakes and catchment area soils, and suggests *in situ* production of relatively more cyclized and methylated brGDGTs within lakes. In agreement with previous studies, we also note higher brGDGT concentrations in lake sediments (median = 8.2 µg g<sup>sed</sup><sup>-1</sup>) in comparison to watershed soils (median = 2.2 µg g<sup>sed</sup><sup>-1</sup>) (e.g. Sinninghe Damsté et al., 2009; Tierney and Russell, 2009) pointing to *in situ* brGDGT production.

BrGDGT fluxes at all depths are generally low throughout the summer months (June–July). A large flux increase at depth (18–30 m) occurs during September, when the lake is strongly stratified. Thus any transfer of brGDGTs from lower depths to the upper water column likely would be minimal. This suggests annual seasonal production of brGDGTs in Basin Pond, with a fall bloom occurring at intermediate (18–30 m) depths. Therefore, brGDGT temperatures recorded in the lake sediments likely reflect a seasonally biased (fall), rather than mean annual, temperature. We make the following observations based on these results. First, peak brGDGT flux is observed at 18-30 m water depth, suggesting that the organisms producing the most brGDGTs thrive in the mid to upper water column (Fig. 3). Secondly, peak brGDGT production occurs in September, suggesting that the sedimentary record will be biased toward brGDGTs produced during this period (Fig. 3). Finally, for the four time-periods sampled, brGDGT distributions (as described by  $MBT'_{5ME}$ ) correlate with temperature (Fig. S1). Interestingly, at depth the water temperature shows little to no seasonal cycle, remaining at approximately 4 °C for the entire year (Frost, 2005). Therefore, if maximum brGDGT production is indeed occurring here, it is possible that another parameter, which covaries with temperature on a seasonal scale (i.e. light duration, water chemistry, nutrient availability), may drive, or contribute to, the distribution of brGDGTs produced at depth at Basin Pond. However, the sediment trap at this depth represents an integrated signal of SPM produced in the water column, which could also be driving the temperature correlation at depth.

Although few studies are available for comparison, Loomis et al. (2014) studied brGDGTs in another temperate lake in the NE US (Lower King Pond, Vermont).

brGDGT production in Lower King Pond peaked during fall and spring and was linked to seasonal full water column mixing events (Loomis et al., 2014), which do not occur at Basin Pond (Frost, 2005). Moreover, Basin Pond is ten times larger by area and four times deeper than Lower King Pond. Similar to Lower King Pond, brGDGT production at Basin Pond seems to be seasonal, and calibration of brGDGTs against seasonal (in this case, fall) temperatures is a necessary area of future work to accurately reconstruct past absolute temperature change for this location. If the behaviour of brGDGTs in Lower King Pond and Basin Pond is representative of all temperate lakes, then calibration to fall or spring temperature may be the most appropriate choice for these settings.

### **5.6.2 Calibration of the 900 year brGDGT record to temperature**

Numerous studies have provided strong evidence for *in situ* brGDGT production in lakes and have shown that application of the global soils calibration to lacustrine sediments often yields temperatures that are unrealistically cold (e.g. Tierney and Russell, 2009; Bechtel et al., 2010; Blaga et al., 2010; Tierney et al., 2010a,b; Tyler et al., 2010; Pearson et al., 2011). Therefore, many lacustrine brGDGT calibrations have been developed (Tierney et al., 2010; Zink et al., 2010; Pearson et al., 2011; Sun et al., 2011; Loomis et al., 2012, Foster et al., 2016). However, many of these are based on relatively few samples or are geographically restricted (e.g. Tierney et al., 2010; Zink et al., 2010; Foster et al., 2016). Furthermore, at present, all available lacustrine brGDGT calibrations except for two (Dang et al., 2018; Russell et al., 2018) were developed using older HPLC methods that did not fully separate brGDGT isomers. As we measured our brGDGTs following the newer method of Hopmans et al. (2016), we investigated Basin Pond temperature reconstructions using only those calibrations based on the same technique.

The Dang et al. (2018) calibration is based on alkaline Chinese lakes and reconstructs temperatures ranging from 4-9 °C, while the Russell et al. (2018) calibration is based on African lakes and yields temperatures ranging from 10-14 °C (Fig. 7). The African lakes calibration from Russell et al. (2018) is based on  $MBT'_{5ME}$  while the Chinese lakes calibration of Dang et al., (2018) is based on fractional abundances of brGDGTs; therefore these two calibrations yield somewhat different trends with the Dang et al. (2018) calibration showing muted variability and some discrepancies from the other proxy records (i.e. during the last 50 years) (Figure 7).

Importantly, caution must be taken when interpreting the Basin Pond reconstructed temperatures using either of these calibrations because application of an African or Chinese calibration to lakes in the NE US is questionable as these regions are climatically different and their lakes differ in terms of stratification and mixing regimes. Furthermore, brGDGTs from Basin Pond are characterized by distinct brGDGT distributions from both the African (Russell et al., 2018) and alkaline Chinese lake sediments (Dang et al., 2018) (Figure 8). This suggests that application of either of these calibrations to Basin Pond sediments may not be appropriate. Local temperature data are available for Basin Pond over the period our measurements were made, but the SPM dataset presented here is not large enough to develop a robust local  $MBT'_{5ME}$  to temperature calibration (see Supplement). We thus present our results in the following discussion and figures simply in terms of the  $MBT'_{5ME}$  index, which provides a relative temperature indicator, where higher values reflect relatively higher temperatures and vice versa (De Jonge et al., 2014b).

Our interpretation of the 900-year MBT'<sub>5ME</sub> record is as follows. Based on the SPM samples, we argue that the downcore brGDGT reconstruction is likely weighted toward September temperature change in the NE US. We note that brGDGTs are present at all depths measured but peak at 18-30 m depth, indicating that the compounds reaching the lake floor represent an integrated signal from the entire water column. Although brGDGT concentrations vary down core, they are not correlated with reconstructed MBT'<sub>5ME</sub> values ( $p=0.25$ ), indicating that brGDGT production and MBT'<sub>5ME</sub> variability are largely decoupled. We observe an overall stepped cooling trend recorded by generally decreasing MBT'<sub>5ME</sub> values over the past 900 years (Fig. 9). Using the calibration of Russell et al. (2018), this overall cooling is on the order of 3.0 °C; however, for the reasons discussed earlier, we advise that caution must be taken when interpreting absolute temperature changes from applying this calibration to Basin Pond sediments.

### **5.6.3 Comparison to Regional Hydroclimate Records in the NE US**

Regional hydroclimate in the NE US has been reconstructed at several sites on similar timescales as the Basin Pond record. The MBT'<sub>5ME</sub> record indicates an overall cooling from ~1300 AD to ~1900 AD (Fig. 9), which is also observed in pollen-derived temperature reconstructions from Basin Pond (Gajewski, 1988). Both records also indicate two major cooling steps, although the exact timing of these differs between records, which may be attributable to age model differences (Fig. 9). Apparent differences between the Basin Pond records are likely also associated with sampling resolution; the pollen record has varying and generally much lower sample resolution in comparison to our MBT'<sub>5ME</sub> record. Furthermore, some of the differences in MBT'<sub>5ME</sub> and pollen reconstructions may be caused by differences in proxy seasonality, with pollen

representing a summer signal (Gajewski, 1988) and MBT'<sub>SME</sub> likely representing a fall signal.

The general long-term cooling trend from Basin Pond is also observed in a hydrogen isotope-based temperature reconstruction from Little Pond, Massachusetts (Gao et al., 2017). Both records show higher temperatures between 1300-1400 AD (Fig. 9). Bog records provide additional, high-resolution reconstructions of hydrological conditions in the NE US over this time period via analysis of testate amoeba (a proxy for water table depth) and the *Sphagnum*/Vascular Ratio (SVR) (Nichols and Huang, 2012; Clifford and Booth, 2013). The testate amoeba records show that the last 400 years (i.e., 1600–2000 AD) have been generally wetter than the preceding 400 years (1200-1600 AD). However, unlike the temperature reconstructions, these records do not show a long-term linear trend (Fig. 9).

These cooling and wetting trends are surprising given the record of fire history at Basin Pond (Miller et al., 2017), which shows five periods of increased charcoal deposition since 1100 AD (Fig. 9). It is important to note that wildfire activity is a complex phenomena, with multiple factors affecting fire occurrence apart from climate variability (Marlon et al., 2017). However, our data suggest that fire activity in the NE US may be influenced more by shorter-term (multi-decadal) variations in climate, particularly seasonal cooling superimposed on dry conditions, as opposed to longer-term, multi-centennial climate trends. Surprisingly, the first 200 years of the record (1100–1300 AD) are dominated by warm and dry conditions, but no fire events were recognized during this period. Three fire events (Fig. 9g), between ~1300 and ~1700 AD, are associated with regionally dry conditions (Fig. 9d-f). Although average Basin Pond

MBT'<sub>5ME</sub> values are higher on a multi-centennial time-scale during this interval, the fire events themselves occur synchronously with multi-decadal cold periods (Fig. 9a-c). Furthermore, two recent fire events occurred during the historical period, which is reconstructed as relatively cool and wet (Fig. 9). Therefore, it appears that at Basin Pond, temperature did not exert a major influence over fire occurrence.

#### **5.6.4 Comparison with Northern Hemisphere records**

A compilation of Northern Hemisphere temperature records for the last 2000 years reveals sustained warmth from 830–1100 AD, just prior to the beginning of our reconstructions (PAGES2k, 2013). Northern Hemisphere climate then entered a cooler phase, though the timing of this transition varied regionally between 1200 and 1500 AD (PAGES2k, 2013). North American pollen data show elevated, though decreasing, temperatures through 1500 AD (Gajewski, 1988; PAGES2k, 2013) (Fig. 10). From 1100–1400 AD, Basin Pond MBT'<sub>5ME</sub> values are high in contrast with European and Arctic temperature reconstructions. From 1500–1900 AD, MBT'<sub>5ME</sub> values are lower, in better agreement with other Northern Hemisphere reconstructions. Moreover, the decadal to centennial scale variability observed in MBT and other records during this time may be linked to variability in Atlantic Multidecadal Oscillation (AMO) and North Atlantic Oscillation (NAO) indices (Figure 8). We note that the brGDGT MBT'<sub>5ME</sub> values are better correlated with regional tree-ring records and compilations of European and Arctic temperatures, which all show warm anomalies, followed by cooling, earlier this century. Thus, the multi-centennial structure of the brGDGT record from Basin Pond is supported by other local, regional, and global records (PAGES2k, 2013). On a multi-decadal scale, there is variability potentially associated with volcanic events recognized as having a

global impact. Five intervals during the last millennium were defined as ‘volcanic-solar downturns’: 1251–1310, 1431–1520, 1581–1610, 1641–1700, and 1791–1820 AD (PAGES2k, 2013). All but the most recent (1908–1950 AD) of the cool events are present in the Basin Pond MBT’<sub>5ME</sub> record during these periods (or within the age model uncertainty) (Fig. 10 highlighted in blue).

There is some similarity between the Basin Pond reconstruction and other Northern Hemisphere reconstructions (PAGES2k, 2013) (Fig. 10). The brGDGT record is also peppered with warm (high MBT’<sub>5ME</sub>) anomalies; many of these seem to be coherent with tree-ring based reconstructions of North American climate (i.e. 1300, 1550, 1830 AD) and are sometimes associated with negative phases of the NAO (Fig. 10). The sensitivity of the Basin Pond sediment record to regional scale climatic variations is highlighted by time series analysis. Multispectral taper method analysis reveals a persistent cycle in the brGDGT-based temperature reconstruction with a period of 57–63 years (Fig. 10). The Northern Hemisphere tree-ring compilation also shows a cyclicity with a period of 60 years (Fig. 10). However, the fact that the two datasets are not significantly correlated indicates the variability at 60-year periods is not exactly in-phase over the 900 year period covered by the two records. Cross-correlation analysis indicates that the correlation between the two datasets is strongest when the tree-ring reconstruction is lagged by 42 years relative to the Basin Pond temperature record ( $r=0.33$ ,  $p=0.04$ ). Significant spectral peaks with a similar period exist in the annually-resolved records from Europe (period = 65 yr), Asia (period = 58 yr) and the Arctic (period = 58 yr) (PAGES2k, 2013). However, the same analyses applied to South American, Australasian, and Antarctic reconstructions do not show spectral peaks at this

period (PAGES2k, 2013). Thus, it appears that the Basin Pond brGDGT record captures variability that is representative of, but not necessarily in-phase with, the Northern Hemisphere at large. One possible mechanism to explain this is the North Atlantic Oscillation (NAO), which exhibits a quasi-periodic oscillation of ~60 yr (Sun et al., 2015). While the NAO has some regionally coherent climatic effects, the signature of positive and negative NAO modes is spatially heterogeneous and complex; this could explain the phase offset in the ~60 yr band between the Basin Pond record and the other Northern Hemisphere reconstructions.

Another possible driver of the MBT'<sub>5ME</sub> changes we see is the AMO, which is based on sea surface temperature anomalies in the North Atlantic and shows variability in quasi-periodic 60–80 yr cycles (Trenberth et al., 2017). An AMO reconstruction spanning the last 400 years shows some similarities to the MBT'<sub>5ME</sub> reconstruction from Basin Pond. Although the records do not show a strong cross correlation ( $r=0.08$ ,  $p=0.53$ ), they feature apparently synchronous cool and warm periods (i.e. 1550 - 1650 AD and 1780 – 1830 AD) (Fig. 10). This suggests that climate at Basin Pond is coupled to Atlantic sea surface temperatures on multi-decadal timescales. Thus, the record presented here may prove useful in the future for reconstructing changes in the AMO earlier in the paleorecord.

### **5.6.5 20th Century temperature, brGDGT Reconstructions and Algal Community Shifts**

Daily temperature averages from meteorological stations in the state of Maine were accessed and obtained through the National Climatic Data Center from 1895 – present day (NOAA, 2014) (Fig. 5.11). Average temperatures in Maine have warmed by

~1.5°C since 1895 AD (Fig. 11). The temperature increase is dominated by changes from 1895-1945 AD and 1985-present; for the forty intervening years mean temperatures were more stable, with a slight cooling observed during fall (Fig. 5.11). Interannual variability of +/- 1°C is observed throughout the record, with the most pronounced variability during the winter (NOAA, 2014).

Interestingly, variations in MBT'<sub>5ME</sub> values for the last 100 years do not agree with instrumental observations. The brGDGT-based reconstruction shows stable values from 1900-1950 AD, followed by an abrupt increase (warming) in MBT'<sub>5ME</sub> of 0.1 until approximately 1975 AD (three data points), and a subsequent continual decrease since then (five data points) (Fig. 5.11). In contrast, instrumental records indicate a slight cooling, or at least a stabilization of warming, starting at the same time (1960s-70s) when the MBT'<sub>5ME</sub> values are increasing (Fig. 5.11). We note decreasing MBT'<sub>5ME</sub> values in the upper 3.5 cm (Fig. 5.11). Low MBT'<sub>5ME</sub> values in surface and core top sediments have been noted in other studies as well (e.g. Sinninghe Damsté et al., 2012; Tierney et al., 2012), indicating that this feature occurs in different regions and environments, and may be driven by mechanisms associated with brGDGT production or preservation. Tierney et al. (2012) note a similar pattern in the brGDGT distributions of Salt Pond (RI) surface sediments that we observe at Basin Pond where the shallow surface sediments are characterized by more methylated brGDGTs. These authors suggest that more methylated brGDGTs present in shallow lake sediments do not survive diagenesis and they also note that deeper sediments yielded reasonable brGDGT reconstructed temperatures (Tierney et al., 2012). This hypothesis requires further testing and additionally, other influences such as changes in brGDGT producer, post-depositional mobility and/or overprinting of the

brGDGT signal, biotic and abiotic compound diagenesis, and anthropogenic impacts to lake ecosystems should be examined as well. Despite the uncertainties about the MBT'<sub>5ME</sub> record during the last 100 years, we believe that the Basin Pond brGDGT record is useful for describing regional climate evolution over the last millennium in the NE US.

It is possible that land-use change and other anthropogenic impacts have affected the brGDGT record over the last 100 years. However, known land use change in the Basin Pond catchment is minimal over the past century (Gajewski, 1988). A complicating factor is the addition of the piscicide rotenone to the lake in 1955 to remove fish species in competition with trout (USGS, 1996). While the estimated lifetime of rotenone in the water column is short (days to weeks), it has been shown to have lasting long-term (years) effects on zooplankton communities and lake productivity (Kiser, 1963; Andersen, 1970; Sanni and Waervagen, 1990).

In lacustrine environments, some classes of lipid biomarkers, specifically sterols and stanols, can give valuable insight into variability of lake productivity of certain types of algae throughout time. Many sterols (and their saturated counterparts, stanols) are indicative of certain groups of source organisms, in particular, specific phytoplankton groups (e.g. Volkman et al., 1998; Volkman, 2003). For example, dinosterol and dinostanol are found in dinoflagellates and are not produced in higher plants, and are therefore used as a biomarker for dinoflagellate species (Volkman et al., 1998). The compounds isololiolide and loliolide are known to be anoxic degradation products of diatom pigments (Klok et al., 1984; Repeta, 1989) while long-chain alkyl diols are produced by eustigmatophyte (yellow-green) algae (Volkman et al., 1998). At Basin

Pond, several algal biomarker concentrations, including isololiolide/loliolide, dinosterol/stanol, and C<sub>30</sub> 1,13 *n*-alkyl diol, decrease following the rotenone treatment in 1955 AD while  $\beta$ -sitosterol (a biomarker of higher plants) increases (Fig. 5.11) suggesting a shift in the overall algal community structure. Additionally, after 1955 contributions of the different algal biomarkers are remarkably stable in comparison to earlier times (Fig. 5.11). Due to the widespread shift in algal community, we posit that bacterial communities and therefore brGDGT production may also have been impacted. However, brGDGT concentrations do not clearly respond to the rotenone treatment, and additional knowledge of brGDGT producers would be required to further investigate this idea.

## 5.7 Conclusions

We find evidence for seasonally-biased, *in situ* production of branched glycerol dialkyl glycerol tetraethers (brGDGTs) in a lake in central Maine, NE US. BrGDGTs are mostly produced in September at Basin Pond, and their downward fluxes in the water column peak at 30 m water depth. A downcore brGDGT-based reconstruction reveals both gradual and transient climate changes over the last 900 years and records cooling and warming events correlated with other Northern Hemisphere records and the NAO and AMO indices. This suggests inland Maine climate is sensitive to hemispheric climate forcing as well as changes in regional atmospheric pressure patterns and North Atlantic sea surface temperatures. Our new MBT'<sub>5ME</sub> temperature reconstruction, supported by a pollen record from the same site, reveals a prominent cooling trend from 1100–1900 AD in this area. Comparison with regional hydroclimate records suggests that despite increasingly cool and wet conditions persisting at Basin Pond over the last 900 years, fire

activity has increased. Although recent fire activity is likely anthropogenically triggered (i.e. via land-use change), our results imply an independent relationship between climate and NE US fire occurrence over the study interval. Thus, the paleotemperature reconstruction presented here alongside site-specific knowledge from Basin Pond informs our understanding of climatic variability in NE US beyond the era of human influence.

### **5.8 Data Availability**

BrGDGT data, including fractional abundances of 5- and 6-methyl isomers, BIT Index values, MBT'<sub>5Me</sub> values, CBT'<sub>5Me</sub> values, 5-methyl isomer ratio (IR), total brGDGT concentrations, and temperature calibrations (Dang et al., 2018; Russell et al., 2018) from Basin Pond watershed soils, SPM, and sediment samples are available at the National Oceanic and Atmospheric Administration National Centers for Environmental Information (NOAA NCEI) Paleoclimate Database. Concentrations of isololiolide/loliolide, C30 1,13 Diol, sitosterol/sitostanol, and dinosterol/dinostanol from the Basin Pond sediment core are also provided where measured. To access these data, please visit: <https://www.ncdc.noaa.gov/data-access/paleoclimatology-data/datasets>.

### **5.9 Author Contributions**

DRM, MHH, and BAK designed the sediment traps, carried out field work, processed samples through all stages of laboratory prep and analysis, and prepared the manuscript for publication. ISC and RSB provided advice throughout the experiment and writing process, aided with field work, contributed to data interpretation, and covered costs of sample analysis. Manuscript revisions were made through contributions from all co-authors.

## **5.10 Competing Interests**

The authors declare that they have no conflict of interest.

## **5.11 Acknowledgements**

The authors thank John Sweeney for his assistance in sediment trap construction and design. Jeff Salacup is acknowledged for technical laboratory assistance. We thank the members of the UMass Biogeochemistry Lab for helpful feedback and discussion. We are grateful to Lucas Groat, Christopher Mode, and Paige Miller-Hughes for their assistance in sediment trap deployment and collection. Dr. Mike Retelle, Dan Frost, Julie Savage, and the Bates College Geology Department are recognized for sediment coring assistance. We are indebted to the Basin-David-Tilton Ponds Association for their cooperation and support. Funding for this project was provided by grant G12AC00001 from the United States Geological Survey and the 2014 and 2015 Joe Hartshorn Memorial Award through the UMass Amherst Department of Geosciences. We thank J. Hou and an anonymous reviewer for their comments. We also acknowledge Liping Zhou and Denis-Didier Rosseau for editing this manuscript. Results are solely the responsibility of the authors and do not necessarily represent the views of the Northeast Climate Adaptation Science Center or the USGS.

## **5.12 Supplementary Information**

### **5.12.1 MBT'<sub>5ME</sub> Calibration to Local Temperature**

As addressed previously, the Basin Pond MBT'<sub>5ME</sub> record is presented without calibration to temperature. While the primary goal of this study was to understand the spatial and temporal variations in brGDGT production in Basin Pond in order to address

potential seasonal bias in a novel 900 year temperature reconstruction, developing a brGDGT to temperature calibration for Basin Pond (or a regional calibration for the NE US) is an important aspect of research that merits focus in future projects and work. As a first step towards this, we investigated a preliminary lake-specific calibration for MBT'<sub>5ME</sub> to air temperature using the SPM samples collected in this study, which shows promise. We compared MBT'<sub>5ME</sub> values to average daily air temperatures recorded at the closest weather station over each collection interval (Table 5.1, Figure 5.12a).

Measurements of water column temperature were not made. We note that during the January 2015 (late fall through spring) sample, only temperatures from ice-free dates were used in the average, as brGDGT production likely decreases drastically or ceases during times when the lake is ice covered. This is an assumption about brGDGT production that should be more thoroughly investigated in future work. Ice-in and ice-out dates (Table 5.1) were provided by the Maine Volunteer Lake Monitoring Program (MVLMP).

Through linear regression, we find a positive relationship between MBT'<sub>5ME</sub> and average temperature for each time period, with a correlation coefficient of  $\sim 0.4$  (Fig 5.12a). We applied this calibration downcore and compared to the two calibrations discussed in the manuscript (Fig 5.12b); the MBT'<sub>5ME</sub> African lakes calibration (Russell et al., 2018) and a calibration from Chinese Lakes (Dang et al., 2018). The Basin Pond calibration has a similar slope to that of Russell et al. (2018), resulting in nearly identical reconstructed temperature trends, with temperature values offset by  $\sim 1-2^{\circ}\text{C}$  (Figure 5.12b). While the Russell et al. (2018) calibration produces slightly lower than observed temperatures, the Dang et al. (2018) calibration produces far lower temperatures ( $10^{\circ}\text{C}$ )

than observed. The Dang et al. (2018) calibration also produces different temperature trends than those reconstructed by the  $MBT'_{5ME}$  calibrations (see section 5.5.2). Although the dataset is too short (4 data points) for a robust lake-specific calibration of  $MBT'_{5ME}$  against temperature, these initial results are promising, and provide support for future efforts to develop a calibration of  $MBT'_{5ME}$  to air and water temperature at Basin Pond. Currently, a new multi-year sampling campaign is underway in Basin Pond, with the goal of getting more data for a  $MBT'_{5ME}$  -temperature correlation to produce a reliable calibration. This campaign includes water column temperature measurements.

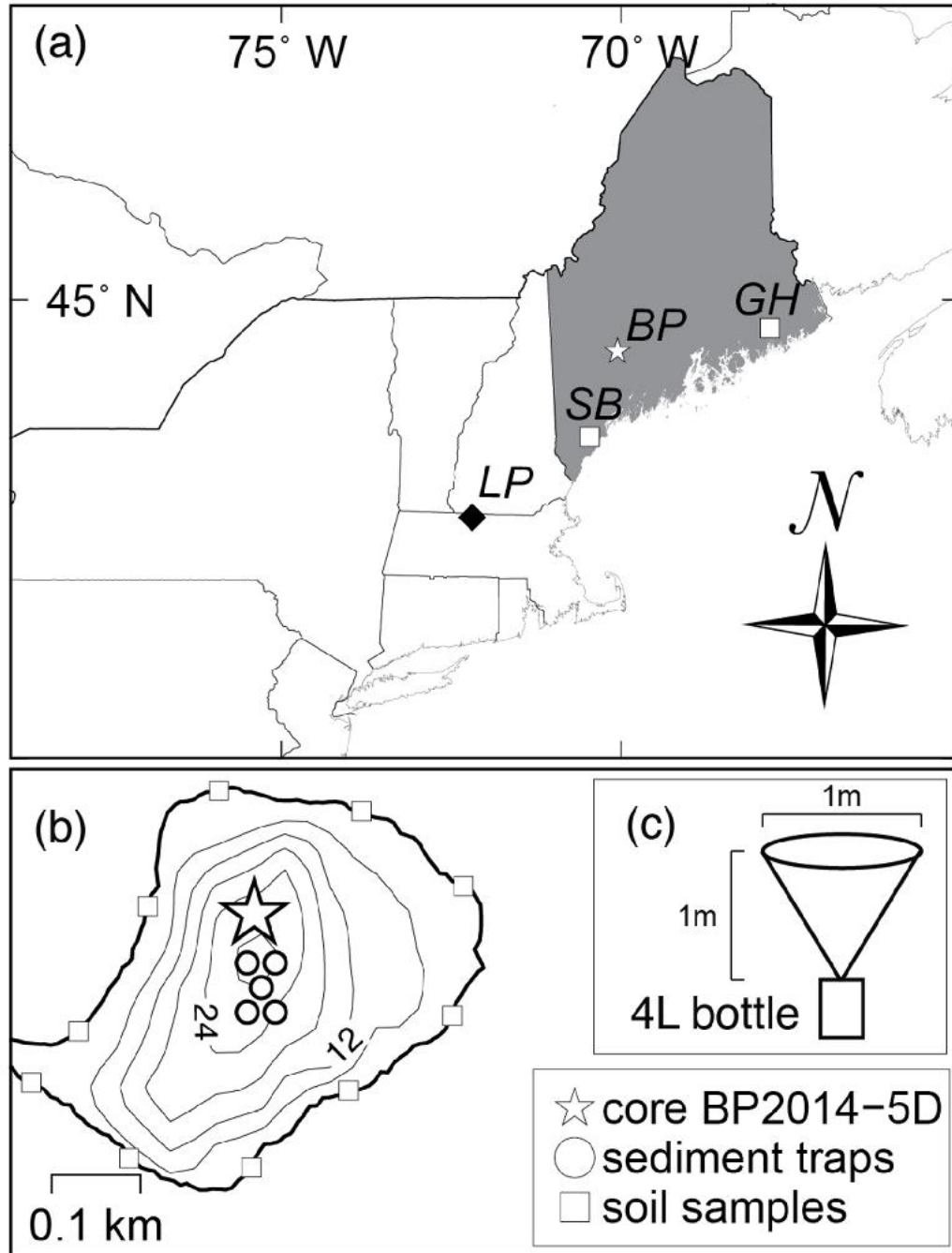


**Figure 5.1: Map of Basin Pond. (a)** The location of Basin Pond (BP) (white star) in Maine, USA. Locations of three other sites are labelled: Little Pond (LP; Gao et al. 2017), Great Heath Lake (GH; Nichols and Huang, 2012; Clifford and Booth, 2013), and Saco Bog (SB; Clifford and Booth, 2013). **(b)** Bathymetric profile (6 m contours) of Basin Pond with position of floating sediment traps (circles), surface soil samples (squares), and core BD-2014-5D used for the downcore temperature reconstruction in this study (star). The pond has an area of approximately 0.14 km<sup>2</sup>. **(c)** Schematic of sediment traps utilized in this study.

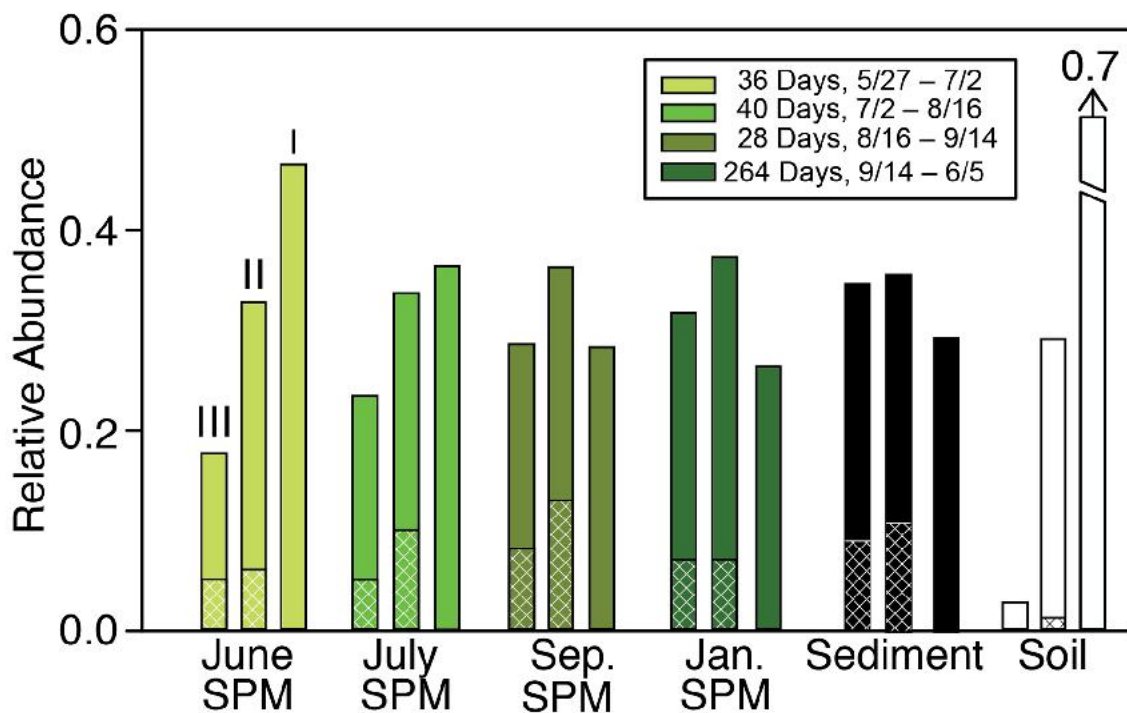


**Figure 5.2: Temporal variation of the relative abundance of group I, II and III brGDGTs in SPM (green shaded bars), sediment (black bars), and catchment soil samples (white bars). As in the plot of June SPM, the brGDGT groups III, II, and I, are displayed from left to right for each collection period and sediment and soil samples. Sediment and soil samples were collected in Spring of 2014. Green shaded bars for SPM samples reflect averages for each date samples were collected, measured in July 2014 (lightest green), August 2014, September 2014 and June 2015 (darkest green). For each category, brGDGT groups III, II, and I are shown in that order (left to right). Lines in each bar represent the relative abundance of 5- and 6-methyl brGDGTs, with cross hatching representing 6- methyl abundances.**

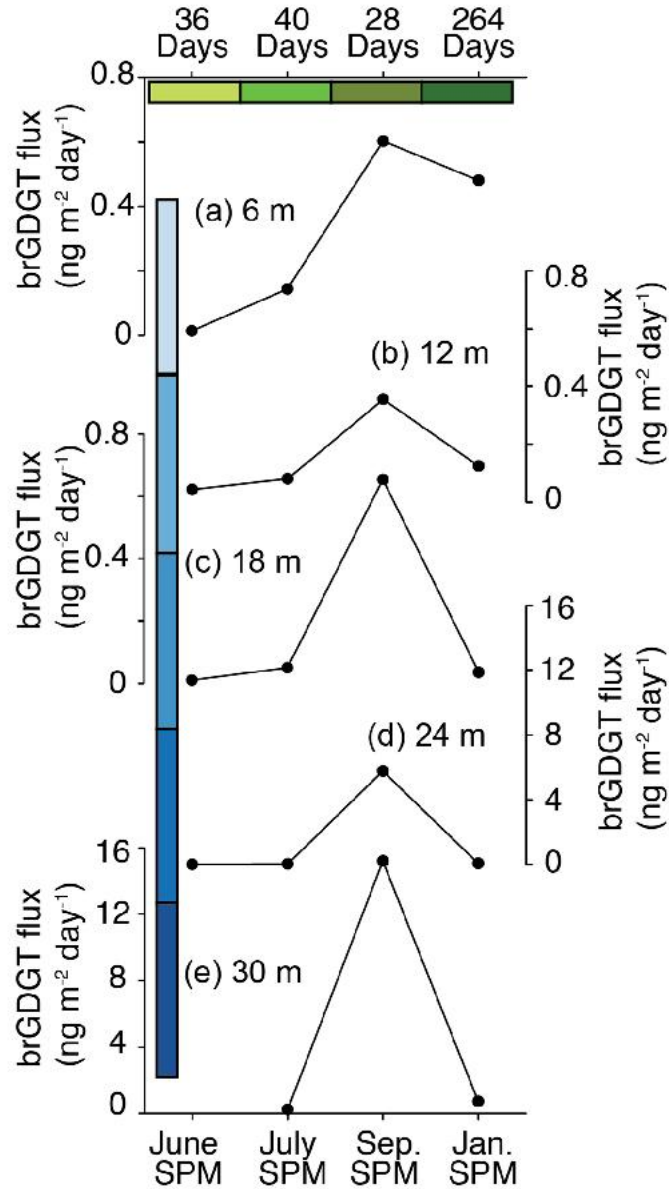


**Figure 5.3: Time series of brGDGT fluxes for each of the sediment traps in Basin Pond. brGDGT fluxes at 6m (a), 12m (b), 18m (c), 24m (d), and 30m (e) are shown. There is no data for trap (e) in July 2014. Note the change of scale for (d) and (e), indicating fluxes an order of magnitude higher for the lowermost traps. Green bars correspond to the time periods in Figure 2. Blue bars correspond to the depth ranges in Figure 5.**

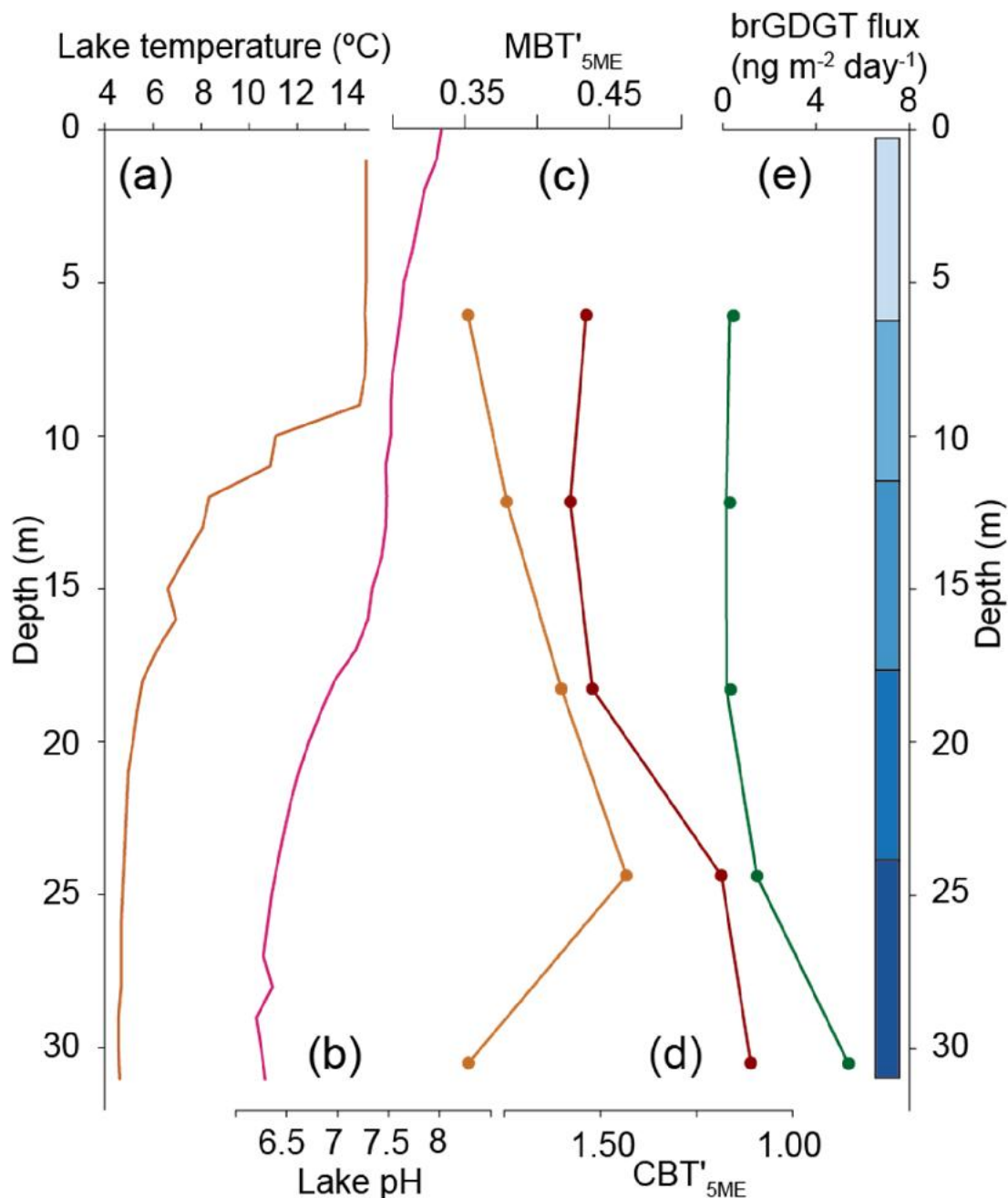


**Figure 5.4: Hydrolab-measured temperature and pH profiles for Basin Pond compared with flux weighted average brGDGT-based reconstructions. (a) Fall lake temperature profile, showing the mixed layer extending to ~9 m water depth, followed by the thermocline (9-15 m) and a cold deep layer (15-32 m). (b) Fall pH profile. the pH ranges from ~7.5 at the surface to ~6.2 at depth. (c) Flux weighted average MBT values measured at sediment traps. (d) Flux weighted average CBT values measured at sediment traps. (e) brGDGT fluxes measured at sediment traps.**

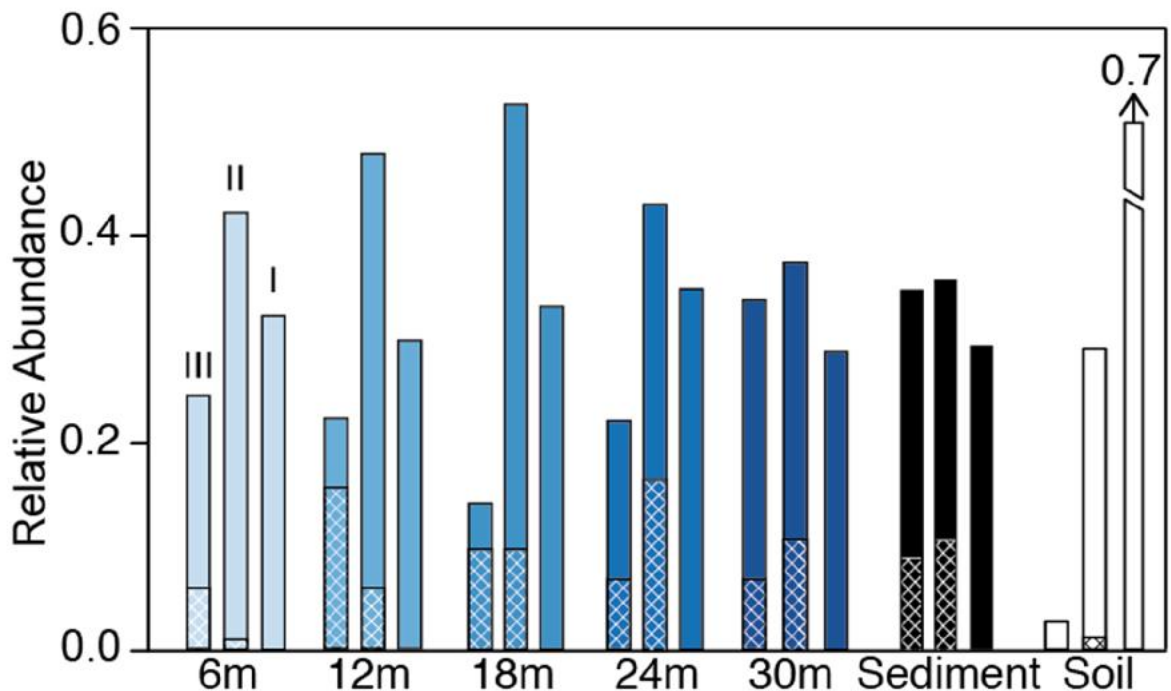


**Figure 5.5: Spatial variation in the water column of the relative abundance of groups I, II and III brGDGTs in SPM as a function of water depth. As in the plot of June SPM, the brGDGT groups III, II, and I, are displayed from left to right for each collection period and sediment and soil samples. For each group, the relative abundance at depths of 6 m (lightest blue), 12 m, 18 m, 24 m, and 30 m (darkest blue) is plotted next to the average surface sediment (black) and catchment soil (white). For each category, brGDGT groups III, II, and I are shown in that order (left to right). Lines in each bar represent the relative abundance of 5- and 6- methyl brGDGTs, with cross hatching representing 6- methyl abundances.**

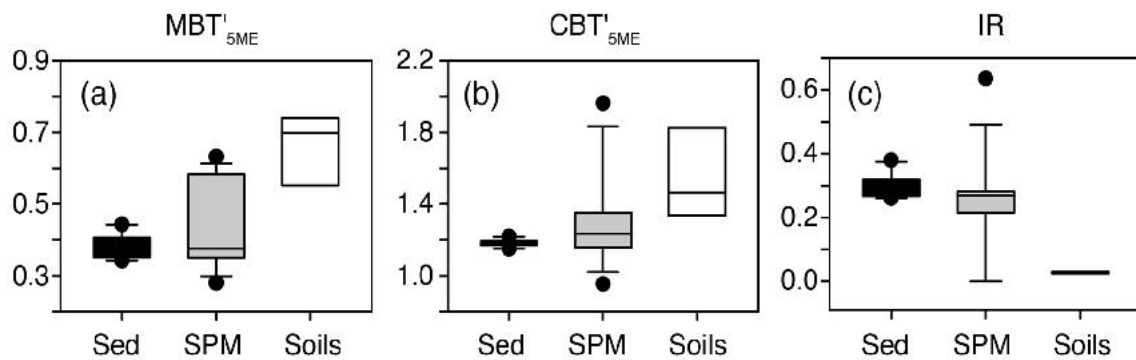


**Figure 5.6: BrGDGT-based proxies measured on surface sediments (black), SPM (gray), and catchment soils (white). (a) Cyclization of Branched Tetraethers (CBT), (b) Methylation of branched tetraethers (MBT'<sub>5ME</sub>), and (c) the Isomer Ratio (IR).**

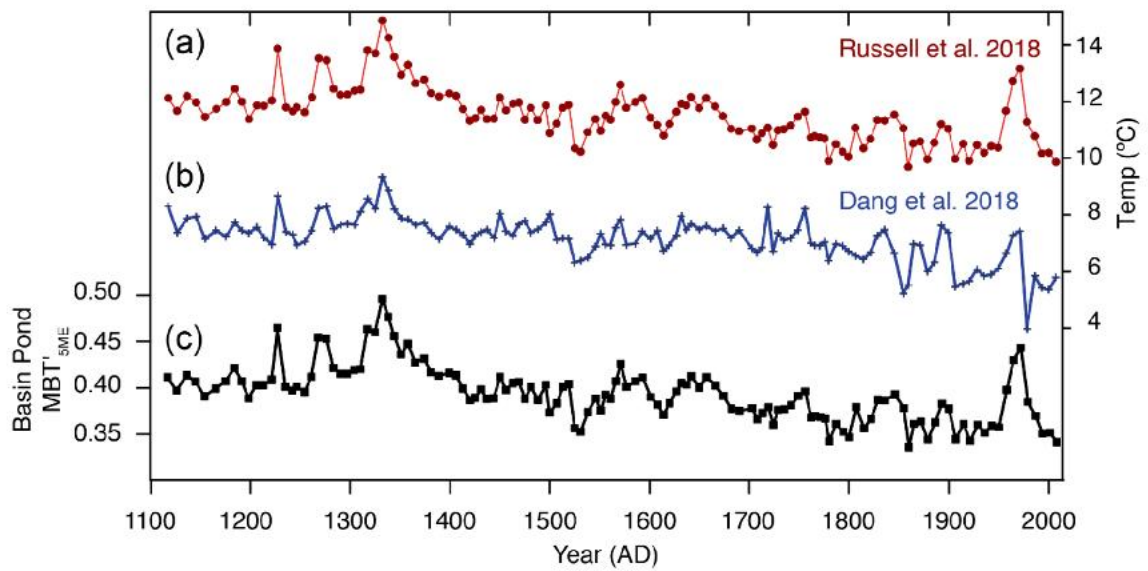


**Figure 5.7: Comparison of Basin Pond MBT'<sub>5ME</sub> with newly published temperature calibrations. (a) Core BP2014-5D plotted using the African Lakes calibration (Russell et al., 2018), and the (b) Chinese lakes calibration (Dang et al., 2018). (c) Basin Pond MBT'<sub>5ME</sub> values.**

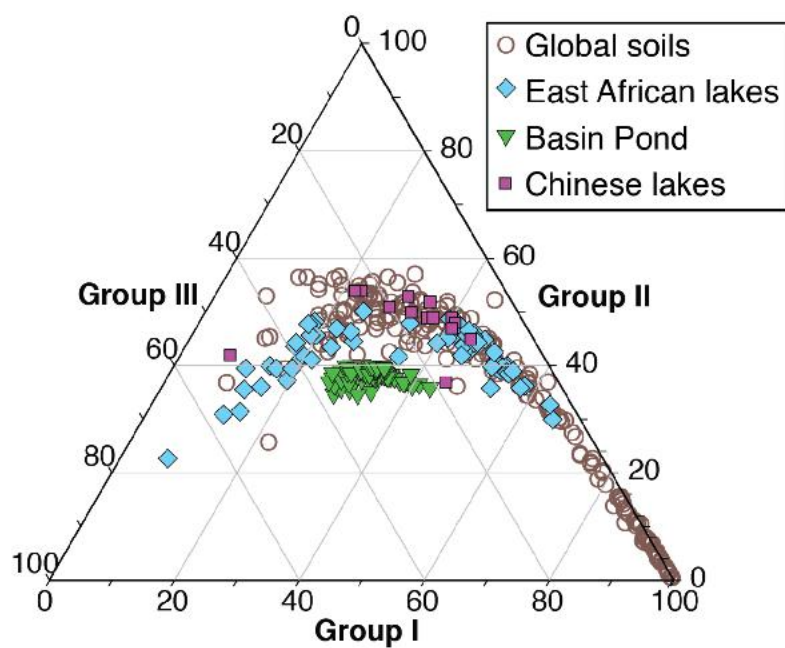


**Figure 5.8: Ternary diagram of brGDGT distributions of lake sediments (Dang et al., 2018; Russell et al., 2018) and global soils (Peterse et al., 2012) and Basin Pond sediments.**

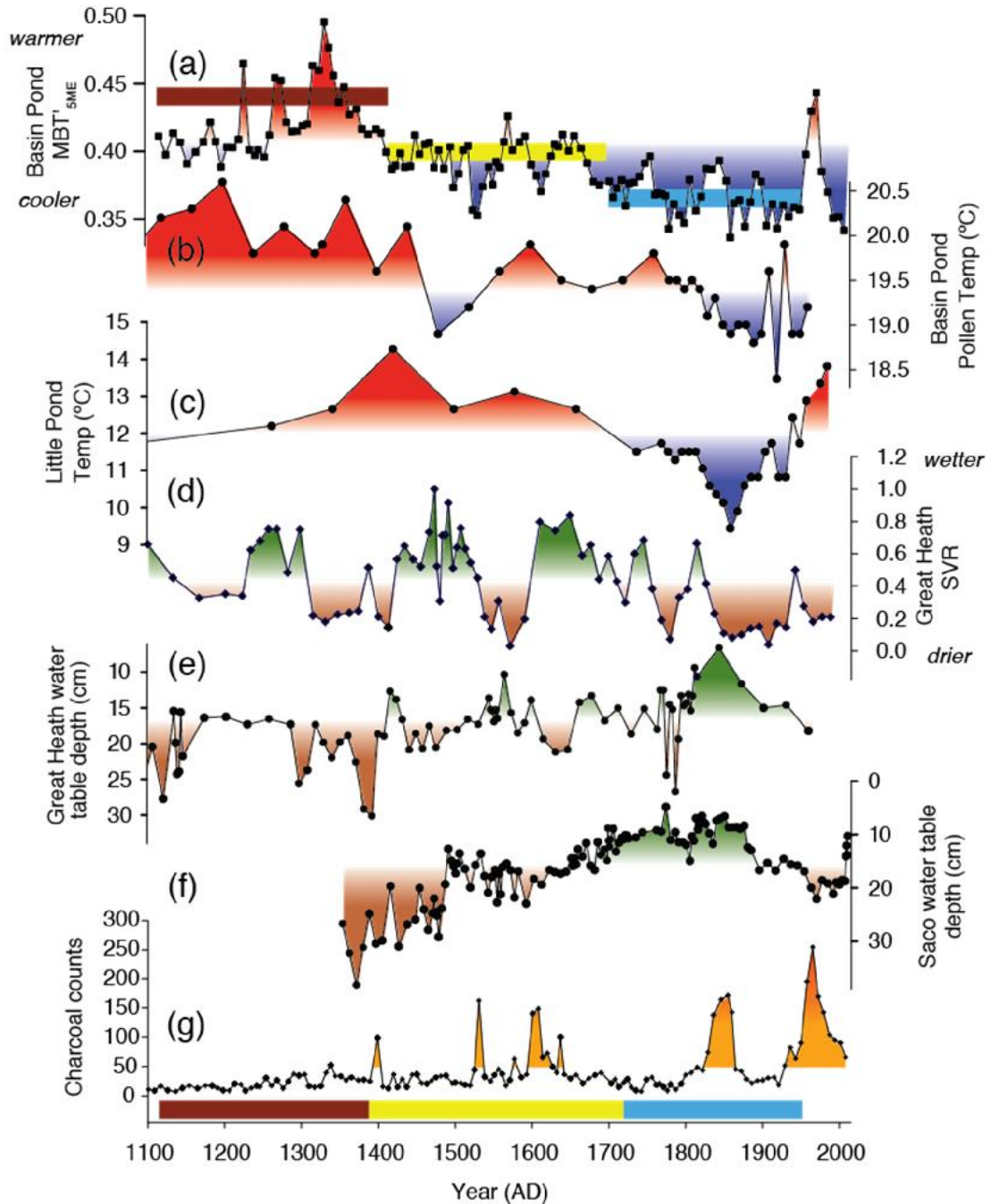


**Figure 5.9: The Basin Pond MBT'<sub>5ME</sub> record compared with other paleoclimate records from the NE US. (a) MBT'<sub>5ME</sub> (this study). Colored bars indicate the three main periods discussed in the text. (b) Pollen-based reconstruction of temperature at Basin Pond (Gajewski, 1988). (c) Deuterium isotope ( $\delta D$ )-based temperature reconstruction at Little Pond (Gao et al., 2017). (d) Great Heath aridity reconstruction based on the *Sphagnum*/Vascular Ratio (SVR) (Nichols and Huang, 2012). (e) Water table reconstruction from Great Heath (Clifford and Booth, 2013). (f) Water table reconstruction from Saco Bog (Clifford and Booth, 2013). (g) Charcoal counts from Basin Pond (Miller et al., 2017).**

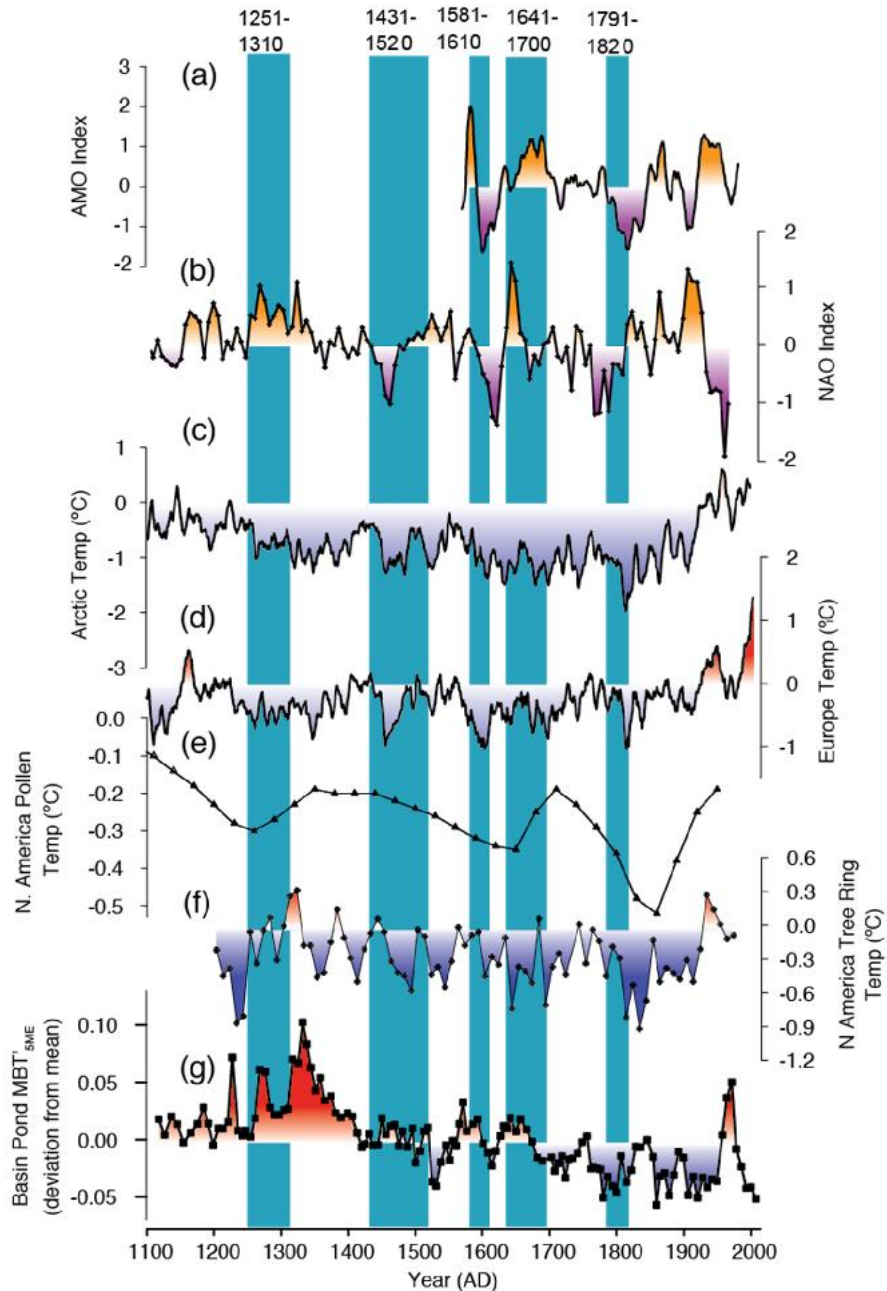


**Figure 5.10: The Basin Pond MBT'<sub>5ME</sub> record compared with regional and global records of temperature change. (a) Tree-ring based reconstruction of the AMO Index (Gray et al., 2004). (b) NAO Index reconstruction (Sun et al., 2015). (c–f) Regional temperature stacks based on composite proxy reconstructions for the Arctic (c), Europe (d), and North America (pollen, (e); tree rings, (f)). The records have been standardized to have the same mean (0) and standard deviation (1) from 1190–1970 AD (PAGES2k 2013). (g) MBT'<sub>5ME</sub> (this study).**

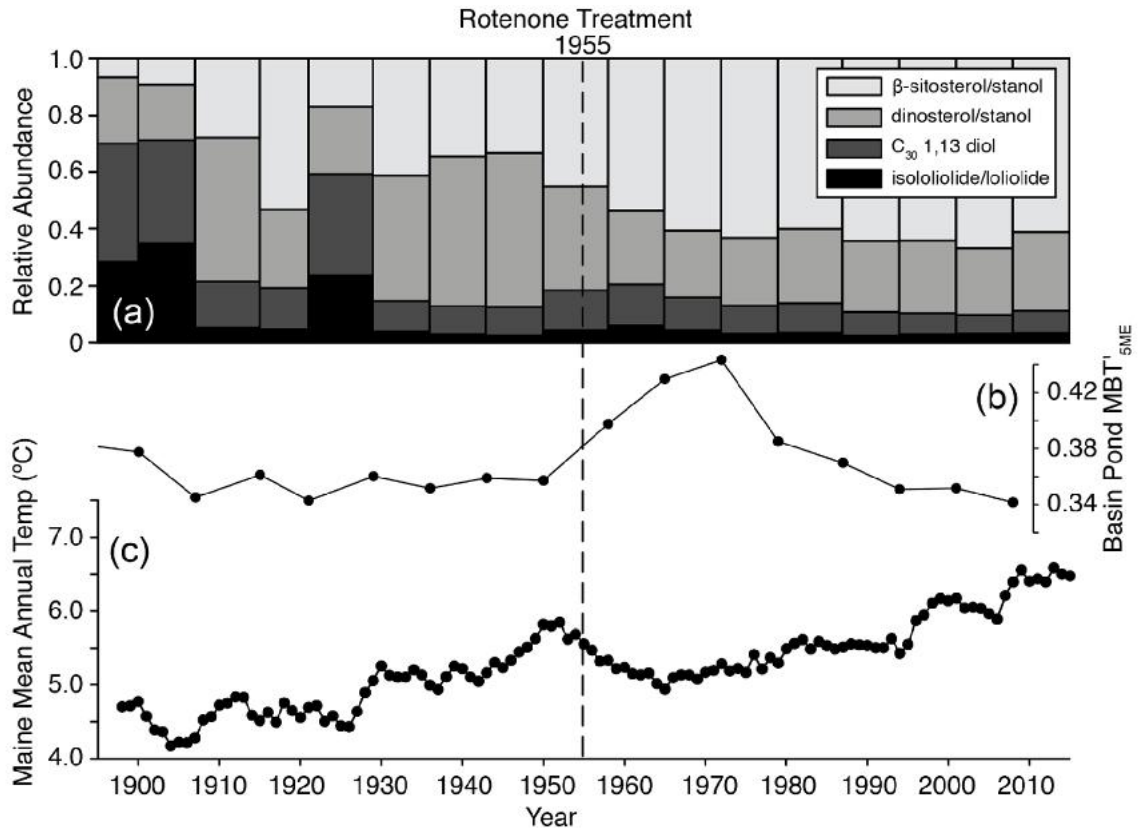


**Figure 5.11: Comparison of historical temperature records for the state of Maine, MBT<sup>5</sup><sub>SME</sub> reconstruction, and algal lipid biomarkers in Basin Pond. (a) Relative abundance of four major algal lipids. (b) MBT<sup>5</sup><sub>SME</sub> record. (c) Maine state-wide average temperature (NOAA, 2014). The black line indicates the rotenone treatment of the lake in 1955.**

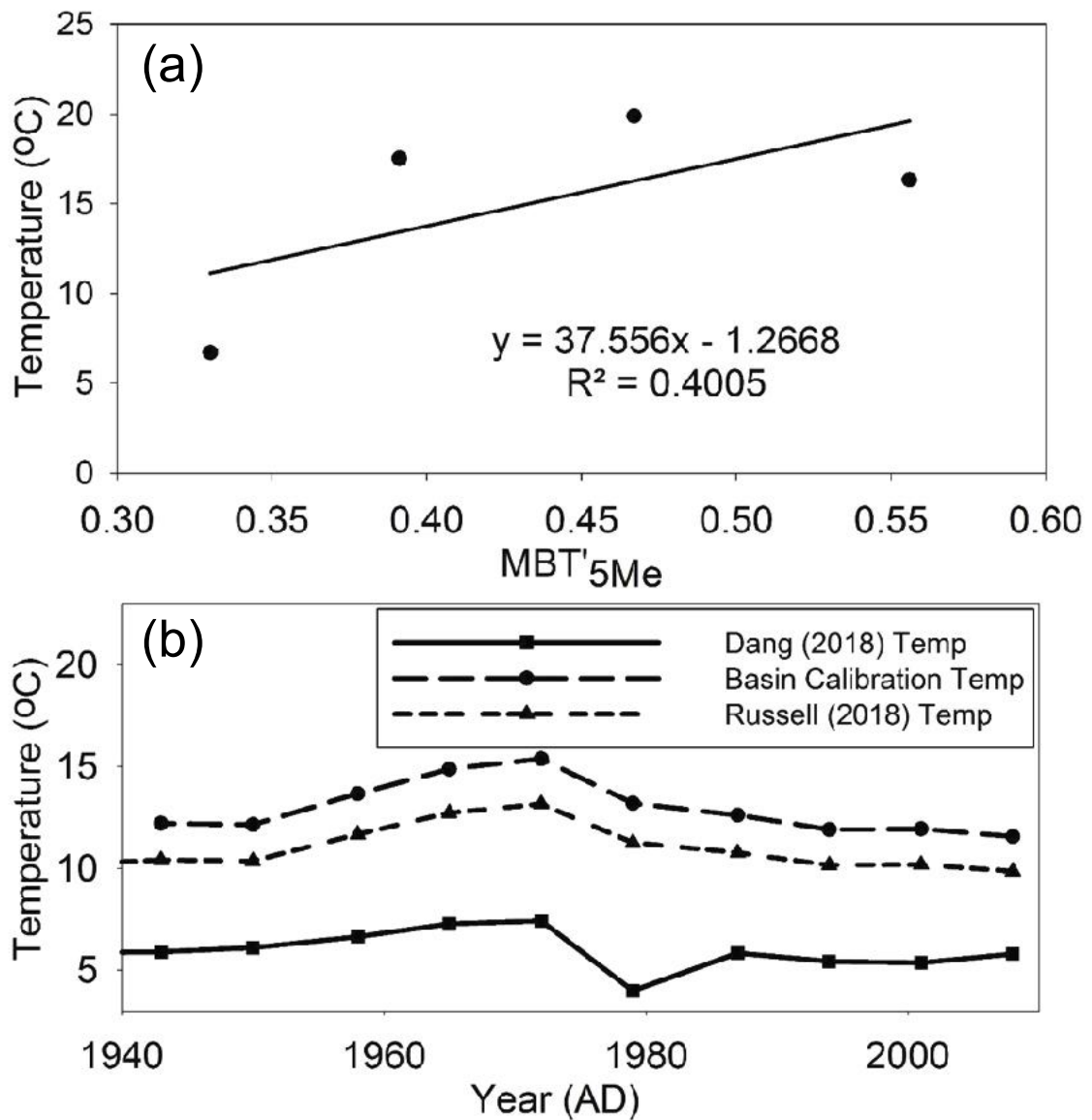


**Figure 5.12: a) Comparison of MBT'<sub>5Me</sub> values from all SPM samples (averaged for each date range) to average air temperatures during each time period. The equation for the plotted linear regression line, along with the correlation coefficient, are shown. b) Downcore reconstructed temperatures (in °C) from the Basin Pond calibration (long dashed line), the Russell et al. 2018 African lakes calibration (short dashed line), and from the Dang et al. 2018 Chinese lakes calibration (solid line).**

<b>Start Date</b>	<b>End Date</b>	<b>Avg Temp (°C)</b>
05/27/2014	07/01/2014	16.31
07/02/2014	08/15/2014	19.90
08/16/2014	09/13/2014	17.52
09/14/2014	06/05/2015	6.71
<i>excluding ice-cover dates (12/2/14-4/26/15)</i>		
09/14/2014	06/05/2015	0.56

**Table 5.1: Meteorological data used for calculating MBT<sub>5Me</sub> to temperature calibration at Basin Pond, ME from June 2014 through June 2015**

<b>ID</b>	<b>Site Name</b>	<b>Type of Proxy</b>	<b>Lat</b>	<b>Lon</b>	<b>Avg. yr/sample</b>	<b>Citation</b>
BP	Basin Pond	Pollen (Summer Temperature)	44.47	-70.05	24	Gajewski (1988)
BP	Basin Pond	Charcoal (Fire)	44.47	-70.05	7	Miller et al. (2017)
LJ	Little Pond	Hydrogen Isotopes (Hydroclimate)	42.68	-72.19	25	Gao et al. (2017)
GH	Great Heath Bog	Testate Amoeba (Water Table Level)	44.7	-67.81	11	Clifford & Booth (2013)
SB	Saco Bog	Testate Amoeba (Water Table Level)	43.55	-70.46	5	Clifford & Booth (2013)
GH	Great Heath Bog	SVR (Hydroclimate)	44.7	-67.81	14	Nichols & Huang (2012)

**Table 5.2: Additional information regarding sites discussed in the main text for comparison with the Basin Pond record.**

## CHAPTER 6

### CONCLUSIONS AND FUTURE WORK

This dissertation describes a variety of methods and studies addressing climatic fire risk in the Northeastern United States in pre-historic times, historical records, and into the future. We find that regional climatic fire risk for the NEUS can be estimated most accurately using the Keetch Byram Drought Index (KBDI) from 20<sup>th</sup> century historical meteorological records from various stations located throughout the region. The KBDI was demonstrated to capture extreme years of fire risk throughout the 20<sup>th</sup> century, with increased KBDI occurring during years of high fire occurrence and low KBDI values occurring during wet and cool years with little to no fire occurrence. Regional fire risk is then estimated through 2100 AD, using the KBDI and dynamically downscaled regional climate models from CMIP5 climate models. Under RCP 8.5, average KBDI and max yearly KBDI is shown to increase by 300% and 500%, respectively, in an exponential trend. Under RCP 4.5, KBDI is also expected to increase through 2100 AD to a lesser extent. Interestingly, these increases in regional fire risk are present regardless of increases in precipitation, indicating that future fire risk in the NEUS is driven largely by changes in temperature as opposed to precipitation.

Employing sedimentary PAHs to investigate regional fire occurrence, as outlined in Chapter 4, highlighted the value of a multi-proxy approach to reconstructing fires in sedimentary records from the region. In order to investigate long-term regional wildfire activity over the past millennium, we examined PAHs and macrocharcoal from a varved sedimentary record from Basin Pond, Fayette, Maine (USA). We found elevated concentrations of the PAH retene were highly correlated with known large-scale regional

wildfire events that occurred in 1761-1762, 1825, and 1947 (A.D.). To distinguish between biomass burning and anthropogenic combustion, the ratio of the PAHs retene and chrysene was examined. The new Basin Pond PAH records, along with a local signal of fire occurrence from charcoal analysis, offers the prospect of using this multi-proxy approach for examining wildfire frequency at the local and regional scale in the NEUS.

Finally, in Chapter 5, seasonally resolved measurements of brGDGT production in the water column, in catchment soils, and in a sediment core from Basin Pond were reported. These observations were used to help interpret a Basin Pond brGDGT-based temperature reconstruction spanning the past 900 years. This record exhibits similar trends to a pollen record from the same site and also to regional and global syntheses of terrestrial temperatures over the last millennium. However, the Basin Pond temperature record shows higher-frequency variability than has previously been captured by such an archive in the NEUS, potentially attributed to large scale atmospheric patterns. These new records of temperature variability and wildfire activity, when compared to regional hydroclimate records, shed insight into pre-historic wildfire risk in the NEUS.

## **6.1 Future Work**

This dissertation highlights the importance and usefulness of utilizing the Keetch Byram Drought Index (KBDI) to estimate future fire risk by forest and fire managers to determine how fire management and suppression practices need to change. For example, in the Bar Harbor/Acadia National Park locality, an area that has been drastically altered by wildfires (i.e., the 1947 wildfires), future fire risk is a critical question managers face, particularly in a widely visited National Park where there are high populations of visitors during the fire season. This method of modeling fire risk using the KBDI can be a

valuable tool for forest and fire managers in making informed decisions about changes in fire suppression practices in the near future, particularly in coastal or southern areas of the NEUS that have deep duff and upper soil layers. Because the KBDI estimates upper soil moisture, extreme end-of-century values will be critical for fire suppression activities in these areas, as suppressing creeping, smouldering, or underground fires (as seen in regions with deep duff layers), which cost much more to suppress than above ground wildfires. Sub-regional, high resolution analyses of these wildfire-prone areas should be done on a case-by-case basis using the KBDI in the future, and compared with other fire indices commonly employed that take into account other aspects of fire risk (i.e. ecological parameters).

The Basin Pond temperature study, as outlined in Chapter 5, provides the foundation for a brGDGT temperature calibration for the Northeastern United States. Currently, numerous water samples are being collected on a biweekly basis at Basin Pond, in order to further develop the preliminary calibration presented in Chapter 5. Furthermore, work on Sebago Lake, a large, deep lake located in southern Maine, will aid in further advancing the development of a refined NEUS temperature calibration for brGDGTs. This will ultimately make brGDGT analysis in this region a reliable and accurate method to reconstruct temperature, which will be a valuable addition to the paleoclimate community. Finally, future work within the brGDGT-community is needed to constrain brGDGT producers. With a better understanding of where, when, and what are the primary producers of these compounds, temperature reconstructions can be more accurately constrained and interpreted.

Employing sedimentary PAHs to investigate regional fire occurrence, as outlined in Chapter 4, highlighted the value of a multi-proxy approach to reconstructing fires in sedimentary records from the region. To date, the vast majority of studies have focused on sedimentary charcoal analysis, which unfortunately have spatial limitations, limiting their ability to investigate regional fire outbreaks. Using PAHs provides an alternative to charcoal analysis, and reconstruct regional outbreaks of wildfires. Furthermore, alternative emerging methods, such as black carbon or analysis of molecular compounds such as levoglucosan, can be used to investigate regional and “super-regional” fire activity. These methods should be employed by future studies to gain better understanding of the spatial extent of PAHs and other wildfire proxies, as well as any regional fire outbreaks in pre-historic times in the NEUS.

## BIBLIOGRAPHY

- Ahad, J.M.E., Jautzy, J.J., Cumming, B.F., Das, B., Laird, K.R., Sanei, H., 2015. Sources of polycyclic aromatic hydrocarbons (PAHs) to northwestern Saskatchewan lakes east of the Athabasca oil sands. *Organic Geochemistry* 80, 35–45.
- Anderson, R.S., 1970. Effects of Rotenone on Zooplankton Communities and a Study of their Recovery Patterns in Two Mountain Lakes in Alberta. *Journal of the Fisheries Research Board of Canada* 27, 1335–1356.
- Appleby, P.G., Oldfield, F., 1978. The calculation of lead-210 dates assuming a constant rate of supply of unsupported <sup>210</sup>Pb to the sediment. *CATENA* 5, 1–8.
- Bachmann, A., Allgower, B., 2001. A consistent wildland fire risk terminology is needed! *Fire Management Today* 61, 28–33.
- Barton, A.M., White, A.S., Cogbill, C.V., 2012. The Changing Nature of the Maine Woods. UPNE.
- Beall, H., 1990. Fire research in Canada's federal forestry service –the formative years. (Information Report No. NOR-X-309), The Art and science of fire management, proceedings of the first Interior West Fire Council annual meeting and workshop. Forestry Canada, Northern Forestry Centre, Edmonton.
- Bechtel, A., Smittenberg, R.H., Bernasconi, S.M., Schubert, C.J., 2010. Distribution of branched and isoprenoid tetraether lipids in an oligotrophic and a eutrophic Swiss lake: Insights into sources and GDGT-based proxies. *Organic Geochemistry* 41, 822–832.
- Bianchi, T.S., Canuel, E.A., 2011. *Chemical Biomarkers in Aquatic Ecosystems*. Princeton University Press.
- Bлага, C.I., Reichart, G.-J., Heiri, O., Sinninghe Damsté, J.S., 2009. Tetraether membrane lipid distributions in water-column particulate matter and sediments: a study of 47 European lakes along a north–south transect. *Journal of Paleolimnology* 41, 523–540.
- Blumer, M., 1961. Benzopyrenes in soils. *Science* 44, 474–475.
- Bracken, C., 2016. Downscaled CMIP3 and CMIP5 Climate and Hydrology Projections–Addendum. Release of Downscaled CMIP5 Climate Projections (LOCA) and Comparison with Preceding Information.
- Bradshaw, L., McCormick, E., 2013. FireFamilyPlus user's Guide, Version 4.1 (General Technical Report No. RMRS-GTR-67-WWW). US Department of Agriculture, Forest Service, Rocky Mountain Research Station, Ogden, UT.

- Buckles, L., Weijers, J.W., Verschuren, D., Sinninghe Damste, J.S., 2014. Sources of core and intact branched tetraether membrane lipids in the lacustrine environment: Anatomy of Lake Challa and its catchment, equatorial East Africa. *Geochimica et Cosmochimica Acta* 140, 106–126.
- Burgan, R.E., 1988. 1988 Revisions to the 1978 National Fire-Danger Rating System (Research Paper No. SE-273). US Department of Agriculture, Forest Service, Southeastern Forest Experiment Station.
- Burgan, R.E., Hartford, R.A., Eidenshink, J.C., 1996. Using NDVI to Assess Departure From Average Greenness and its Relation to Fire Business (General Technical Report No. INT-GTR-333). US Department of Agriculture, Forest Service, Intermountain Research Station, Ogden, UT.
- Burgan, R.E., Klaver, R.W., Klaver, J.M., 1998. Fuel Models and Fire Potential From Satellite and Surface Observations. *International Journal of Wildland Fire* 8, 159–170.
- Butler, J., 2014. *Wildfire loose: the week Maine burned*. Down East Books.
- Carlson, J.R., 2013. A Synopsis of Prescribed Fire in New England [WWW Document]. Ecological Landscape Alliance. URL <https://www.ecolandscaping.org/07/uncategorized/a-synopsis-of-prescribed-fire-in-new-england/> (accessed 9.27.18).
- C. Hopmans, E., Schouten, S., Sinninghe-Damste, J., 2015. The effect of improved chromatography on GDGT-based palaeoproxies. *Organic Geochemistry* 93. doi:10.1016/j.orggeochem.2015.12.006
- Clarke, H.G., Smith, P.L., Pitman, A.J., 2011. Regional signatures of future fire weather over eastern Australia from global climate models. *International Journal of Wildland Fire* 20, 550–562.
- Clark, J.S., 1988. Particle Motion and the Theory of Charcoal Analysis: Source Area, Transport, Deposition, and Sampling. *Quaternary Research* 30, 67–80.
- Clark, J.S., Patterson, W.A., 1997. Background and Local Charcoal in Sediments: Scales of Fire Evidence in the Paleorecord, in: Clark, J.S., Cachier, H., Goldammer, J.G., Stocks, B. (Eds.), *Sediment Records of Biomass Burning and Global Change*, NATO ASI Series. Springer Berlin Heidelberg, pp. 23–48.
- Clark, J.S., Royall, P.D., 1994. Pre-Industrial Particulate Emissions and Carbon Sequestration from Biomass Burning in North America. *Biogeochemistry* 24, 35–51.

- Clark, J.S., Royall, P.D., 1995. Transformation of a northern hardwood forest by aboriginal (Iroquois) fire: charcoal evidence from Crawford Lake, Ontario, Canada. *The Holocene* 5, 1–9.
- Clark, J.S., Royall, P.D., 1996. Local and Regional Sediment Charcoal Evidence for Fire Regimes in Presettlement North-Eastern North America. *The Journal of Ecology* 84, 365.
- Clark, J.S., Royall, P.D., Chumbley, C., 1996. The Role of Fire During Climate Change in an Eastern Deciduous Forest at Devil’s Bathtub, New York. *Ecology* 77, 2148.
- Clifford, M., Booth, R.K., 2013. Increased probability of fire during late Holocene droughts in northern New England. *Climate Change* 119, 3–4.
- Colcord, D.E., Cadieux, S.B., Brassell, S.C., Castañeda, I.S., Pratt, L.M., White, J.R., 2015. Assessment of branched GDGTs as temperature proxies in sedimentary records from several small lakes in southwestern Greenland. *Organic Geochemistry* 82, 33–41.
- Coolidge, P., 1963. *History of the Maine Woods*. Furbush-Roberts Printing Co., Bangor, ME.
- Chuvieco, E., Congalton, R.G., 1989. Application of remote sensing and geographic information systems to forest fire hazard mapping. *Remote Sensing of Environment* 29, 147–159.
- Dang, X., Ding, W., Yang, H., D. Pancost, R., David A. Naafs, B., Xue, J., Lin, X., Lu, J., Xie, S., 2018. Different temperature dependence of the bacterial brGDGT isomers in 35 Chinese lake sediments compared to that in soils. *Organic Geochemistry* 119. doi:10.1016/j.orggeochem.2018.02.008
- Davis, M., Gratton, L., Adams, J., Goltz, J., Stewart, C., Buttrick, S., Zinger, N., Kavanagh, K., Sims, M., Mann, G., n.d. *New England-Acadian forests | Ecoregions | WWF [WWW Document]*. World Wildlife Fund. URL <https://www.worldwildlife.org/ecoregions/na0410> (accessed 2.8.18).
- Deeming, J.E., Burgan, R.E., Cohen, J.D., 1977. *The National Fire-Danger Rating System - 1978 (General Technical Report No. INT-39)*. US Department of Agriculture, Forest Service, Intermountain Research Station, Ogden, UT.
- Deeming, J.E., Lancaster, J.W., Fosberg, M.A., Furman, W.R., Schroeder, M.J., 1972. *The National Fire-Danger Rating System (Research Paper No. RM-84)*. US Department of Agriculture, Forest Service, Rocky Mountain Forest and Range Experiment Station, Fort Collins, CO.

- De Jonge, C., Hopmans, E.C., Stadnitskaia, A., Rijpstra, W.I.C., Hofland, R., Tegelaar, E., Sinninghe Damsté, J.S., 2013. Identification of novel penta- and hexamethylated branched glycerol dialkyl glycerol tetraethers in peat using HPLC–MS2, GC–MS and GC–SMB-MS. *Organic Geochemistry* 54, 78–82.
- De Jonge, C., Hopmans, E.C., Zell, C.I., Kim, J.-H., Schouten, S., Sinninghe Damsté, J.S., 2014a. Occurrence and abundance of 6-methyl branched glycerol dialkyl glycerol tetraethers in soils: Implications for palaeoclimate reconstruction. *Geochimica et Cosmochimica Acta* 141, 97–112.
- De Jonge, C., Stadnitskaia, A., Hopmans, E.C., Cherkashov, G., Fedotov, A., Sinninghe Damsté, J.S., 2014b. In situ produced branched glycerol dialkyl glycerol tetraethers in suspended particulate matter from the Yenisei River, Eastern Siberia. *Geochimica et Cosmochimica Acta* 125, 476–491.
- De Jonge, C., Stadnitskaia, A., Hopmans, E.C., Cherkashov, G., Fedotov, A., Streletskaia, I.D., Vasiliev, A.A., Sinninghe Damsté, J.S., 2015. Drastic changes in the distribution of branched tetraether lipids in suspended matter and sediments from the Yenisei River and Kara Sea (Siberia): Implications for the use of brGDGT-based proxies in coastal marine sediments. *Geochimica et Cosmochimica Acta* 165, 200–225.
- Denis, E.H., Toney, J.L., Tarozo, R., Scott Anderson, R., Roach, L.D., Huang, Y., 2012. Polycyclic aromatic hydrocarbons (PAHs) in lake sediments record historic fire events: Validation using HPLC-fluorescence detection. *Organic Geochemistry* 45, 7–17.
- Domec, J.-C., Rivera, L.N., King, J.S., Peszlen, I., Hain, F., Smith, B., Frampton, J., 2013. Hemlock woolly adelgid (*Adelges tsugae*) infestation affects water and carbon relations of eastern hemlock (*Tsuga canadensis*) and Carolina hemlock (*Tsuga caroliniana*). *New Phytologist* 199, 452–463.
- Enache, M.D., Cumming, B.F., 2006. Tracking recorded fires using charcoal morphology from the sedimentary sequence of Prosser Lake, British Columbia (Canada). *Quaternary Research* 65, 282–292.
- Fabbri, D., Chiavari, G., Prati, S., Vassura, I., Vangelista, M., 2002. Gas chromatography/mass spectrometric characterisation of pyrolysis/silylation products of glucose and cellulose. *Rapid Communications in Mass Spectrometry* 16, 2349–2355.
- Fahey, T.J., Reiners, W.A., 1981. Fire in the Forests of Maine and New Hampshire. *Bulletin of the Torrey Botanical Club* 108, 362.
- Fobes, C.B., 1948. Historic Forest Fires in Maine. *Economic Geography* 24, 269.

- Fosberg, M.A., 1978. Weather in wildland fire management: the Fire Weather Index. Presented at the Conference on Sierra Nevada Meteorology, Lake Tahoe, CA, pp. 1–4.
- Foster, D., J Aber, 2004. *Forest In Time: Ecosystem Structure and Function as a Consequence of 1000 Years of Change*. Yale University Press.
- Foster, D.R., O’Keefe, J., 2000. *New England Forests Through Time, Insights from the Harvard Forest Dioramas*. Harvard University Press, Cambridge, MA.
- Foster, D.R., Oswald, W.W., Faison, E.K., Doughty, E.D., Hansen, B.C.S., 2006. A Climatic Driver for Abrupt Mid-Holocene Vegetation Dynamics and the Hemlock Decline in New England. *Ecology* 87, 2959–2966.
- Foster, L.C., Pearson, E.J., Juggins, S., Hodgson, D.A., Saunders, K.M., Verleyen, E., Roberts, S.J., 2016. Development of a regional glycerol dialkyl glycerol tetraether (GDGT)-temperature calibration for Antarctic and sub-Antarctic lakes. *EARTH AND PLANETARY SCIENCE LETTERS* 433, 370–379.
- Frost, D.S., 2005. *Paleoclimate Reconstruction using Physical Sedimentology and Organic Matter Biogeochemistry of Varved Sediments, Basin Pond, Fayette, ME (Undergraduate Thesis)*. Bates College.
- Gajewski, K., 1988. Late holocene climate changes in eastern North America estimated from pollen data. *Quaternary Research* 29, 255–262.
- Gajewski, K., Swain, A.M., Peterson, G.M., 1987. Late Holocene Pollen Stratigraphy in Four Northeastern United States Lakes. *Géographie physique et Quaternaire* 41, 377.
- Gao, L., Huang, Y., Shuman, B., Oswald, W.W., Foster, D., 2017. high-resolution hydrogen isotope record of behenic acid for the past 16 kyr in the northeastern United States. *Quaternary International* 449, 1–11.
- Gardner, J., Whitlock, C., 2001. Charcoal accumulation following a recent fire in the Cascade Range, northwestern USA, and its relevance for fire-history studies. *The Holocene* 11, 541–549.
- Gill, A.M., Bradstock, R.A., 1995. Extinction of biota by fires. *Conserving biodiversity: threats and solutions* 309–322.
- Giorgi, F., Jones, C., Asrar, G., 2008. Addressing climate information needs at the regional level: The CORDEX framework. *WMO Bull* 53.
- Goodrick, S.L., 2002. Modification of the Fosberg Fire Weather Index to include drought. *International Journal of Wildland Fire* 11, 205–221.

- Gould, J.S., Patriquin, M.N., Wang, S., McFarlane, B.L., Wotton, B.M., 2013. Economic evaluation of research to improve the Canadian forest fire danger rating system. *Forestry: An International Journal of Forest Research* 86, 317–329.
- Grimalt, J., van Drooge, B., Ribes, A., Fernandez, P., Appleby, P., 2004. Polycyclic aromatic hydrocarbon composition in soils and sediments of high altitude lakes. *Environmental Pollution* 131, 13–24.
- Haines, D.A., 1988. A lower atmospheric severity index for wildland fire. *National Weather Digest* 13, 23–27.
- Holz, A., Haberle, S., Veblen, T.T., De Pol-Holz, R., Southon, J., 2012. Fire history in western Patagonia from paired tree-ring fire-scar and charcoal records. *Clim. Past* 8, 451–466.
- Hopmans, E.C., Weijers, J.W., Schefuß, E., Herfort, L., Damsté, J.S.S., Schouten, S., 2004. A novel proxy for terrestrial organic matter in sediments based on branched and isoprenoid tetraether lipids. *Earth and Planetary Science Letters* 224, 107–116.
- Horton, R., Yohe, G., Easterling, W., Kates, R., Ruth, M., Sussman, E., Whelchel, A., Wolfe, D., Lipschultz, F., 2014. Ch. 16: Northeast. *Climate Change Impacts in the United States: The Third National Climate Assessment*. doi:10.7930/J0SF2T3P
- Hou, J., D'Andrea, W.J., Huang, Y., 2008. Can sedimentary leaf waxes record D/H ratios of continental precipitation? Field, model, and experimental assessments. *Geochimica et Cosmochimica Acta* 72, 3503–3517.
- Huang, Y., Shuman, B., Wang, Y., Webb, T., 2004. Hydrogen isotope ratios of individual lipids in lake sediments as novel tracers of climatic and environmental change: a surface sediment test. *Journal of Paleolimnology* 31, 363–375.
- Irland, L.C., 2013. Extreme value analysis of forest fires from New York to Nova Scotia, 1950–2010. *Forest Ecology and Management, The Mega-fire reality* 294, 150–157.
- J. Barsugli, J., Guentchev, G., Horton, R., Wood, A., Mearns, L., Liang, X., Dixon, K., Hayhoe, K., Rood, R., Goddard, L., Ray, A., Buja, L., Ammann, C., 2013. The Practitioner's Dilemma: How to Assess the Credibility of Downscaled Climate Projections. *Eos Transactions American Geophysical Union* 94, 424–425.
- Karmalkar, A., Thibeault, J.M., Bryan, A.M., Seth, A., in review. A framework for selecting CMIP5 GCMs for analyses of climate change and its impacts in the northeastern United States. *Climate Change*.

- Keetch, J.J., Byram, G.M., 1968. A Drought Index for Forest Fire Control. Res. Pap. SE-38. Asheville, NC: U.S. Department of Agriculture, Forest Service, Southeastern Forest Experiment Station. 35 p. 038.
- Kerr, G.H., DeGaetano, A.T., Stoof, C.R., Ward, D., 2018. Climate change effects on wildland fire risk in the Northeastern and Great Lakes states predicted by a downscaled multi-model ensemble. *Theoretical and Applied Climatology* 131, 625–639.
- Kirchgeorg, T., Schüpbach, S., Kehrwald, N., McWethy, D.B., Barbante, C., 2014. Method for the determination of specific molecular markers of biomass burning in lake sediments. *Organic Geochemistry* 71, 1–6.
- Kiser, R.W., Donaldson, J.R., Olson, P.R., 1963. The Effect of Rotenone on Zooplankton Populations in Freshwater Lakes. *Transactions of the American Fisheries Society* 92, 17–24.
- Klok, J., Baas, M., Cox, H.C., de Leeuw, J.W., Schenck, P.A., 1984. Loliolides and dihydroactinidiolide in a recent marine sediment probably indicate a major transformation pathway of carotenoids. *Tetrahedron Letters* 25, 5577–5580.
- Krawchuk, M.A., Moritz, M.A., 2014. Burning issues: statistical analyses of global fire data to inform assessments of environmental change. *Environmetrics*.
- Kunkel, K.E., 2013. Regional climate trends and scenarios for the US National Climate Assessment. US Department of Commerce, National Oceanic and Atmospheric Administration, National Environmental Satellite, Data, and Information Service.
- Kuo, L.-J., Louchouart, P., Herbert, B.E., Brandenberger, J.M., Wade, T.L., Crecelius, E., 2011. Combustion-derived substances in deep basins of Puget Sound: historical inputs from fossil fuel and biomass combustion. *Environmental Pollution* 159, 983–990.
- Le Goff, H., Flannigan, M., Bergeron, Y., 2009. Potential changes in monthly fire risk in the eastern Canadian boreal forest under future climate change. *Canadian Journal of Forest Research* 39, 2369–2380.
- Levis, S., Bonan, B., Vertenstein, M., Oleson, K., 2004. ), The Community Land Model's Dynamic Global Vegetation Model (CLM-DGVM): Technical Description and User's Guide (NCAR Tech Note No. TN-459+IA). NCAR, Boulder, CO.
- Liu, Y., Goodrick, S.L., Stanturf, J., 2013. Future U.S. Wildfire Potential Trends Projected Using a Dynamically Downscaled Climate Change Scenario. *Forest Ecology and Management* 294, 120–135.

- Liu, Y., Stanturf, J., Goodrick, S., 2010. Wildfire potential evaluation during a drought event with a regional climate model and NDVI. *Ecological Informatics* 5:418-428  
5, 418–428.
- Loomis, S.E., Russell, J.M., Heures, A.M., D'Andrea, W.J., Sinninghe Damsté, J.S., 2014. Seasonal variability of branched glycerol dialkyl glycerol tetraethers (brGDGTs) in a temperate lake system. *Geochimica et Cosmochimica Acta* 144, 173–187.
- Loomis, S., Russell, J.M., Ladd, B., Street-Perrott, A., Sinninghe Damsté, J.S., 2012. Calibration and application of the branched GDGT temperature proxy on East African lake sediments. *Earth and Planetary Science Letters* 357-358, 277–288.
- Lorimer, C.G., 1977. The Presettlement Forest and Natural Disturbance Cycle of Northeastern Maine. *Ecology* 58, 139.
- Marlon, J.R., Bartlein, P.J., Carcaillet, C., Gavin, D.G., Harrison, S.P., Higuera, P.E., Joos, F., Power, M.J., Prentice, I.C., 2008. Climate and human influences on global biomass burning over the past two millennia. *Nature Geoscience* 1, 697–702.
- Marlon, J.R., Pederson, N., Nolan, C., Goring, S., Shuman, B., Robertson, A., Booth, R., Bartlein, P.J., Berke, M.A., Clifford, M., Cook, E., Dieffenbacher-Krall, A., Dietze, M.C., Hessler, A., Hubeny, J.B., Jackson, S.T., Marsicek, J., McLachlan, J., Mock, C.J., Moore, D.J.P., Nichols, J., Peteet, D., Schaefer, K., Trouet, V., Umbanhowar, C., Williams, J.W., Yu, Z., 2017. Climatic history of the northeastern United States during the past 3000 years. *Clim. Past* 13, 1355–1379.
- Meyers, P.A., 1997. Organic geochemical proxies of paleoceanographic, paleolimnologic, and paleoclimatic processes. *Organic Geochemistry* 27, 213–250.
- Miller, D.R., Castañeda, I.S., Bradley, R.S., MacDonald, D., 2017. Local and regional wildfire activity in central Maine (USA) during the past 900 years. *Journal of Paleolimnology* 58, 455–466.
- Moritz, M., Parisien, M., Batllori, E., Krawchuk, M., Van Dorn, J., Ganz, D., Hayhoe, K., 2012. Climate change and disruptions to global fire activity - Moritz - 2012 - *Ecosphere* - Wiley Online Library. *Ecosphere* 3.
- Moss, R., Edmonds, J., Hibbard, K., Manning, M., Rose, S., Vuuren, D., Carter, T., Emori, S., Kainuma, M., Kram, T., Meehl, G., Mitchell, J., Nakicenovic, N., Riahi, K., Smith, S., Ronald, S., Thomson, A., Weyant, J., Wilbanks, T., 2010. The Next Generation of Scenarios for Climate Change Research and Assessment. *Nature* 463, 747–56.

- Musa Bandowe, B.A., Srinivasan, P., Seelge, M., Sirocko, F., Wilcke, W., 2014. A 2600-year record of past polycyclic aromatic hydrocarbons (PAHs) deposition at Holzmaar (Eifel, Germany). *Palaeogeography, Palaeoclimatology, Palaeoecology* 401, 111–121.
- National Interagency Fire Center, 2016. Federal Firefighting Costs (Suppression Only) [WWW Document]. URL [https://www.nifc.gov/fireInfo/fireInfo\\_documents/SuppCosts.pdf](https://www.nifc.gov/fireInfo/fireInfo_documents/SuppCosts.pdf).
- National Oceanic and Atmospheric Administration (NOAA), 2014. National Climatic Data Center [WWW Document]. URL [www.ncdc.noaa.gov](http://www.ncdc.noaa.gov) (accessed 10.17.14).
- Nichols, J.E., Huang, Y., 2012. Hydroclimate of the northeastern United States is highly sensitive to solar forcing: NORTHEAST US SENSITIVE TO SOLAR FORCING. *Geophysical Research Letters* 39, n/a–n/a.
- O’Sullivan, P.E., 1983. Annually-laminated lake sediments and the study of Quaternary environmental changes — a review. *Quaternary Science Reviews* 1, 245–313.
- Oswald, W., Faison, E.K., Foster, D.R., Doughty, E.D., Hall, B.R., Hansen, B.C.S., 2007. Post-glacial changes in spatial patterns of vegetation across southern New England. *Journal of Biogeography* 34, 900–913.
- Page, D.S., Boehm, P.D., Douglas, G.S., Bence, A.E., Burns, W.A., Mankiewicz, P.J., 1999. Pyrogenic polycyclic aromatic hydrocarbons in sediments record past human activity: a case study in Prince William Sound, Alaska. *Marine Pollution Bulletin* 38, 247–260.
- PAGES2k Consortium, P. 2k, Ahmed, M., Anchukaitis, K.J., Asrat, A., Borgaonkar, H.P., Braida, M., Buckley, B.M., Büntgen, U., Chase, B.M., Christie, D.A., Cook, E.R., Curran, M.A.J., Diaz, H.F., Esper, J., Fan, Z.-X., Gaire, N.P., Ge, Q., Gergis, J., González-Rouco, J.F., Goosse, H., Grab, S.W., Graham, N., Graham, R., Grosjean, M., Hanhijärvi, S.T., Kaufman, D.S., Kiefer, T., Kimura, K., Korhola, A.A., Krusic, P.J., Lara, A., Lézine, A.-M., Ljungqvist, F.C., Lorrey, A.M., Luterbacher, J., Masson-Delmotte, V., McCarroll, D., McConnell, J.R., McKay, N.P., Morales, M.S., Moy, A.D., Mulvaney, R., Mundo, I.A., Nakatsuka, T., Nash, D.J., Neukom, R., Nicholson, S.E., Oerter, H., Palmer, J.G., Phipps, S.J., Prieto, M.R., Rivera, A., Sano, M., Severi, M., Shanahan, T.M., Shao, X., Shi, F., Sigl, M., Smerdon, J.E., Solomina, O.N., Steig, E.J., Stenni, B., Thamban, M., Trouet, V., Turney, C.S.M., Umer, M., Ommen, T. van, Verschuren, D., Vial, A.E., Villalba, R., Vinther, B.M., Gunten, L. von, Wagner, S., Wahl, E.R., Wanner, H., Werner, J.P., White, J.W.C., Yasue, K., Zorita, E., 2013. Continental-scale temperature variability during the past two millennia. *Nature Geoscience* 6, 339–346.

- Parnell, A., 2015. Radiocarbon Dating, Age-Depth Modeling, Relative Sea Level Rate Estimation, and Non-Parametric Phase Modelling. (R package No. version 4.2.5).
- Parshall, T., Foster, D.R., Faison, E., MacDonald, D., Hansen, B.C.S., 2003. Long-term history of vegetation and fire in pitch pine–oak forests on cape cod, massachusetts. *Ecology* 84, 736–748.
- Patterson, W.A., Edwards, K.J., Maguire, D.J., 1987. Microscopic charcoal as a fossil indicator of fire. *Quaternary Science Reviews* 6, 3–23.
- Pearson, E.J., Juggins, S., Talbot, H.M., Weckström, J., Rosén, P., Ryves, D.B., Roberts, S.J., Schmidt, R., 2011. A lacustrine GDGT-temperature calibration from the Scandinavian Arctic to Antarctic: Renewed potential for the application of GDGT-paleothermometry in lakes. *Geochimica et Cosmochimica Acta* 75, 6225–6238.
- Pederson, D.C., Peteet, D.M., Kurdyla, D., Guilderson, T., 2005. Medieval Warming, Little Ice Age, and European impact on the environment during the last millennium in the lower Hudson Valley, New York, USA. *Quaternary Research* 63, 238–249.
- Peterse, F., van der Meer, J., Schouten, S., Weijers, J.W.H., Fierer, N., Jackson, R.B., Kim, J.-H., Sinninghe Damsté, J.S., 2012. Revised calibration of the MBT–CBT paleotemperature proxy based on branched tetraether membrane lipids in surface soils. *Geochimica et Cosmochimica Acta* 96, 215–229.
- Pierce, D.W., Cayan, D.R., Maurer, E.P., Abatzoglou, J.T., Hegewisch, K.C., 2015. Improved bias correction techniques for hydrological simulations of climate change. *Journal of Hydrometeorology* 16, 2421–2442.
- Pierce, D.W., Cayan, D.R., Thrasher, B.L., 2014. Statistical Downscaling Using Localized Constructed Analogs (LOCA). *Journal of Hydrometeorology* 15, 2558–2585.
- Pyne, S., 1982. *Fire in America: A cultural history of wildland fire and rural fire*. University of Washington Press, Seattle, WA.
- Ramdahl, T., 1983. Retene—a molecular marker of wood combustion in ambient air. *Nature* 306, 580–582.
- Repeta, D.J., 1989. Carotenoid diagenesis in recent marine sediments: II. Degradation of fucoxanthin to loliolide. *Geochimica et Cosmochimica Acta* 53, 699–707.
- Roads, J., Fujioka, F., Chen, S., Burgan, R., 2005. Seasonal fire danger forecasts for the USA. *International Journal of Wildland Fire*. 14: 1-18 14, 1–18.

- Rothermel, R., 1972. A Mathematical Model for Predicting Fire Spread in Wildland Fuels (Research Paper No. INT-115). US Department of Agriculture, Forest Service, Intermountain Forest and Range Experiment Station, Ogden, UT.
- Russell III, J., Hopmans, E.C., Loomis, S., Liang, J., Sinninghe-Damste, J., 2018. Distributions of 5- and 6-methyl branched glycerol dialkyl glycerol tetraethers (brGDGTs) in East African lake sediment: Effects of temperature, pH, and new lacustrine paleotemperature calibrations. *Organic Geochemistry* 117, 56–69.
- San-Miguel-Ayanz, J., Carlson, J.D., Alexander, M., Tolhurst, K., Morgan, G., Sneeuwjagt, R., Dudfield, M., 2003. Current Methods to Assess Fire Danger Potential, in: *Wildland Fire Danger Estimation and Mapping - the Role of Remote Sensing Data*, Series in Remote Sensing. World Scientific Publishing Co. Pte. Ltd., Singapore, pp. 21–61.
- Sanni, S., Wærvågen, S.B., 1990. Oligotrophication as a result of planktivorous fish removal with rotenone in the small, eutrophic, Lake Mosvatn, Norway. *Hydrobiologia* 200-201, 263–274.
- Santos, R.A.L. dos, Deckker, P.D., Hopmans, E.C., Magee, J.W., Mets, A., Damsté, J.S.S., Schouten, S., 2013. Abrupt vegetation change after the Late Quaternary megafaunal extinction in southeastern Australia. *Nature Geoscience* 6, 627–631.
- Schlachter, K.J., Horn, S.P., 2010. Sample preparation methods and replicability in macroscopic charcoal analysis. *Journal of Paleolimnology* 44, 701–708.
- Scholze, M., Knorr, W., Arnell, N.W., Prentice, I.C., 2006. A climate-change risk analysis for world ecosystems. *Proceedings of the National Academy of Sciences* 103, 13116–13120.
- Schoon, P.L., Kluijver, A. de, Middelburg, J.J., Downing, J.A., Sinninghe Damste, J., Schouten, S., 2013. Influence of lake water pH and alkalinity on the distribution of core and intact polar branched glycerol dialkyl glycerol tetraethers (GDGTs) in lakes. *Organic Geochemistry* 60, 72–82.

- Schouten, S., Hopmans, E.C., Rosell-Melé, A., Pearson, A., Adam, P., Bauersachs, T., Bard, E., Bernasconi, S.M., Bianchi, T.S., Brocks, J.J., Carlson, L.T., Castañeda, I.S., Derenne, S., Selver, A.D., Dutta, K., Eglinton, T., Fosse, C., Galy, V., Grice, K., Hinrichs, K.-U., Huang, Y., Huguet, A., Huguet, C., Hurley, S., Ingalls, A., Jia, G., Keely, B., Knappy, C., Kondo, M., Krishnan, S., Lincoln, S., Lipp, J., Mangelsdorf, K., Martínez-García, A., Ménot, G., Mets, A., Mollenhauer, G., Ohkouchi, N., Ossebaar, J., Pagani, M., Pancost, R.D., Pearson, E.J., Peterse, F., Reichart, G.-J., Schaeffer, P., Schmitt, G., Schwark, L., Shah, S.R., Smith, R.W., Smittenberg, R.H., Summons, R.E., Takano, Y., Talbot, H.M., Taylor, K.W.R., Tarozo, R., Uchida, M., van Dongen, B.E., Van Mooy, B.A.S., Wang, J., Warren, C., Weijers, J.W.H., Werne, J.P., Woltering, M., Xie, S., Yamamoto, M., Yang, H., Zhang, C.L., Zhang, Y., Zhao, M., Damsté, J.S.S., 2013. An interlaboratory study of TEX86 and BIT analysis of sediments, extracts, and standard mixtures. *Geochemistry, Geophysics, Geosystems* 14, 5263–5285.
- Schouten, S., Hopmans, E.C., Schefuß, E., Damsté, J.S.S., 2002. Distributional variations in marine crenarchaeotal membrane lipids: a new tool for reconstructing ancient sea water temperatures? *Earth and Planetary Science Letters* 204, 265–274.
- Shanahan, T.M., Overpeck, J.T., Hubeny, J.B., King, J., Hu, F.S., Hughen, K., Miller, G., Black, J., 2008. Scanning micro-X-ray fluorescence elemental mapping: A new tool for the study of laminated sediment records: XRF MAPPING OF LAMINATED SEDIMENTS. *Geochemistry, Geophysics, Geosystems* 9, n/a–n/a.
- Shuman, B., Huang, Y., Newby, P., Wang, Y., 2006. Compound-specific isotopic analyses track changes in seasonal precipitation regimes in the Northeastern United States at ca 8200calyrBP. *Quaternary Science Reviews* 25, 2992–3002.
- Sinninghe Damsté, J.S., Ossebaar, J., Abbas, B., Schouten, S., Verschuren, D., 2009. Fluxes and distribution of tetraether lipids in an equatorial African lake: constraints on the application of the TEX86 palaeothermometer and BIT index in lacustrine settings. *Geochimica et Cosmochimica Acta* 73, 4232–4249.
- Sinninghe Damsté, J.S., Ossebaar, J., Schouten, S., Verschuren, D., 2012. Distribution of tetraether lipids in the 25-ka sedimentary record of Lake Challa: extracting reliable TEX86 and MBT/CBT palaeotemperatures from an equatorial African lake. *Quaternary Science Reviews* 50, 43–54.
- Sinninghe Damsté, J.S., Rijpstra, W.I.C., Foesel, B.U., Huber, K.J., Overmann, J., Nakagawa, S., Kim, J.J., Dunfield, P.F., Dedysh, S.N., Villanueva, L., 2018. An overview of the occurrence of ether- and ester-linked iso-diabolic acid membrane lipids in microbial cultures of the Acidobacteria: Implications for brGDGT paleoproxies for temperature and pH. *Organic Geochemistry* 124, 63–76.

- Sinninghe Damsté, J.S.S., Hopmans, E.C., Pancost, R.D., Schouten, S., Geenevasen, J.A.J., 2000. Newly discovered non-isoprenoid glycerol dialkylglycerol tetraether lipids in sediments. *Chemical Communications* 0, 1683–1684.
- Sinninghe Damsté, J.S.S., Rijpstra, W.I.C., Hopmans, E.C., Weijers, J.W.H., Foesel, B.U., Overmann, J., Dedysh, S.N., 2011. 13,16-Dimethyl octacosanedioic acid (iso-diabolic acid), a common membrane-spanning lipid of *Acidobacteria* subdivisions 1 and 3. *Applied and Environmental Microbiology* 77, 4147–4154.
- Snover, A.K., Mantua, N.J., Littell, J.S., Alexander, M.A., McClure, M.M., Nye, J., 2013. Choosing and Using Climate-Change Scenarios for Ecological-Impact Assessments and Conservation Decisions. *Conservation Biology* 27, 1147–1157.
- Sun, C., Li, J., Jin, F.-F., 2015. A delayed oscillator model for the quasi-periodic multidecadal variability of the NAO. *Climate Dynamics* 45, 2083–2099.
- Sun, Q., Chu, G., Liu, M., Xie, M., Li, S., Ling, Y., Wang, X., Shi, L., Jia, G., Lu, H., 2011. Distributions and temperature dependence of branched glycerol dialkyl glycerol tetraethers in recent lacustrine sediments from China and Nepal. *Geophysical Research* 116.
- Swain, A.M., 1973. A history of fire and vegetation in northeastern Minnesota as recorded in lake sediments. *Quaternary Research, The Ecological Role of Fire in Natural Conifer Forests of Western and Northern America* 3, 383–396.
- Tang, Y., Zhong, S., Luo, L., Bian, X., Heilman, W.E., Winkler, J., 2015. The Potential Impact of Regional Climate Change on Fire Weather in the United States. *Annals of the Association of American Geographers* 105, 1–21.
- Taylor, K.E., Stouffer, R.J., Meehl, G.A., 2011. An Overview of CMIP5 and the Experiment Design. *Bulletin of the American Meteorological Society* 93, 485–498.
- Taylor, S.W., Pike, R., Alexander, M., 1996. Field guide to the Canadian Forest Fire Behavior Prediction System.
- Tierney, J.E., Russell, J.M., 2009. Distributions of branched GDGTs in a tropical lake system: Implications for lacustrine application of the MBT/CBT paleoproxy. *Organic Geochemistry* 40, 1032–1036.
- Tierney, J.E., Russell, J.M., Eggermont, H., Hopmans, E.C., Verschuren, D., Damsté, S., S, J., 2010. Environmental controls on branched tetraether lipid distributions in tropical East African lake sediments. *GEOCHIMICA ET COSMOCHIMICA ACTA* 74, 4902–4918.

- Tierney, J.E., Schouten, S., Pitcher, A., Hopmans, E.C., Sinninghe Damsté, J.S., 2012. Core and intact polar glycerol dialkyl glycerol tetraethers (GDGTs) in Sand Pond, Warwick, Rhode Island (USA): Insights into the origin of lacustrine GDGTs. *Geochimica et Cosmochimica Acta* 77, 561–581.
- Trenberth, K., Zhang, R., NCAR Staff (Eds), 2017. The Climate Data Guide: Atlantic Multi-decadal Oscillation (AMO). [WWW Document]. URL <https://climatedataguide.ucar.edu/climate-data/atlantic-multi-decadal-oscillation-amo>
- Tyler, J.J., Nederbragt, A.J., Jones, V.J., Thurow, J.W., 2010. Assessing past temperature and soil pH estimates from bacterial tetraether membrane lipids: Evidence from the recent lake sediments of Lochnagar, Scotland. *Journal of Geophysical Research: Biogeosciences* 115. doi:10.1029/2009JG001109
- United States Forest Service, 2015. The Rising Cost of Wildfire Operations: Effects on the Forest Service's Non-Fire Work [WWW Document]. URL <http://www.fs.fed.us/about-agency/budget-performance/cost-fire-operations>
- United States Geological Survey (USGS), 1996. Basin Pond Survey and Bathymetric Mapping, Fayette, ME [WWW Document].
- Van Wagner, C., 1987. Development and structure of the Canadian Forest Fire Weather Index System (Forestry Technical Report No. 35). Canadian Forest Service, Ottawa, ON, Canada.
- Van Wagner, C., Pickett, T.L., 1985. Equations and FORTRAN program for the Canadian Forest Fire Weather Index System (Forestry Technical Report No. 33). Canadian Forest Service, Ottawa, ON, Canada.
- Volkman, J., 2003. Sterols in microorganisms. *Applied Microbiology and Biotechnology* 60, 495–506.
- Volkman, J.K., Barrett, S.M., Blackburn, S.I., Mansour, M.P., Sikes, E.L., Gelin, F., 1998. Microalgal biomarkers: A review of recent research developments. *Organic Geochemistry* 29, 1163–1179.
- Wang, H., Liu, W., Zhang, C.L., Wang, Z., Wang, J., Liu, Z., Dong, H., 2012. Distribution of glycerol dialkyl glycerol tetraethers in surface sediments of Lake Qinghai and surrounding soil. *Organic Geochemistry* 47, 78–87.
- Wang, X., Thompson, D., A Marshall, G., Tymstra, C., Carr, R., Flannigan, M., 2015. Increasing frequency of extreme fire weather in Canada with climate change. *Climatic Change* 130. doi:10.1007/s10584-015-1375-5

- Webb, T., Shuman, B., Leduc, P., Newby, P., Miller, N., 2003. Late Quaternary Climate History of Western New York. *Bul. Buffalo Soc. Natural History* 37, 11–17.
- Weber, Y., De Jonge, C., Rijpstra, W.I.C., Hopmans, E.C., Stadnitskaia, A., Schubert, C.J., Lehmann, M.F., Damsté, S., S, J., Niemann, H., 2015. Identification and carbon isotope composition of a novel branched GDGT isomer in lake sediments: evidence for lacustrine branched GDGT production. *Geochimica et Cosmochimica Acta* 154, 118–129.
- Werf, G.R. van der, Randerson, J.T., Collatz, G.J., Giglio, L., Kasibhatla, P.S., Arellano, A.F., Olsen, S.C., Kasischke, E.S., 2004. Continental-Scale Partitioning of Fire Emissions During the 1997 to 2001 El Niño/La Niña Period. *Science* 303, 73–76.
- Wetzel, A., 1983. Biogenic structures in modern slope to deep-sea sediments in the sulu sea basin (Philippines). *Palaeogeography, Palaeoclimatology, Palaeoecology* 42, 285–304.
- Whitlock, C., Larsen, C., 2001. Charcoal as a Fire Proxy, in: Smol, J.P., Birks, H.J.B., Last, W.M., Bradley, R.S., Alverson, K. (Eds.), *Tracking Environmental Change Using Lake Sediments, Developments in Paleoenvironmental Research*. Springer Netherlands, pp. 75–97.
- Whitlock, C., Millspaugh, S.H., 1996. Testing the assumptions of fire-history studies: an examination of modern charcoal accumulation in Yellowstone National Park, USA. *The Holocene* 6, 7–15.
- W.H. Weijers, J., Schouten, S., C. van den Donker, J., C. Hopmans, E., Sinninghe-Damste, J., 2007. Environmental controls on bacterial tetraether membrane lipid distribution in soils. *Geochimica et Cosmochimica Acta* 71, 703–713.
- Woodruff, J.D., Martini, A.P., Elzidani, E.Z.H., Naughton, T.J., Kekacs, D.J., MacDonald, D.G., 2013. Off-river waterbodies on tidal rivers: Human impact on rates of infilling and the accumulation of pollutants. *Geomorphology* 184, 38–50.
- Wright, J.G., 1937. Preliminary improved fire hazard index tables for pine forests at Petawawa Forest Experiment Station. Canada Department of Mines Resources, Dominion Forest Service.
- Yan, B., Abrajano, T.A., Bopp, R.F., Chaky, D.A., Benedict, L.A., Chillrud, S.N., 2005. Molecular tracers of saturated and polycyclic aromatic hydrocarbon inputs into Central Park Lake, New York City. *Environmental science & technology* 39, 7012–7019.
- Yunker, M.B., Backus, S.M., Graf Pannatier, E., Jeffries, D.S., Macdonald, R.W., 2002. Sources and Significance of Alkane and PAH Hydrocarbons in Canadian Arctic Rivers. *Estuarine, Coastal and Shelf Science* 55, 1–31.

- Zell, C., Kim, J.-H., Moreira-Turcq, P., Abril, G., Hopmans, E.C., Bonnet, M.-P., Sobrinho, R.L., Damsté, J.S.S., 2013. Disentangling the origins of branched tetraether lipids and crenarchaeol in the lower Amazon River: Implications for GDGT-based proxies. *Limnology and Oceanography* 58, 343–353.
- Zennaro, P., Kehrwald, N., Marlon, J., Ruddiman, W.F., Brücher, T., Agostinelli, C., Dahl-Jensen, D., Zangrando, R., Gambaro, A., Barbante, C., 2015. Europe on fire three thousand years ago: Arson or climate? *Geophysical Research Letters* 42, 5023–2033.
- Zhang, Z., Smittenberg, R.H., Bradley, R.S., 2016. GDGT distribution in a stratified lake and implications for the application of TEX86 in paleoenvironmental reconstructions. *Scientific Reports* 6.
- Zhu, C., Weijers, J.W., Wagner, T., Pan, J.-M., Chen, J.-F., Pancost, R.D., 2011. Sources and distributions of tetraether lipids in surface sediments across a large river-dominated continental margin. *Organic Geochemistry* 42, 376–386.
- Zink, K.-G., Vandergoes, M.J., Mangelsdorf, K., Dieffenbacher-Kral, A.C., Schwark, L., 2010. Application of bacterial glycerol dialkyl glycerol tetraethers (GDGTs) to develop modern and past temperature estimates from New Zealand lakes. *Organic Geochemistry* 41, 1060–1066.
- Zolitschka, B., Pike, J., von Gunten, L., Kiefer, T., 2014. Annual Recorders of the Past. *Past Global Changes* 22, 1–56.